Prebiotic Synthesis of Inorganic Pyrophosphate (PP_i) Driven by a Geochemical Redox Reaction

Dissertation

for the award of the degree

"Doctor rerum naturalium"

of the Georg-August University of Göttingen

Within the doctoral program *Chemistry*

of Georg-August University School of Science (GAUSS)

Submitted by

Atida Nasufovska, nee Avmedovska

from Brostica

Göttingen 2021

Thesis Committee

Prof. Dr. Ulf Diederichsen
Institute of Organic and Biomolecular Chemistry, University of Göttingen

Prof. Dr. Hans-Joachim Fritz
Institute of Organic and Biomolecular Chemistry, University of Göttingen

Members of the Examination Board

Referee: Prof. Dr. Ulf Diederichsen
Institute of Organic and Biomolecular Chemistry, University of Göttingen

2nd Referee: Prof. Dr. Hans-Joachim Fritz
Institute of Organic and Biomolecular Chemistry, University of Göttingen

Further Members of the Examination Board

Prof. Dr. Franc Meyer
Institute of Inorganic Chemistry, University of Göttingen

Prof. Dr. Joachim Reitner
Department of Geobiology, Centre for Geosciences, University of Göttingen

Prof. Dr. Reinhard Jahn

Department of Neurobiology, Max Planck institute for Biophysical Chemistry

Dr. Holm Frauendorf

Institute of Organic and Biomolecular Chemistry, University of Göttingen

Date of oral examination: September 10, 2021

The work described in this thesis was carried out under the supervision of Prof. Dr. Ulf Diederichsen at the Institute of Organic and Biomolecular Chemistry of the Georg-August University of Göttingen between July 2017 and September 2021 in close cooperation with Prof. Dr. Hans-Joachim Fritz.

Declaration of Authorship

Hereby, I declare that I prepared the doctoral thesis entitled “Prebiotic synthesis of inorganic pyrophosphate driven by a geochemical redox reaction” on my own and with no other sources and aids than quoted.

Göttingen, July 27, 2017

To my Son

To my Family

Abstract

Bioenergetics deals with energy conversion in organisms and is essential for the understanding of living systems. In all extant organisms adenosine triphosphate (ATP) is the energy carrier and transmitter of free energy from exergonic to endergonic processes. Since ATP is a complex molecule, it was unlikely available on prebiotic Earth. Considerations of plausible energy-rich compounds have to be made. After many compounds were mentioned, the most attention got LIPMANNS proposal that inorganic pyrophosphate (PP_i) could be a precursor of ATP. However, a robust synthesis under prebiotic conditions was not yet achieved.

In this thesis, a synthesis of PP_i under prebiotic conditions is indicated by condensation of orthophosphate (P_i) in aqueous solution. The P_i dimerization was coupled to a reaction, which was known to form C/C-bonds from present carbon monoxide (CO), methanethiol (CH_3SH) under transition metal catalysis (FeS, NiS). This reaction compounds can be considered at certain hydrothermal vents, which were referred to be the cradle of the origin of life.

Formed PPi in the reaction was monitored with fluorescence spectroscopy using a fluorescent PPi-sensor assay based on enhanced fluorescence upon binding of PP_i to a sensor fluorophore. Furthermore, the formation of PPi under reaction conditions was confirmed with a another more sensitive *PP_i-Light* assay by measuring the luminescence of PP_i-containing samples.

Acetyl phosphate (AcP) was also considered as energy carrier on early Earth and therefore measurements of the hydrolytically kinetics of both AcP and PPi were carried out to draw conclusions about the stability of the compound at certain temperatures.

In a side project of this thesis, attempts were made towards synthesizing a peptidic minimal model of the active site A-Cluster in acetyl CoA synthase (ACS), which is a key enzyme in combination with carbon monoxide dehydrogenase (CODH) in ancient WOOD-LJUNGDAHL pathway. New findings indicated that metal sulfides catalyse the CO_2 fixation in CODH/ACS enzyme. A precursor of the A-cluster, which is able to catalyse the formation of thioester from

CO and e.g. thioacetic acid in analogy to the ACS enzyme would corroborate to the concept that primordial biochemical metabolisms have geochemical roots.

Contents

1. Introduction

In living systems energy conversion is coupled to electrochemical gradients across lipid membranes controlled by complex protein systems. A disequilibrium of pH-, concentration-, and redox gradients have to be sustained due to harnessing the proton-motive-force. To this process known as *chemiosmotic coupling* the ATP-synthase-catalysed formation of Adenosine triphosphate (ATP) is coupled from Adenosine diphosphate (ADP) and phosphate (P_i). ATP is referred as the universal *energy currency* of extant organisms due to available energy in the phosphoanhydride bonds.

The enzyme-based formation of ATP is complex and unlikely on early Earth ~4.0 Ga ago, to provide an energy source for metabolic reactions. LIPMANN proposed that inorganic pyrophosphate (PP_i) could be a plausible predecessor of ATP considering the rule that complex compounds may evolve from simpler ones.[1] However, PP_i is a simpler molecule with energy-rich phosphoanhydride bond and could be considered as plausible energy-rich source on prebiotic Earth.

Since there is no clue about available polyphosphate deposits on (early) Earth, PP_i must have been synthesized [2]. Many scientists made experimental attempts to couple PP_i condensation of P_i to the hydrolysis of condensing agents of doubtful availability on early Earth.[3–6] Without using condensing agents PP_i synthesis was not realized.[7]

The intention of this work was no further consideration of PP_i condensation by condensing agents and instead to couple the dimerization of P_i to a sustainable geochemical redox process with the result of energy driven condensation of PP_i (Figure 1.1, eq. 3). Great advantages of PP_i as prebiotic energy currency were the ability to distribute the energy stored in the phosphoanhydride bond to drive energy dependent reactions and its stability to hydrolysis.

For this approach the geochemical redox reaction (Figure 1.1, equation 2), in which C/C-bonds were formed, catalysed by transition metal sulfides (FeS, NiS) from inorganic molecules only, seems to be suitable and was originally performed by HUBER and WÄCHTERSHÄUSER.[8] The

experimental conditions were comparable to some underwater volcanos known as hydrothermal systems, in which CO, CH_3SH and transition metal sulfid were available. Under these reaction conditions it was shown that FeS and NiS can catalyse reactions in absence of proteins. Additionally, recent investigations demonstrated that in the ancient acetyl-CoA (WOOD-LJUNGDAHL pathway) pathway the CO_2 fixation is accomplished by metal sulfide-clusters in the key enzymes carbon monoxide dehydrogenase (CODH) and acetyl-CoA synthase (ACS). These findings indicated that some of the oldest features of today's biochemistry not only have similarities to the primary metabolisms, but also provide clues to their inanimate precursors and thus to the path from geochemistry to biochemistry. Between the Hadean ocean and the underwater volcanos temperature-, pH-, concentration- and redox gradients were expected and thus form a plausible region to drive early carbon and energy metabolism.

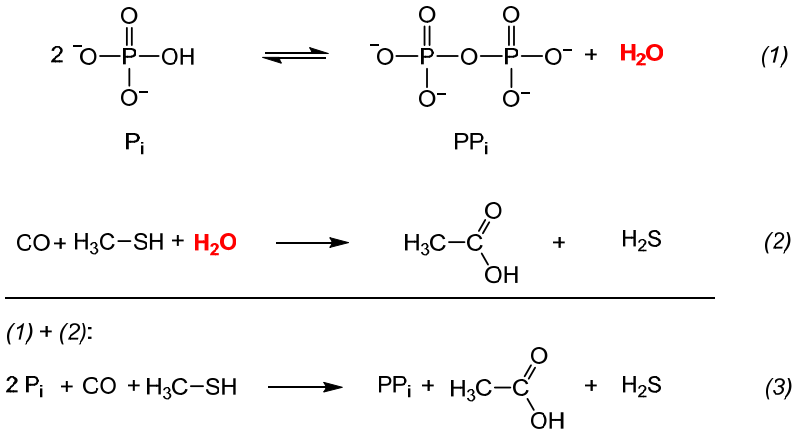

Scheme 1.1 In Equation (1) the condensation of P_i to PP_i is shown. In (2) the acetic acid formation from CO, CH_3SH in aqueous solution is presented. The combination of both (1) and (2) lead to PP_i condensation.

This thesis targets the following two main points: First, coupling the P/P-bond formation to the prebiotically plausible geochemical redox reaction (Figure 1.1, eq. 2) to yield energy-rich PP_i. This would indicate that in prebiotic Earth thioester, which were considered as energy carrier before inorganic phosphate entered the building blocks of life and PP_i had been present simultaneously and therefore is no need to imply a *thioester world* [9] as a distinct evolutionary stage of preceding phosphoanhydride-based bioenergetics. Both energy carriers may have

been present from the beginning with the later shift to PP_i (later ATP) as more efficient catalyst.

Second, to carry out experiments towards synthesizing a peptidic minimal model as prebiotic precursor of the active site A-cluster in ACS enzyme from very ancient carbon fixation Acetyl-CoA pathway (WOOD-LJUNGDAHL pathway). The A-cluster consists of metal sulfide-cluster and catalyses the formation of acetyl-CoA from CO, CH_3-residue and Coenzyme A to acetyl-CoA. A peptidic minimal model, which is able to catalyse the formation of thioester from CO and e.g. thioacetic acid in analogy to the ACS enzyme would corroborate to the concept that primordial biochemistry has been of geochemical origin.

2. Fundamentals of Origin of Life

2.1 Early Earth

The Earth is about 4.6 billion years (Ga) old.[10] This was determined with geochemistry and comparisons to meteorites from other solar system, since geological record is scare. The moon formed ~4.45 Ga ago (Figure 2.1), when the Earth collided with a Mars-sized object, which melted and vaporized (~ 20%) the Earth mantle [10]. This lead to temperatures above 2000 K on early Earth and transferred all water into the gas phase, as well as accreted carbon into carbon monoxide.[11] 1-2 Ga later the Earth cooled down (Figure 2.1) and a primordial ocean was formed, but twice as deep as today's oceans due to later onset of the primordial crust through hydrothermal convection currents.[12]

2.1.1 Early Earth Atmosphere

Many attempts were made to find a satisfactory answer to the composition of the atmosphere, surface area and the primeval ocean on early Earth. UREY and others argued that the gas phase have been strongly reducing based on models of the early terrestrial atmosphere.[13] In MILLERS famous experiment to investigate the prebiotic synthesis of organic molecules, a reducing atmosphere containing CH_4, NH_3 and H_2O, was exposed to electrical discharge and led to the formation carboxylic acids, amino acids and other building blocks of life.[14,15] The accumulation of these compounds in surface environments at the ocean or lakes could contribute to a plausible chemical evolution. After publishing the very promising results of the MILLER-UREY-Experiment [15], the scepticism about the composition of the atmosphere on early Earth increased. [16] More and more scientist favoured the idea of recent models, which indicated that the atmosphere was rather neutral than reducing, dominated by CO_2 and N_2 with traces of H_2.[17] However, it is plausible that the formation of the atmosphere, dominated by the gases CO_2 and N_2 seemed to be a natural consequence of planetary accretion in the terrestrial planet region. [18,19]

2.2 Emergence of Life

The first indications of life was dated ca. 3.8 Ga ago (Figure 2.1) and were found in the form of carbon isotope signature, microbial structures and microfossils in the Eoarchean sedimentary rocks in Canada (Isua supracrustal belt rocks).[20,21] However, the interpretation of the findings was controversial discussed.[22] More indications of life were found in 3.5 Ga old stromatolites preserved microbial mats of deposition by photosynthetic prokaryotes. [23] First widely accepted evidence for biological activity in stromatolites, microfossils were found in Archean rocks of the Pilabara Craton in Australia (Figure 2.1). [24] It is still unclear when life emerged due to absent records on Earth. It is assumed that that first important steps, which lead to the emergence of life happened in the late Hadean (~4.0 Ga), since potentially liquid water, molecular compounds and energy were available. The oldest zircon with an age of ~4.4 Ga was found in Australia and analysis have shown that it has undergone low-temperature interactions with a liquid hydrosphere. These findings indicated that in the period 4.4-4.0 Ga the Earth was may cool enough for the presence of liquid water and allow the survival of organic compounds (Figure 2.1). From this can be derived that key steps in the emergence of first life may have started 4.4-4.0 Ga ago.[25]

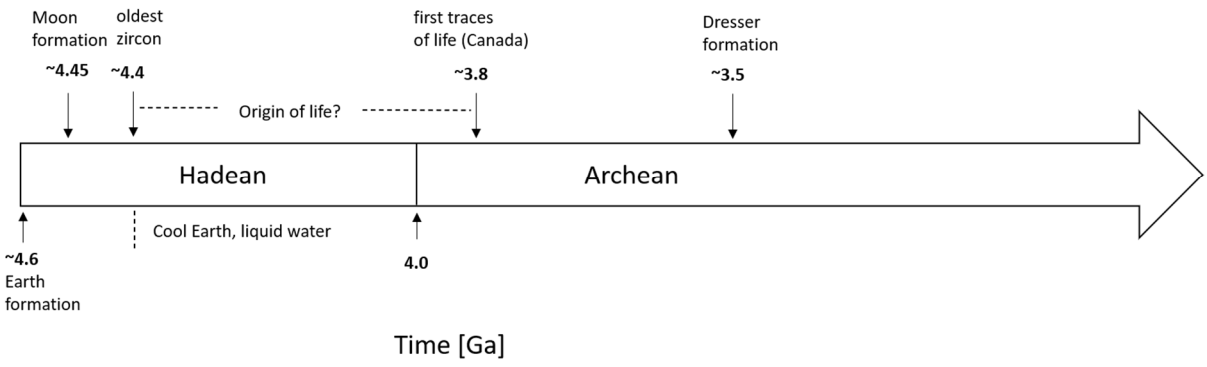

Figure 2.1 Events on early Earth in Hadean and Archean time period. Earth and Moon formation were major events in the Hadean. The oldest found zircon is ca. 4.4 Ga old leads to the assumption of cool Earth and presence of liquid water. First traces of life were found in Isua, Canada ca. 3.8 Ga ago.[25]

It can be assumed that in a narrow time window of 200-600 Ma on early Earth, first cells may have evolved.

2.2.1 Chemoautotrophic Origin of Life

The theory about the chemoautotrophic origin of life indicated that first life developed in a metabolic system, before replication processes could evolve and was supported by WÄCHTERSHÄUSER (see chapter 2.6.2).[26][27] The first living cells, these so-called *pioneer organisms*[28], which evolved chemoautotrophically may have populated sites at reducing volcanic exhalations like hydrothermal vents.[29] The author claimed that first metabolisms could develop on the surface of certain minerals like pyrites (FeS_2), which were according to geological data abundant on prebiotic Earth. The suggestion of WÄCHTERSHÄUSER was that the required free energy for carbon fixation on prebiotic Earth was provided by the oxidative pyrite (FeS_2) formation from iron sulfide (FeS).

$$FeS + H_2S \longrightarrow FeS_2 + 2H^+ + 2e^- \qquad \Delta G^0 = -38.4\ kJ/mol$$

The energy source had to fulfil following requirements: [30]

- Geochemical abundant on early Earth
- Selective and work under mild conditions (UV radiation is excluded)
- Direct electron flow to the reducing agent (CO_2)
- Sufficient reduction potential for all reduction reactions

Chemoautotrophs are able to exist and develop under extreme conditions. The form of energy conversion is considered to be the oldest on Earth. It is suggested that first free-living cells emerged 3.8 Ga ago and had been chemoautotrophic prokaryotes such as eubacteria and archaebacteria. These organisms may populate deep sea vents or acidic environments (see chapter 2.3).

A physical law of thermodynamics (Boltzmann entropy law) is that life only exists far from equilibrium. Only a system that actively maintains disequilibria is able to decrease the entropy locally and thus to generate building blocks of life.[31]

Life could be understood as self-organizing system driven by disequilibrium, which could be e.g. temperature, pH and redox gradients. Those far-from-equilibrium states of living systems keep metabolic systems going and are highly relevant for the emergence of life on early Earth. Hydrothermal settings could be considered as geochemical and physical non-equilibrium settings with existing pH-, temperature and mineral concentration gradients.[32]

2.3 Hydrothermal Settings

The discussion about plausible first emergence of life scenarios was expanded by the discovery of hydrothermal vents in 1977. [33][34] These hydrothermal systems are unique ecosystems and the hydrothermal circulation is assumed to form the basis of life for the organisms.

As soon as the sea water seeps through fissures in the ocean crust, a series of chemical reactions occur (Figure 2.2). This influences the chemistry of the ocean by changes of the sea water composition and that of the volcanic rocks.

The idea that the first organisms on early Earth were anaerobic and chemoautotrophs (Chapter 2.2.1), which were able to metabolise CO_2 in combination with reducing agents like hydrogen (H_2) is widely accepted in science. [35]

Experiments have shown that transition metal compounds (FeS, NiS, etc.), which were present in hydrothermal fluid could serve as a catalysts to synthesize various small molecules including methanethiol (CH_3SH) from CO_2 and H_2S [36] or to accomplish C-C-bond formation to acetic acid from CO and CH_3SH on FeS/NiS-cluster.[8] Hydrothermal vents were suggested to be the place, where those reactions can occur and where first life may have evolved.[37]

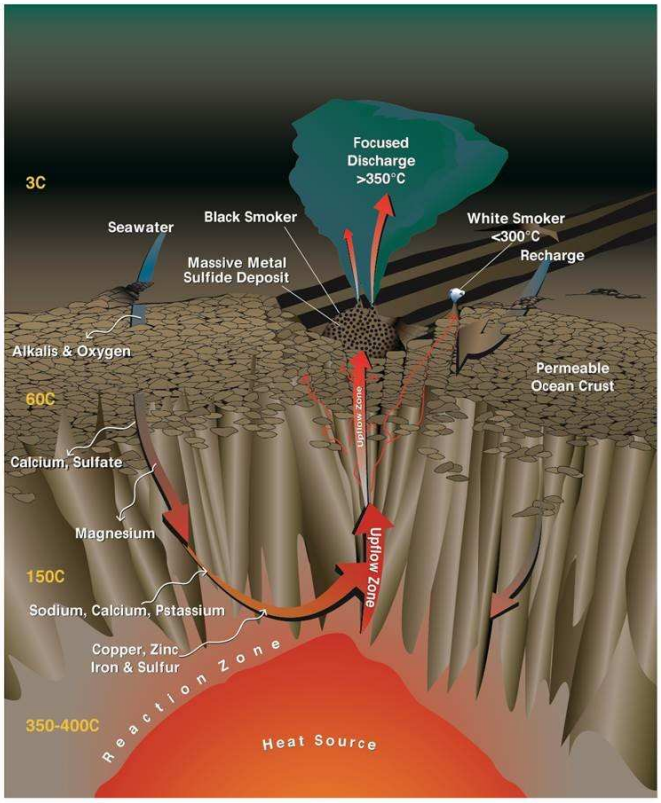

Figure 2.2 Hydrothermal circulation on the mid Atlantic ridge (MAR) [30]. Cold sea water seeps through fissures in the ocean crust and accumulates through various reactions with metals and minerals. The fluid is heated up to 400 °C as it reaches deeper layers in the ocean crust and is pushed with high pressure to the sea surface. [38][39]

In figure 2.3 a tentative pathway for CO_2 fixation with inorganic transition metal sulphides as catalysts is illustrated. H_2 is formed due the geochemical serpentinization[40] process and therefore considered as plausible reducing agent for the reduction of CO_2 to CO. Since HEINEN and LAUWERS demonstrated that CH_3SH can be successfully synthesized under FeS catalysis from carbon dioxide and sulphur species in the presence of H_2, the formation of energy-rich compounds including *e.g.* methyl thio esters is plausible and was indicated by HUBER and WÄCHTERSHÄUSER (1997). The reducing power of hydrothermal vents makes this area particularly interesting as starting point for the origin of biochemistry.[41]

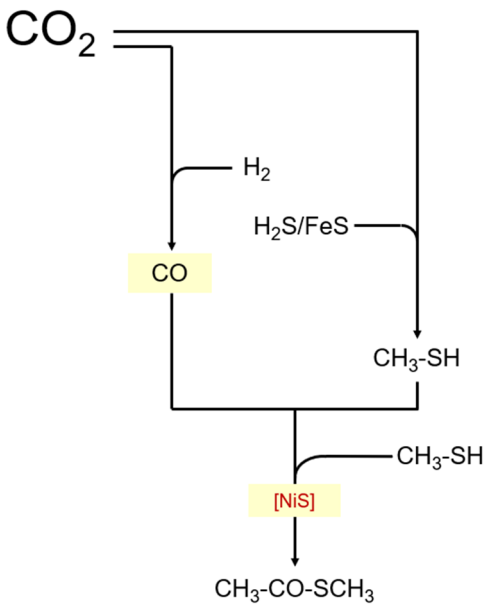

Figure 2.3 Suggested carbon-fixation pathway on primordial Earth, in which inorganic transition metal compound e.g. NiS catalyses the CO_2 fixation to energy-rich compounds.

2.4 Last Universal Common Ancestor (LUCA)

The last universal ancestor (LUCA) could be understood as an evolutionary stage that links the abiotic phase on early Earth with the first biotic signatures in 3.8 Ga old rocks.[11,20] It is considered that LUCA is the common ancestor of bacteria and archaea (Figure 2.4).

LUCA is a theoretical structure and was assumed to have a simple construction like prokaryotes. In literature exist many theories how LUCA was physically assembled and which characteristics it possessed, but nothing concrete can be said about its nature.[42] This hypothesis lead to propose an unrooted universal phylogenetic tree of life, that emerged from ribosomal RNA (rRNA) sequence.[43]

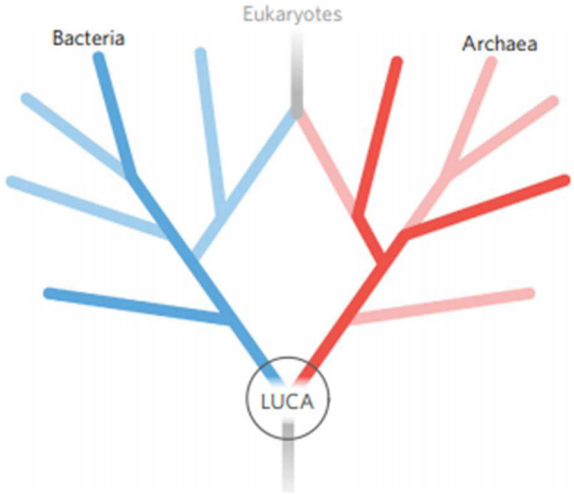

Figure 2.4 Schematic unrooted phylogenetic tree of life. The tree is splitted in two main branches and illustrates that is assumed as the last common ancestor of archaea and bacteria [44]. LUCA can be understood as interface between abiotic early Earth and the first biotic traces of life in old rocks.[20]

The primary branches demonstrated (Figure 2.4) a common predecessor of RNA, transcription compounds and few other genes. It became an organismal tree during the grow process and evolving of many more functions, especially their crystallization. [45] It is assumed that LUCA was not a particular organism, but rather a loosely knit, a conglomeration of primitive cells, which possibly developed and became the primary lines of descent.[45,46]

Scientists reconstructed the genomic data by removing transdomain lateral gene transfers (LGT) in proteins up to LUCA and concluded that it emerges as an anaerobic autotroph. [44,47] It´s assumed that LUCA used a WOOD-LJUNDAHL pathway (Chapter 2.5) and inhabited hydrothermal settings.[48]

2.5 Wood-Ljungdahl Pathway

Autotrophy is the fixation of inorganic carbon into organic material and is a requirement for the explanation of the biological evolution. The most ancient pathway of CO_2 fixation known as acetyl-CoA pathway or WOOD-LJUNGDAHL pathway for carbon assimilation and energy conservation was suggested to be used by LUCA.[49] The acetyl CoA formation from CO_2 in acetogenic bacteria was studied especially by LJUNGDAHL, WOOD and THAUER.[49–52] This

autotrophic acetyl-CoA pathway is highly relevant for the emergence of life on early Earth and was first investigated and descibed in the thermophilic acetogen *Moorrella thermoacetica* (formerly *Clostridium themoaceticum*).[51,52] The fundamental reactions of the WOOD-LJUNGDAHL pathway are schematically illustrated in Figure 2.5.

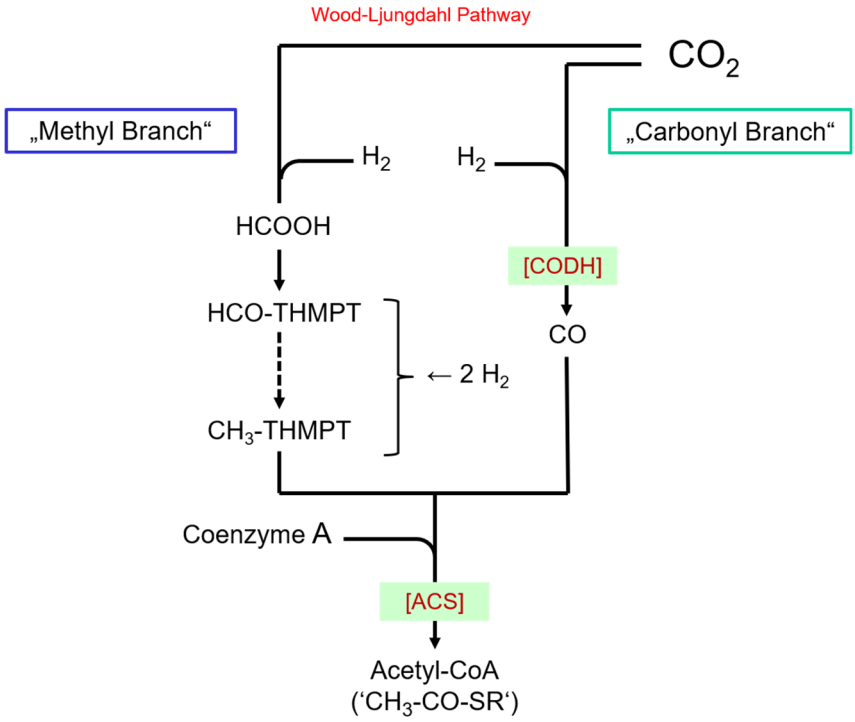

Figure 2.5 Fundamental reactions of CO_2 fixation in the WOOD-LJUNGDAHL pathway. CO_2 is CODH assisted reduced to CO in the “Carbonyl Branch” and in the “Methyl Branch” transformed to a CH_3-residue. ACS converts both compounds and Coenzyme A (CoA) to acetyl CoA.

In the carbon fixation is CO_2 reduced to a CH_3-residue in the “Methyl Branch” and to CO in the “Carbonyl Branch”.

The first reaction of the *Methyl Branch* is the reduction of CO_2 to formic acid (HCOOH). [53] With 10-formyl-H_4folate synthetase HCOOH is catalysed to formyl-H_4folate.[54] The next two steps were catalysed by H_4folate cyclohydrolase to methenyl H_4folate and with H_4folate dehydrogenase to methylene H_4folate. [55] In the last step of the *Methyl Branch* CH_3-H_4folate is formed due catalysis with methylene H_4folate reductase.[56]

CO_2 is reduced in the *Carbonyl Branch* of acetogens to CO by the enzyme CO dehydrogenase (CODH).[57] CODH is a *homodimeric* enzyme and contains five metal clusters [58], in which the

C-Cluster (Figure 2.6) is the catalytical active site for the reduction process. [59] The structure of the C-Cluster can be described as a combination of a [3Fe-4S] cluster with a binuclear [NiFe] cluster (Figure 2.6).[60]

Then the enzyme acetyl-CoA synthase (ACS) catalyzes the reaction from Coenzyme A, the CH_3-residue from the "Methyl Branch" and the CO from "Carbonyle Branch" to the energy-rich acetyl-CoA (Figure 2.5). As mentioned above the C-Cluster (Figure 2.6, A) in CODH is the active site and the A-Cluster (Figure 2.6, B) in ACS is indicated to be the catalytical active site for the condensation of acetyl CoA.[61] In the A-cluster a [4Fe4S] cluster is bridged through a cysteine to a proximal Ni, which is connected to a peptide coordinated distal Ni.[62,63]

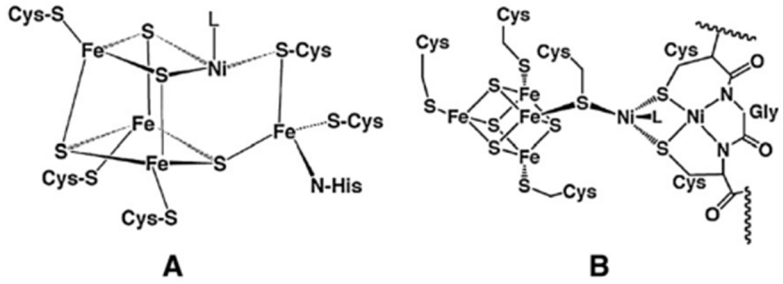

Figure 2.6 Ni-metallocentres are the catalytic active centers of the bifunctional CODH/ACS protein. A: $Ni[Fe_4S_4]$ C-Cluster in CODH and B: $Ni_2[Fe_4S_4]$ A-Cluster in ACS.[61]

This key enzymes in the WOOD-LJUNGDAHL pathway is called *bifunctional CODH/ACS* complex and is a *heterotetrameric* protein.

As mentioned above, carbon records indicated that first life emerged *ca*. 3.8 Ga ago. From Carbon isotopic fractions can be deduced that these anaerobic organisms used the WOOD-LJUNGDAHL pathway to metabolise inorganic compounds like CO_2 and H_2. [64] The simplicity of the WOOD-LJUNGDAHL pathway for carbon fixation makes it plausible to be the first metabolism on early Earth.[41]

Enzymes like bifunctional CODH/ACS were unlikely available on early Earth to catalyse the transformation to acetyl-CoA. Therefore, transition metals compounds e.g. heteroleptic Fe,Ni-complexes could be considered as prebiotic precursor of ACS in analogy to the A-cluster.[65][66]

2.6 Bioenergetics on Early Earth

2.6.1 Modern Bioenergetics

All extant organisms use adenosine triphosphate (ATP, Figure 2.7) as mobile molecular system of energy storage and retrieval. Available energy is stored in the phosphor anhydride-bonds between the phosphates and released 30.5 kJ/mol upon to hydrolysis.[67]

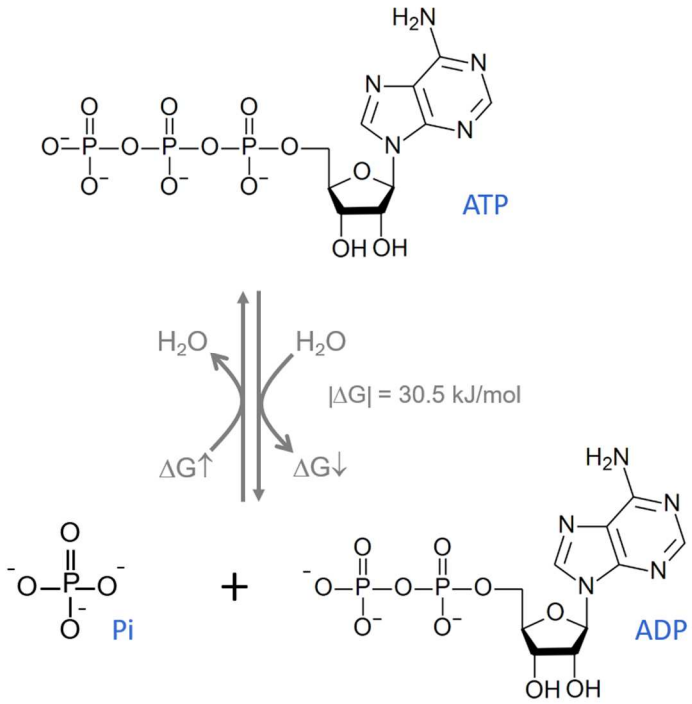

Figure 2.7 ATP released 30.5 kJ/mol due to hydrolysis to adenosine diphosphate (ADP) and phosphate (Pi). Cells require this energy to drive reactions that need to be activated, to transport substances across membranes or to do mechanical work.[67] For ATP synthesis from ADP and P_i energy (30.5 kJ/mol) is required.

The contemporary bioenergetics of anaerobic organisms is well understood and described. [68] In chemolithotrophs electrons are transferred from the major donors H_2 and H_2S to the major acceptors CO_2 and NO_3^-, in which CO_2 is reduced to organic compounds. The electro chemical energy is used to pump protons through the membranes. The energy from the proton gradient is used to synthesize ATP catalyzed by transmembrane incorporated ATP-synthase (Figure 2.8).

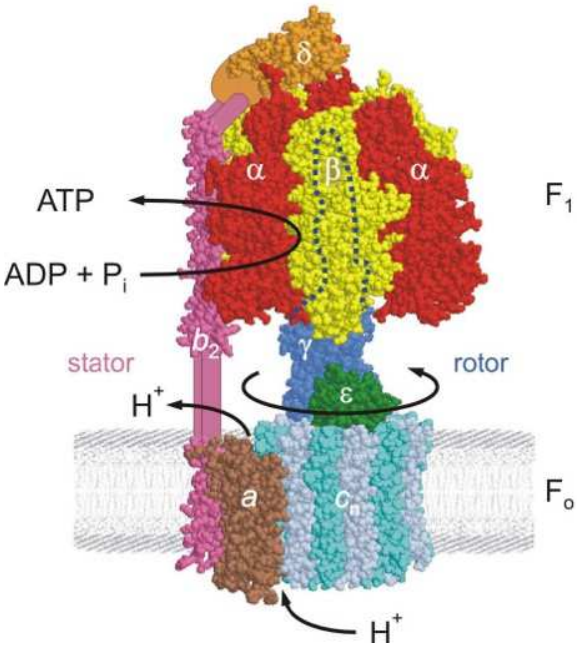

Figure 2.8 Molecular model of ATP synthase[69]. The F_0-unit consists of various sub-units (F_{0a}, F_{0b}, F_{0c}) and is incorporated into the membrane. The F_1-unit consists of three α- and β- proteins, which are connected to the F_0-unit via γ-, δ-, an ε-units. [69,70]

The F_0-unit of ATP synthase is incorporated into the membrane and consists of three subunits. It was suggested that the F_{0c} complex rotates. Experiments indicated that in the subunit of F_{0c} the protonation and deprotonation of aspartic acid could considerably change the structure of the subunit.[71] The so called "head" of ATP-synthase consists of three α-and β-units. Each α- and β-subunit forms a functional unit with a binding site and active center for ATP, ADP and P_i. The three pairs of F_1-unit are in three different states at any point in time. [72] The F_0- and F_1 complex are connected through a central and peripheric stalk of γ–, δ- and ε-subunits (Figure 2.8).

The modern bioenergetics of ATP formation by ATP-synthase is a very progressive and complex enzyme. Therefore, this enzyme-catalysed process is an unlikely scenario to produce energy sources on early Earth. In the following, especially sulfur and phosphate compounds will be discussed as plausible energy sources in the evolution from small organic molecules to biomolecules of life.

2.6.2 Sulfur Chemistry On Early Earth

As described in chapter 2.4. (Hydrothermal Settings), CH_3SH and CO should have been present in reasonable concentrations under vent conditions. Available sulfur on early Earth is of great interest since the absence of molecular oxygen leads to an abundance of elemental sulfur or hydrogen sulfide (H_2S) or to high concentrations of iron sulfides (FeS). [27,73] WÄCHTERSHÄUSER considered that the reaction of H_2S with transition metals (Fe, Ni, etc.) yields insoluble transition metal sulfides and generates electrons, which can be used by other compounds to activate reactions. Under FeS/NiS catalysis the formation of acetyl thioester was demonstrated [8] only by using inorganic compounds like CO and methanethiol (CH_3SH) as reactants. The authors presented a notional mechanism of the prebiotic reaction (Figure 2.9) based on the *Monsanto acetic acid process* [74]. They assumed that a bimodal precipitated NiS-FeS surface is formed in the reaction and acts as an active site on which the reactants CO and CH_3SH can adsorb (Figure 2.9, a). Bound on the NiS-FeS surface, the groups could undergo various migration steps (Figure 2.9, b-d) until activated acetic acid is formed. The activated intermediate can be cleaved from the surface by hydrolysis to acetic acid, or by an attack of aniline or methanethiol to yield N-acetaniline or methyl thio ester respectively Figure 2.9, e).

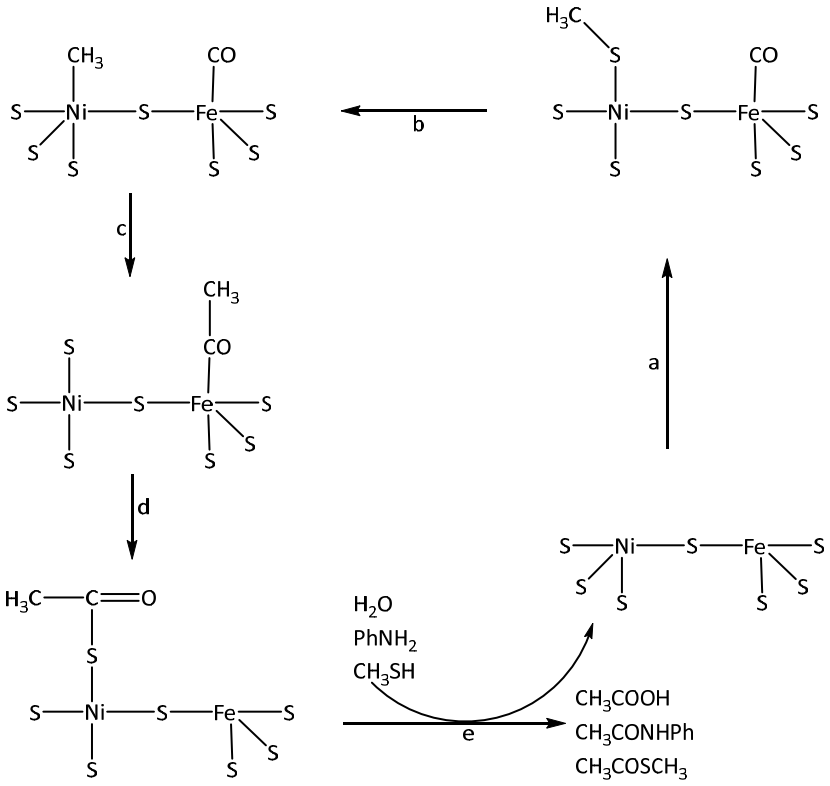

Figure 2.9 Notional mechanism of acetic acid, N-acetylaniline and methyl thioacetate formation from CO and CH_3SH on a NiS-FeS cluster.[8] The mechanism is based on established *Monsanto acetic acid* process. [74]

The experiment to form C/C-bonds and energy-rich thioester from small organic molecules under plausible prebiotic conditions was widely noticed and a great progress in the investigation of the origin of life.

Thioesters are uncontested energy rich compounds, likely available on early Earth and therefore especially from DE DUVE considered as prebiotic energy carriers.[9,75] DE DUVE has recognized the prebiotic potential of sulfur as he proposed that thioesters could have served as activating agents for chemical reactions in the first primitive metabolic pathway before ATP.[9] Prominent scientists have demonstrated the synthesis of acetyl thioesters (Huber and Wächtershäuser 1997) or α-amin acid thioesters[76] under possible prebiotic conditions. WIELAND [77] described spontaneous formation of peptide bonds in aqueous solutions from amino acid thioesters and the elongation of decapeptide in the presence of thioglutamic acid by ORGEL and MAUREL.[78] All these achievements from many scientists lead to the conclusion

that sulfur chemistry has to be considered for the understanding of the early Earth bioenergetics.

2.6.3 Phosphate Chemistry On Early Earth

WÄCHTERSHÄUSER and HUBER have experimentally shown that the metal-sulphide catalysed formation of methyl thioester under prebiotic conditions is possible. [8] However, thioesters are more or less prone to hydrolysis and DE DUVE proposed in addition to hydrolysis of the thioester bond, the transfer of acetyl group to inorganic phosphate as a conceivable step.[9] This would ultimately lead to the formation acetyl phosphate (AcP) and the free thiol. DE DUVE claimed that an attack from inorganic phosphate compounds could have been plausible to generate AcP and suggested that reactions of this type could be the entry of phosphate into bioenergetic pathways. However, plausible phosphate or polyphosphate sources on prebiotic earth have to be discussed first.[79]

2.6.3.1 Phosphate and Polyphosphate Sources

Poly phosphate minerals are not available on contemporary Earth except few kilograms of a calcium diphosphate mineral in New Jersey.[7] YAMAGATA et al. made an interesting discovery that acidic basalts containing apatite are able to release phosphorus pentoxide (P_4O_{10}) when the rock is heated up to 1200 °C.
In addition, they also found tripolyphosphate and pyrophosphate (5 µM) in a fumarole near Uzo in Hokkaido, Japan.[80] The reaction in the basalt could be:

$$4\ H_3PO_4 \longrightarrow P_4O_{10} + 6\ H_2O$$

Scheme 2.1 Proposed reaction in the basalt, which probably leads to the found polyphosphates in the fumarole in Uzo, Japan.[80]

However, the areas where those reactions can occur and produce poly phosphates are very rare and unlikely the main providers of phosphates or polyphosphates for phosphorylation reactions.

The predominant phosphate minerals currently on Earth are hydroxy apatite ($Ca_{10}(PO_4)_6(OH)_2$), fluoro apatite ($Ca_5(PO_4)_3F$) and other apatites. The solubility of calcium phosphate minerals in aqueous solutions is low and actual sedimentary phosphate mineral estimations of 48 x 10^{19} kg would produce ca. 0.2 µM dissolved phosphate in the ocean [81]. Concentrations in micromolar area are too low for phosphorylation reactions and therefore other scenarios must be considered, how phosphate got available on early Earth. It was supposed that phosphorus on prebiotic Earth was present in lower oxidation states than today. Therefore, the formation of more soluble calcium phosphates was favoured instead of apatite and thus higher concentrations of phosphate in the ocean could be expected.

It is assumed that the pH value of the primordial ocean was around 6 and thus more acidic than modern ocean (ca. 8.2).[18] GEDULIN and ARRHENIUS [82] observed that in the pH-range of 6-7.5 the only precipitated mineral is brushite ($CaHPO_4 \cdot 2H_2O$), which crystallizes when phosphate is initiated into sulfate-free seawater medium. The great advantage of $CaHPO_4 \cdot 2H_2O$ is the higher solubility compared to apatite minerals. Under this circumstances $CaHPO_4 \cdot 2H_2O$ could be considered as potential phosphate source on early Earth. Experimental approaches from Hagan et al. have shown that the solubility of $CaHPO_4 \cdot 2H_2O$ depends on the pH and the concentrations of Ca^{2+}-ions. Derived from their results a tentative estimation points out that the phosphate concentration in primordial ocean was 10^2-10^3 times higher than today.[83] Since these results are very interesting it has to be noted that magnesium ions (Mg^{2+}) have been intentionally ignored in the experimental procedures to avoid replacing Ca^{2+} in the brushite by Mg^{2+}, which would decrease the phosphate solubility.

GLINDEMANN et al. showed in model experiments that ca. 11 % of phosphate minerals (hydroxy apatite, fluoro apatite, etc.) can be converted into phosphite salts with electrical discharges under CH_4/N_2 (10 % CH_4) atmosphere.[84] The chosen prebiotic gas mixture from GLINDEMANN did not correspond to assumed geologically plausible neutral prebiotic atmosphere containing mainly CO_2 and N_2. Therefore, DE GRAAF and SCHWARTZ repeated the experiment, but they changed the composition of the atmosphere to CO_2 and N_2 as main gas components and added small amounts of the reducing gases CO and H_2. Also in this attempt the formation of

phosphite salts could be observed and the yield was proportional to the concentration of CO and H_2.[85] The chosen composition of the atmosphere is often criticized as too reducing, but it is speculated that those reducing conditions prevailed at limited areas on early Earth for shorter periods e.g. after volcanic eruptions.

2.6.3.2 Acetyl Phosphate (AcP)

In chapter 2.6.1 was mentioned that acetyl thioester are more or less prone to hydrolysis and DE DUVE proposed in addition to hydrolysis of the thioester bond, the transfer of acetyl group to inorganic phosphate (P_i) as conceivable step.[9,86] He supposed that an attack from inorganic phosphate on thioesters would lead to AcP formation (Figure 2.10).

$$R'SCOR + H_2PO_4^- \longleftrightarrow R'SH + RCOPO_4H^-$$

Scheme 2.2 De Duve proposed that probably phosphate enterted the bioenergetic pathways on early Earth by attacking thioesters phosphorytically to form energy-rich acetyl phosphates (AcP).[41]

AcP is a reactive and energy rich compound with a high phosphorylation potential. The hydrolysis of AcP releases free energy of approximately ΔG_0 = - 43 kJ/mol [87] and is therefore considered as a plausible source of prebiotic energy.

The synthesis of AcP under prebiotic conditions was investigated and indicated by NICK LANE et al.[88] AcP formation was described from orthophosphate and thioacetic acid in water at temperatures of approx. 20-50 °C under neutral to slightly alkaline conditions without using catalysts. It was pointed out that AcP is reasonably stable to hydrolysis under the mentioned conditions. In addition, the formed AcP was able to acetylate Glycine to N-acetylglycine and phosphorylation of adenosine and of ribose under slightly alkaline conditions was observed too. Nevertheless, a polymerization driven by AcP was not obtained. Based on the experimental findings the authors concluded that AcP is a credible primordial energy currency. AcP is worth considering as key intermediate in the prebiotic context, especially since it was experimentally pointed out that PP_i can be synthesized from AcP and Pi.[3,4,89,90]

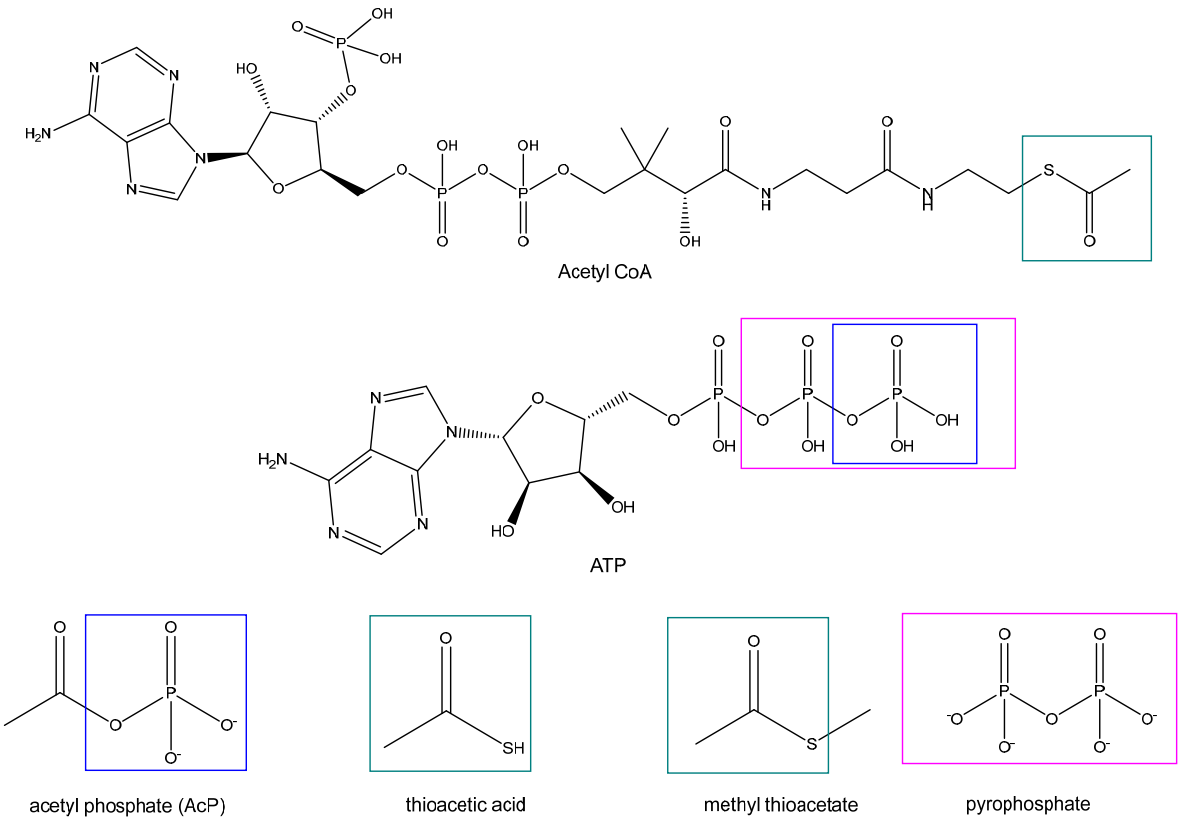

Figure 2.10 Structures of key molecules of modern and possibly prebiotic biochemistry. The thioester group (green), which is known from the carbon fixation acetyl CoA has analogues to the possibly prebiotic relevant molecules thioacetic acid and methyl thioacetate. AcP and PP_i (see chapter 2.6.3.3) shows structural analogues (blue and pink highlighted) to the present-day universal energy currency ATP and is a phosphorylation agent, too.[88]

2.6.3.3 Attempts to form Pyrophosphate (PP_i) under prebiotic conditions

Inorganic pyrophosphate (PP_i) is considered as plausible precursor of ATP in a prebiotic world. The required chemical energy to drive or activate reactions is present in the phosphor anhydride bonds between the phosphates. Since there are no clues about a pyrophosphate or polyphosphate source on Earth, it would need to be synthesized. LIPMANN and BALTSCHEFFSKY proposed PP_i as first phosphate energy currency. [82,91] This hypothesis leads to great efforts to synthesize PP_i under prebiotic

conditions in laboratories all over the world with more or less promising results. The great advantage of PP_i over AcP as precursor of ATP is its much higher stability to hydrolysis. This fact is not surprising and was shown experimentally in this thesis (Chapter 4.3).

- First experimental approaches to form PPi under prebiotic conditions were made by Stanley Miller and Michael Parris.[5] A synthesis reaction of PP_i was described by reacting cyanate and hydroxyapatite under aqueous conditions at pH 8 and 35 °C. They proposed that first may a carbamyl phosphate intermediate be formed, which reacts with a second phosphate molecule to PP_i (Scheme 2.3).

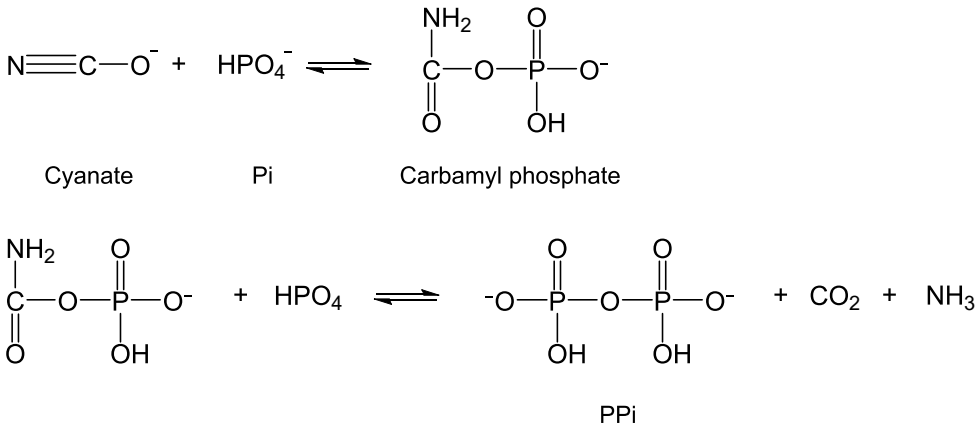

Scheme 2.3 Proposed mechanism of PP_i synthesis from cyanate and Pi *via* carbamyl phosphate as high energy phosphate intermediate.[5]

The authors mentioned that LIPMANN and JONES [92] proposed carbamyl phosphates as possible high energy phosphates on early Earth and that the experimental data supported this hypothesis.

- Further approaches of PP_i formation under prebiotic conditions were made by WEBER in 1981.[3] WEBER described the synthesis of PP_i with N, S-Diacyl cysteamine as condensing agent at pH 7 and 8 at 50 °C. The author assumed that initially acetyl phosphate (AcP) is formed from the thioester and the orthophosphate, which reacts further with a second orthophosphate to PP_i. In 1982 WEBER published another synthesis reaction for PP_i formation under prebiotic conditions.[4] The experimental

procedure of PP_i formation was like the described in 1981, in which thioesters were used as condensing agents and sodium phosphate as phosphate source. However, in this approach the formation of PP_i occurs on the site of the most abundant phosphate mineral hydroxyapatite.

- HERSCHLAG and JENCKS published PP_i synthesis reacting AcP and Pi under concentrated aqueous (6.4 M) sodium perchlorate conditions at 54 °C.[90] The necessarily high concentrations of sodium perchlorate to achieve significant amounts of PP_i could be required to overcome the electrostatic repulsion between AcP and Pi. It was assumed that the sodium ions bridged the negatively charged oxygen atoms of the compounds AcP and Pi (Figure 2.11).

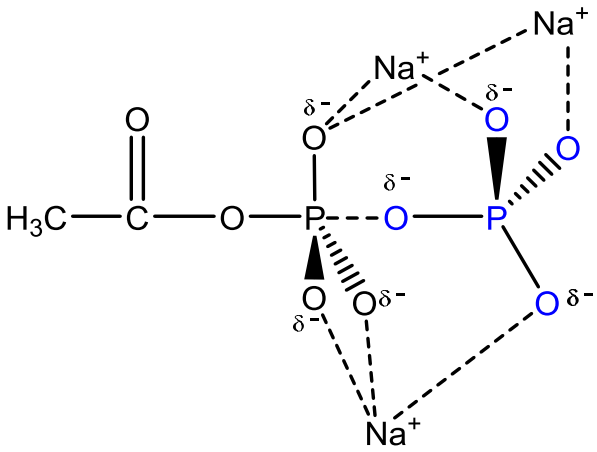

Figure 2.11 Schematic structure of the sodium bridged compounds AcP and Pi. Negative charged oxygen atoms of AcP and Pi are bridged by sodium to overcome electrostatic repulsion.[90]

- A controversial discussion about *Are Polyphosphates or Phosphate Esters Prebiotic Reagents?* was published in 1995 by MILLER and KEEFE.[7] The authors state the occurrence of polyphosphates in nature was present in very low amounts and therefore, a significant accumulation of natural polyphosphates in the early ocean could be neglected. They continued, if polyphosphates were not available naturally then maybe synthesized under prevailing conditions on early Earth. They pointed out that many attempts to polymerize phosphates under prebiotic conditions have been made, but a solid synthesis was not achieved yet. Either were the plausible phosphates

e.g. cyanovinyl phosphate poor phosphorylation agents or the used condensing agents were unlikely on early Earth. The authors explained in some experimental attempts soluble Pi concentration was set higher than 10^{-3} M, which would not correspond to the estimated concentration of Pi in primeval ocean. Also, utilizing Pi on apatite surfaces to form PP_i was not convincing, because some phosphate minerals would hydrolyse phosphate anhydrides.[93]

MILLER and KEEFE concluded that all attempts to synthesize polyphosphate under plausible prebiotic conditions were unconvincing. Therefore, they deduced that phosphate may not play a role in the formation of the first living cell and refer to such theories, which were already proposed by CAIRN-SMITH [94] and DE DUVE.[9]

This judgement may have been premature.

- HERMES-LIMA and VIEYRA have shown a synthesis route for PP_i formation at low temperatures from phosphor(enol)pyruvate (PEP) adsorbed onto precipitated calcium phosphate without using condensing agents.[95] PEP was described by the authors as an analogue of the high energy compound cyanovinyl phosphate, which was synthesized under prebiotic conditions [6]. From the experimental results they concluded that calcium phosphate can catalyse PP_i formation enzyme-like. In further experiments the authors tried to synthesize PP_i with PEP in the presence of precipitated magnesium phosphate and dimethyl sulfoxide.[96] Also, with this approach PP_i synthesis was detected. Adsorption of PEP onto precipitated magnesium phosphate was observed and a reaction of the phosphoryl group of PEP with the phosphate containing magnesium precipitate was assumed. The authors suggested that the magnesium structure not only provides a phosphate group, but also catalyses the formation of PP_i.[96]
- BARGE and co-worker published in 2014 a method to synthesize PP_i in iron mineral films and membranes simulating prebiotic submarine hydrothermal precipitates. [97] They simulated iron-rich inorganic membranes at early Earth alkaline hydrothermal vents. In a solid phase reaction Pi and AcP were precipitated with iron sulfides or iron silicates. In agreement of the findings of HERSCHLAG and JENKS detected the higher the AcP

concentration in the reaction, the higher the PP_i yield.[90] The authors assume that the membrane stabilizes the reactants against hydrolysis and that the compounds can accumulate in the membranes. BARGE et al. pointed out that PP_i synthesis under prebiotic alkaline vent conditions is possible, if AcP is present in the membrane. They don't use condensing agents or very high salt concentrations to overcome electrostatic repulsion between the reactants.

3. Outline

3.1 Prebiotic PP_i Condensation Reaction

The understanding of Bioenergetics is highly relevant for living systems and must be considered on prebiotic Earth. In modern bioenergetics adenosine triphosphate (ATP) is referred to be the universal energy storing system of extant organisms. ATP and its complex enzyme-based formation is unlikely to be the energy source on prebiotic Earth.

LIPMANN hypothesized that inorganic pyrophosphate (PP_i) should be considered as plausible precursor of ATP. Many attempts in the past to find experimental support for LIPMANNS proposal were in vein. PP_i condensation occurred only by using condensing agents of doubtful prebiotic availability on early Earth.

The aim of this project was to couple the P/P-bond formation to a geochemical redox reaction, in particular to drive endergonic condensation of orthophosphate (P_i) to metastable inorganic pyrophosphate (PP_i). The motivation was to find and establish a synthesis route for energy-rich pyrophosphate without using prebiotically unplausible condensing agents.

The geochemical redox reaction from HUBER and WÄCHTERSHÄUSER appears to be a candidate reaction for this approach. The authors demonstrated C/C-bond formation under transition metal catalysis (FeS, NiS) by reacting inorganic compounds like CH_3SH and CO. The reactants and transition metals were available at hydrothermal systems, where its assumed that first life evolved.

We suppose that if ortho phosphate (P_i) is added as further nucleophile next to CH_3SH to the geochemical redox reaction, the acetyl group will be transferred from the catalyst to P_i and acetyl phosphate (AcP) would be formed (Figure 3.1)

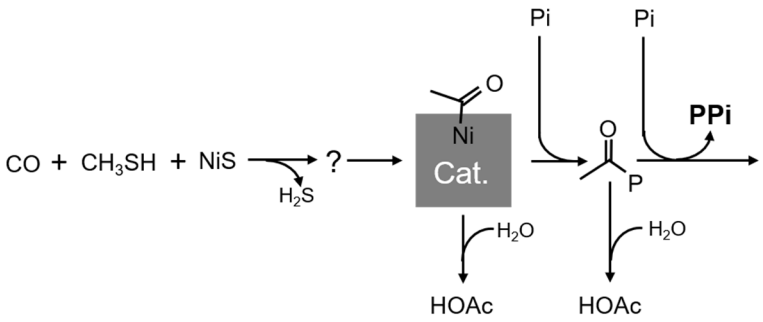

Figure 3.1 Schematic overview of PP_i condensation linked to the geochemical redox reaction of HUBER and WÄCHTERSHÄUSER. Carbon monoxide (CO) and methanethiol (CH_3SH) adsorb at NiS surface and an acetyl group is assembled catalyst bound [8]. A nucleophilic attack of orthophosphate (P_i) yields acetyl phosphate (AcP). Inorganic pyrophosphate (PP_i) is formed due to a nucleophilic attack at of Pi at AcP

In the next step AcP reacts with another P_i to pyrophosphate (PP_i) and would thus present a synthesis route for metastable, energy-rich PP_i under plausible prebiotic conditions (Figure 3.1).

3.2 Experiments towards Peptidic Minimal Models of Acetyl coenzyme A Synthase

Acetyl CoA synthase (ACS) is a key enzyme in the WOOD-LJUNGDAHL pathway, which is assumed to be the oldest metabolic pathway on Earth. The active site for ACS activity is the A-cluster (Figure 3.2) and contains three components, a cuboidal Fe_4S_4 unit, a square planar distal Ni_d coordinated by two peptide backbone amide nitrogens and two cysteine side chains thiolates and a four coordinated proximal nickel site.

It is considered that the evolution of ACS could have started from inorganic transition metal sulfides like NiS in the hydrothermal fluids to peptide coordinated Ni-compounds, which evolved over the time to complex enzymes like ACS.

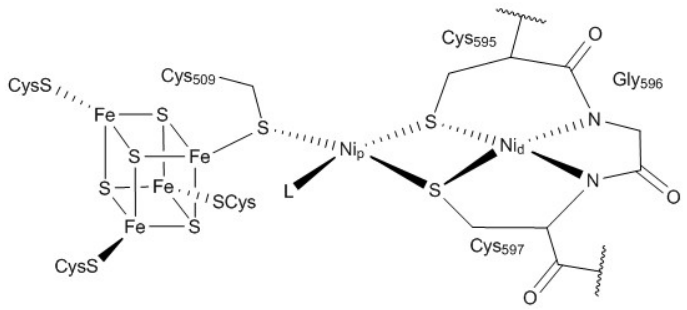

Figure 3.2 A-cluster of acetyl coenzyme A synthase (ACS) containing a cuboidal Fe_4S_4 unit, a peptide coordinated distal Ni_d and a proximal metal (M_p), which is known to be Ni_p in the active site.[98]

The motivation for this part of the project was to synthesize a peptidic minimal model as precursor of the active site of ACS.

First, the square planar coordinated distal Ni-center has to be synthesized with a peptide sequence from thermophilic acetogen *Moorella Thermoacetica* (594-598), containing the amino acids serine (S), cysteine (C), glycine (G), cystein (C) and phenylalanine (F). Afterwards the peptide coordinated Ni-complex would be expanded by a second proximal Ni-center and connected to a Fe-S-cluster in analogy to the A-cluster (Figure 3.2).

Experimental results about a prebiotic, catalytically active precursor of ACS would corroborate to the hypothesis that first biochemical metabolisms have geochemical origin.

4. Results and Discussion

4.1. Prebiotic PP_i Condensation Reaction

HUBER and WÄCHTERSHÄUSER [8] demonstrated plausible that C-C-bond formation is accomplished from small organic molecules under prebiotic conditions (see chapter 2.6.2). The authors proposed that at hydrothermal settings carbon monoxide, methanethiol (CH_3SH) and hydrothermal fluids containing metal sulfides such as nickel sulfides (NiS) were likely present. In a widely noticed experiment they reacted CO, CH_3SH transition metal catalysed (FeS, NiS) in an aqueous suspension at 100 °C and detected acetic acid and methyl thioester. If other nucleophiles like aniline were present in the reaction, then N-acetylaniline was detected (Figure 4.1).

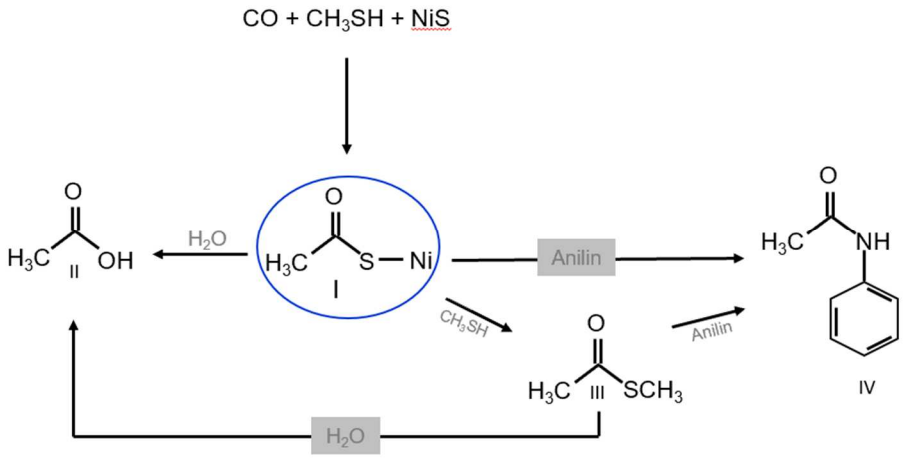

Figure 4.1. Tentative reaction scheme of acetic acid, methylthioacetate and N-acetylaniline under prebiotic reaction conditions. Detachment of the covalently bound acetyl group from the catalyst by water (II) or excess methanethiol to yield acetic acid or methylthioacetate (III) respectively. Aniline as competing nucleophile to CH_3SH and H_2O in the reaction mixture and would yield N-acetylaniline (IV).

The results from the experiment indicated formation of acetyl group on NiS surface from CO and CH_3SH, which covalently bound on the catalyst.

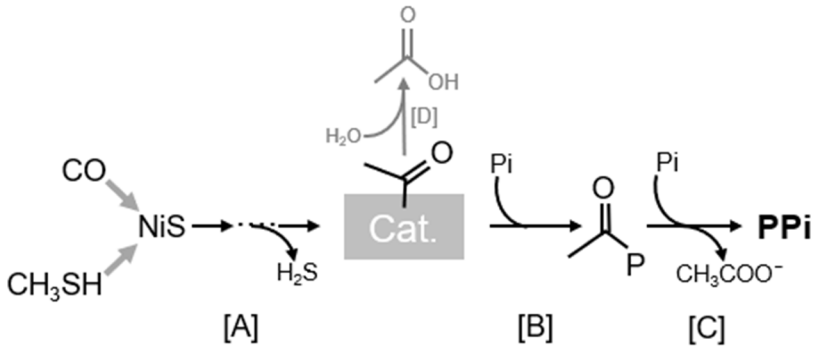

Figure 4.2 Proposed reaction scheme of PP_i synthesis by linking the P/P-bond formation to geochemical redox reaction from HUBER and WÄCHTERSHÄUSER. Reaction [A] described the formation of acetyl bound catalyst, which detached AcP by a P_i attack [B]. An attack of P_i on the phosphate moiety of AcP yield PP_i [C].

Detachment of the covalently bound acetyl group from the catalyst by water or excess methanethiol leads to acetic acid (Figure 4.2, A) or methyl thioacetate, respectively (Figure 4.1, A).[8,99] If inorganic phosphate (P_i) is present in the reaction mixture, formation of acetyl phosphate (AcP) would be expected (Figure 4.2, B) and an attack of a second molecule P_i would ultimately lead to pyrophosphate (PP_i) with energy storage in a hydrolytically stable molecule (Figure 4.2, C). Before linking P/P-condensation to the geochemical redox reaction, it was examined whether PP_i formation can be accomplished with AcP and P_i in aqueous solution (Scheme 4.1).

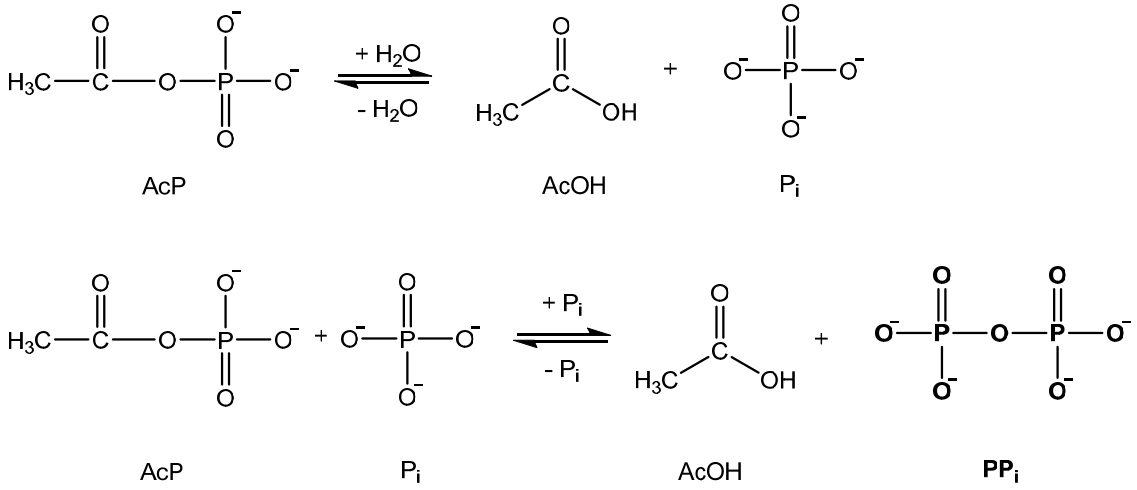

Scheme 4.1 Reaction scheme for PP_i formation from AcP and P_i in aqueous solution. AcP can hydrolyse to acetic acid (AcOH) and P_i. In competition to hydrolysis the phosphate-moiety of AcP can be attacked by P_i to produce PP_i.

To form PP_i, AcP need to be attacked by P_i in the solution, but under pH 8 reaction conditions AcP and P_i are negatively charged (Scheme 4.1). Therefore, a suitable molecular additive need to be found to overcome electrostatic repulsion in the reaction mixture. In a similar case HERSCHLAG and JENCKS [90] demonstrated that the electrostatic repulsion to form PP_i from AcP and P_i can be overcome with high salinity of the reaction medium. They used sodium perchlorate concentrations up to 7 M to increase the PP_i yields due to bridging the negatively charged oxygen atoms of the reactants by sodium ions. Applied to the results of HERSCHLAG and JENCKS calcium phosphate ($Ca_3(PO_4)_2$) was considered to be a suitable and prebiotic plausible compound to assist overcoming the electrostatic repulsion between P_i and AcP. The calcium cations could shield the negatively charged oxygen ions of P_i and AcP to form calcium cation bridges between the reactants (Figure 4.3).

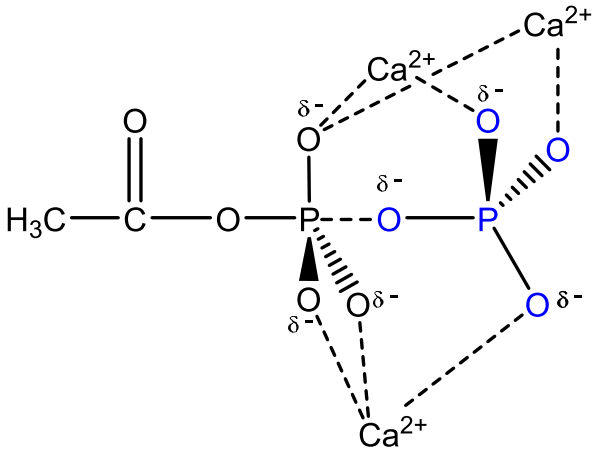

Figure 4.3 Proposed structure of bridged AcP and P_i by calcium cations inspired by HERSCHLAG and JENCKS.[90,100] AcP (black atoms) and P_i (blue atoms) bridged by the calcium cations from $Ca_3(PO_4)_2$ to overcome the electrostatic repulsion between the reactants and to yield PP_i formation.

With the knowledge of the results from HERSCHLAG and JENKS an experiment was performed to confirm the formation of PP_i from AcP and P_i. Commercially available AcP, freshly precipitated $Ca_3(PO_4)_2$ and a 100 mM solution of orthophosphate (pH 8) as P_i source were reacted at 50 °C.

To detect synthesized PP_i in the reaction a commercial fluorophore was used to bind PP_i with high affinity and high selectivity towards PP_i.[101] The naphthalene-based fluorescent sensor detected PP_i with high affinity in aqueous solution over a wide pH range. In Figure 4.4 LEE proposed a mechanism for the binding mode for PP_i at the sensor is illustrated and shows that the two sets of oxygen anions of PP_i bind to the binuclear zinc complex by bridging the two metal ions.[101] Furthermore, the charged sensor shows emission (λ_{Em}) shift to higher wavelength upon addition of PP_i. Summarized can be concluded that PP_i -ligands bonded to the sensor increase the quantum yield of fluorescence (for more details see Experimental Section).

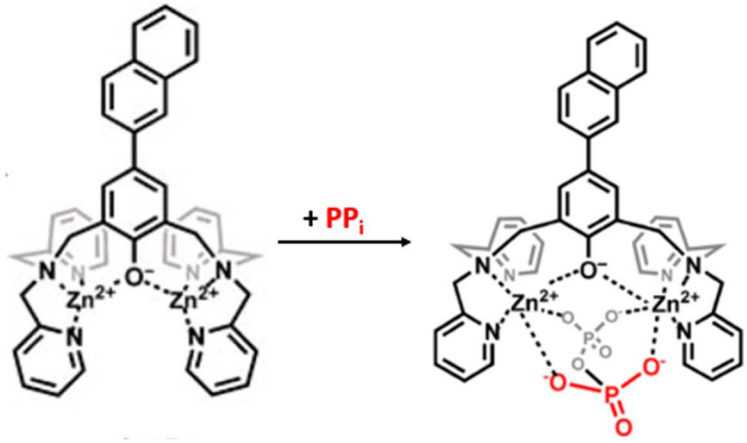

Figure 4.4 Proposed mechanism for the complexation of fluorescent PP_i sensor by PP_i. LEE proposed that the two sets of oxygen anions of PP_i bind to the binuclear zinc complex by bridging the two metal ions. [101]

In Figure 4.5 fluorescent spectra of sampled aliquots at indicated time points of reacted AcP with soluble and insoluble P_i were shown. The first fluorescence signal is detected directly after 0 h caused by PP_i contaminated AcP, which was also confirmed by NMR spectrometry (see NMR-spectra in Appendix A.3). However, the increasing signals after 3-6 hours can be attributed to synthesized PP_i in the reaction mixture. Also, the emission shift to higher wavelength is noticeable due to increasing synthesis of PP_i over the reaction time. After 6 h no further increase of fluorescence intensity was observed. That can be explained by the half-life time ($T_{1/2}$) of AcP, which was determinde to be $T_{1/2}$ = 3 h at 39 °C.[102] Therefore, it can be concluded that AcP is consumed after 6 h under prevailing reaction conditions with the result that no more PP_i can be formed and thus further fluorescence intensity is not monitored.

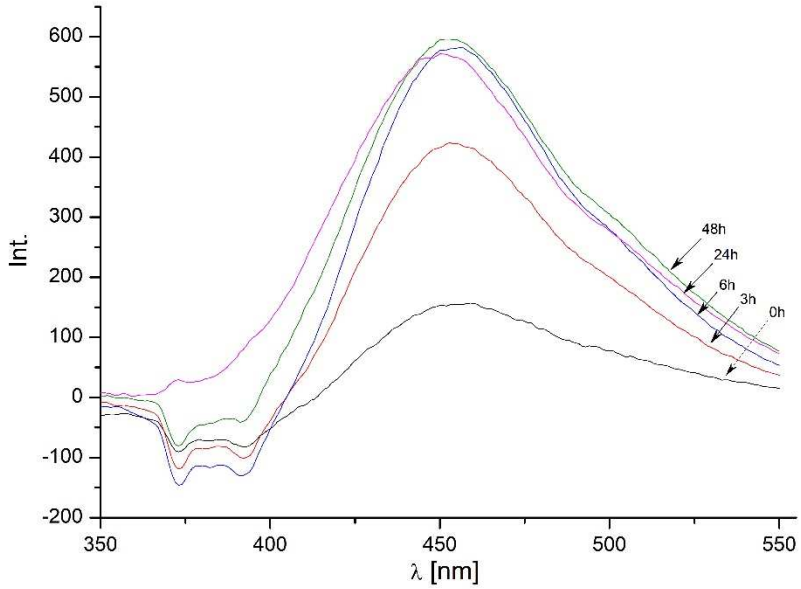

Figure 4.5 Fluorescence spectra of sampled aliquots (10^{-3} diluted with 20 mM TRIS·HCl-buffer, pH 8) after 0, 3, 6, 24 and 48 h to monitor PP_i formation. Excitation wavelength was λ_{Ex} = 316 nm. An increasing of fluorescence intensity is obtained up to 6 h and stays within 48 h unchanged, because of consumed reactant AcP, which has a half-life time below 3 h under reaction conditions. [102]

The experimental results demonstrated formation of PP_i from AcP with orthophosphate as P_i source and freshly precipitated calcium phosphate to overcome electrostatic repulsion between the negatively charged reactants.

Since the results from the reaction of AcP and PP_i were convincing (Figure 4.5), the next step was to link the of P/P-bond formation in analogy to the C/C-bond formation to the geochemical redox reaction from HUBER and WÄCHTERSHÄUSER (Figure 4.1). In the reaction scheme (Scheme 4.2) is illustrated, how PP_i formation can be carried out without using condensing agents. In this process synthesized active species (Figure 4.1) is utilized as acetyl transferring compound to build the key intermediate AcP, which can under reaction conditions lead to formation of PP_i.

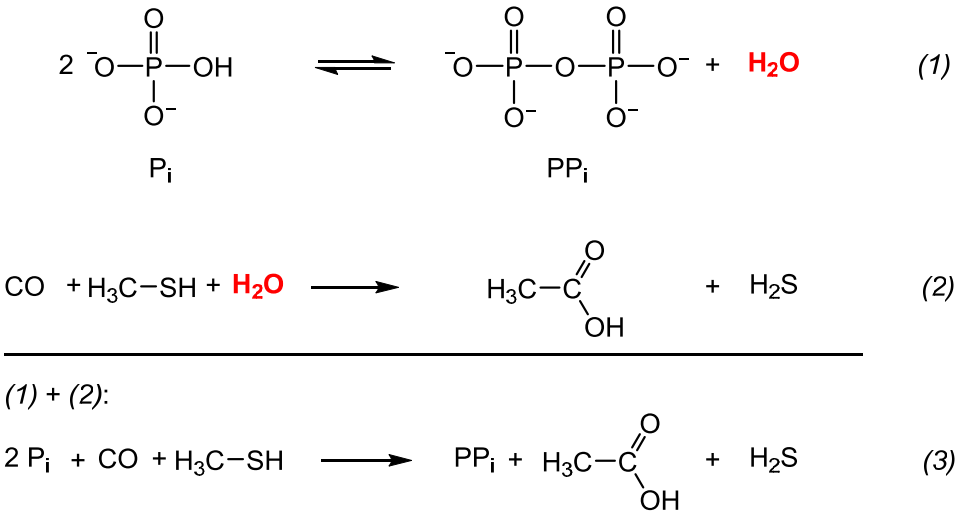

Scheme 4.2 Condensation of P_i to PP_i (1). Acetic acid formation from CO and methanethiol under aqueous conditions (2). Coupled reaction (1)+(2) to form PP_i.

In the experimental procedure NiS was precipitated from $NiSO_4$ and Na_2S under CO atmosphere at 60°C. Soluble aqueous solution of orthophosphate (Na_2HPO_4, pH 8) and insoluble, freshly precipitated calcium phosphate ($Ca_3(PO4)_2$) were added to the suspension. With a constant stream of CO (1 bar) and CH_3SH the reaction mixture was stirred for 8 h at 60 °C. Aliquots were taken at indicated time points and PP_i formation was monitored with previously described fluorescent PP_i sensor (Figure 4.4).

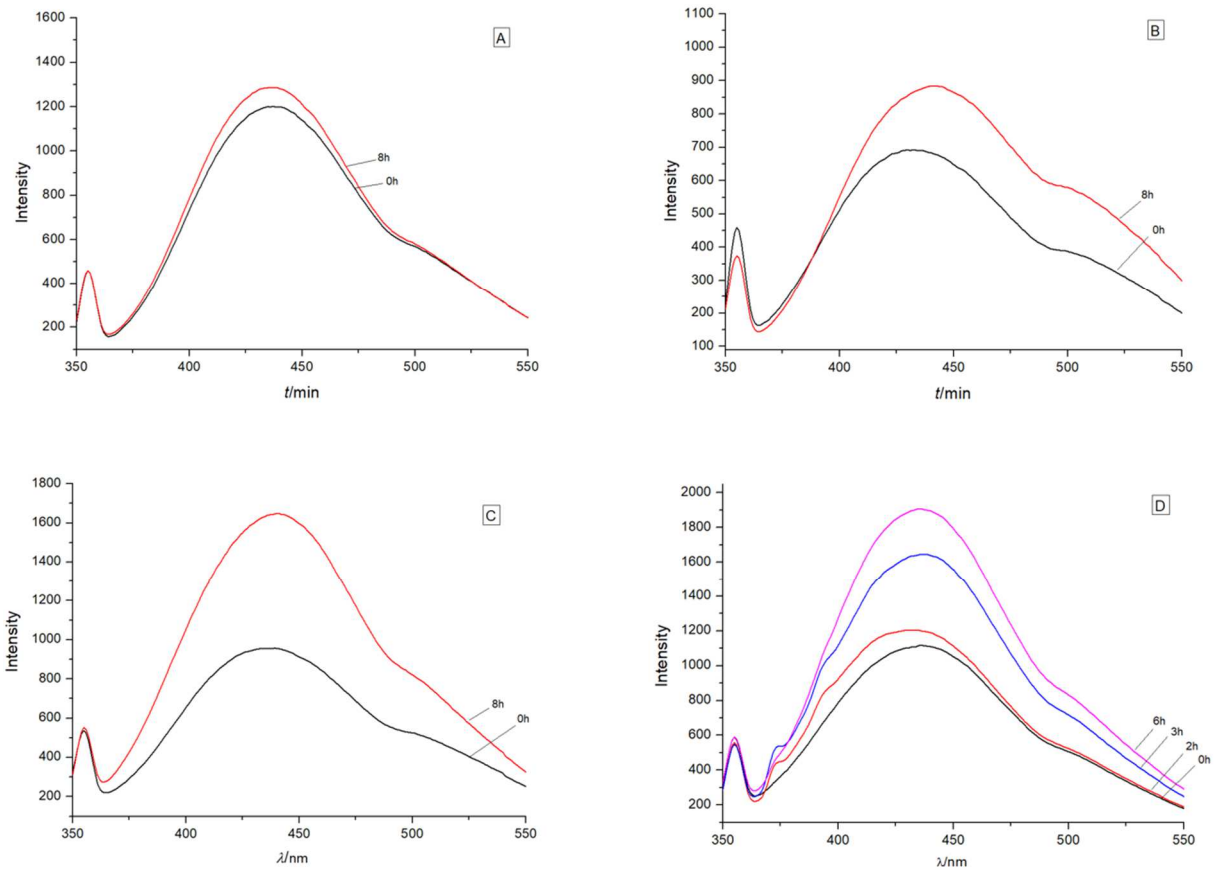

Figure 4.6 Monitored PP_i -formation of the reaction at 60°C, pH 8 by fluorescent PP_i -sensor. The ordinate shows intensities of fluorescence emission in arbitrary units and the excitation wavelength was adjusted at 316 nm. In panel A unsoluble $Ca_3(PO_4)_2$ was not added to the reaction mixture. Panel B: Same as in panel A, but soluble $NaHPO_4$ was left out. Panel C: Both soluble and insoluble P_i present in the reaction mixture. Panel D: Same as in Panel C, but aliquots were withdrawn in shorter time points.

At the beginning of the reaction (after 0 h) fluorescence signal is detected at all panels (Figure 4.6, A-D), which can be attributed to fluorescence of the free sensor (for spectra see Appendix) and may to the presence of PP_i traces in the commercial $NaHPO_4$. However, the increasing fluorescence intensity (Figure 4.6, red line, panel C and D) over the reaction time is interpreted to be caused by synthesized PP_i. This analysis is supported also by the fluorescence spectra at panel D, in which an ordered increasing of the fluorescence signal is observed due to PP_i formation in the reaction mixture. In the absence of insoluble or soluble P_i no or not significant

amounts of growing fluorescence signal is detectable (Figure 4.6, Panel A and B). These results corroborate that PP_i can only be formed in the presence of soluble and insoluble P_i. [4,100,103] and experimentally in Figure 4.6 confirmed. Due to electrostatic repulsion of negatively charged AcP and P_i in the reaction mixture it seems to be necessary to add a compound to connect the reactants by bridging them (Figure 4.3). The results from Figure 4.6 were reproduced in several experiments.

Nevertheless, an alternative assay was used to confirm the observations and conclusions from Figure 4.6 to get higher reliability for the interpretation of the results. The PP_i formation in the reaction was monitored with a bioluminescence assay for the detection of PP_i [104], which consists of two coupled enzymatic reactions. In the first reaction PP_i reacts with AMP under energy consumption to ATP, which again hydrolyses to PP_i and AMP in a second reaction. To the hydrolysis of ATP the luciferin/luciferase oxidation is linked, which caused the emission of light. The produced light is directly proportional to the amount of PP_i present in the sample and shows linearity between 0.02-10 µM PP_i concentrations, which was confirmed in reference measurements (Figure 4.7). The ordinate in Figure 4.7 indicates the luminescence intensity in relative light units (RLUs) of PP_i -reference concentrations from 0.02-10 µM PP_i. The light output is detected by a luminometer, which measures electrical current and read arbitrary light units, usually referred as RLUs. [105]

The reference curves from Figure 4.7 demonstrated that present P_i in the reaction samples inhibits the luminescence of PP_i in the sample.

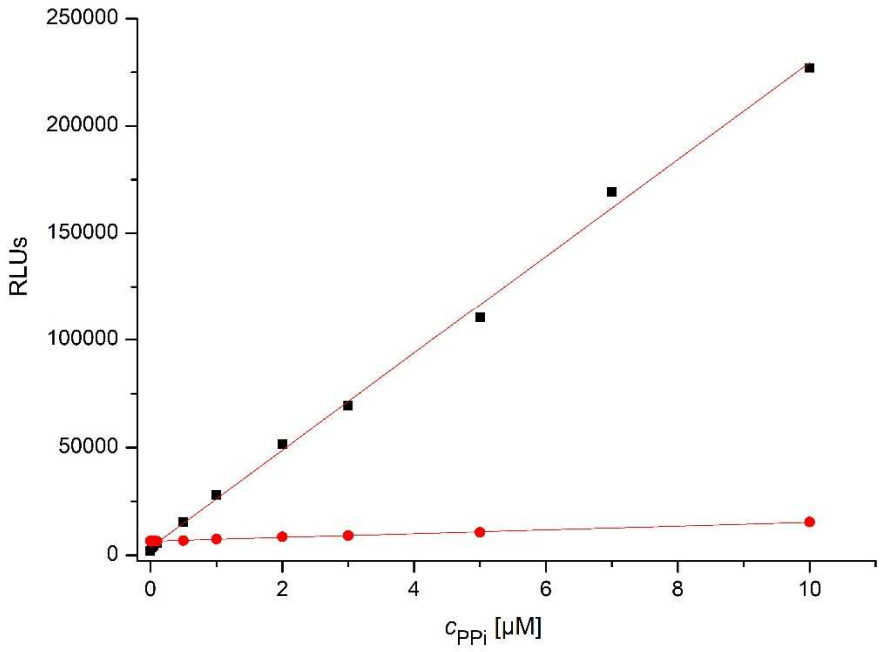

Figure 4.7 Reference curves from a mixture containing 100 mM P_i and PP_i in varying concentrations between 0.02-10 µM (red circles) and only PP_i samples (black squares).

Therefore, attempts for separation of P_i / PP_i containing samples with HPLC at strong anion exchange column (SAX) were performed. P_i is at maximum 3-fold negatively charged and was expected to eluate faster than at maximum four-fold negatively charged PP_i (Figure 2.10). Since PP_i and P_i have no chromophores, no signal in the chromatogram is detectable. However, purification attempts on HPLC were carried out with assistance of reference chromatograms of the nucleotides AMP, ADP, ATP and Adenosine on strong anion exchange column (4.8). The retention time of P_i and PP_i could be then estimated from the retention times of the equally charged nucleotides.

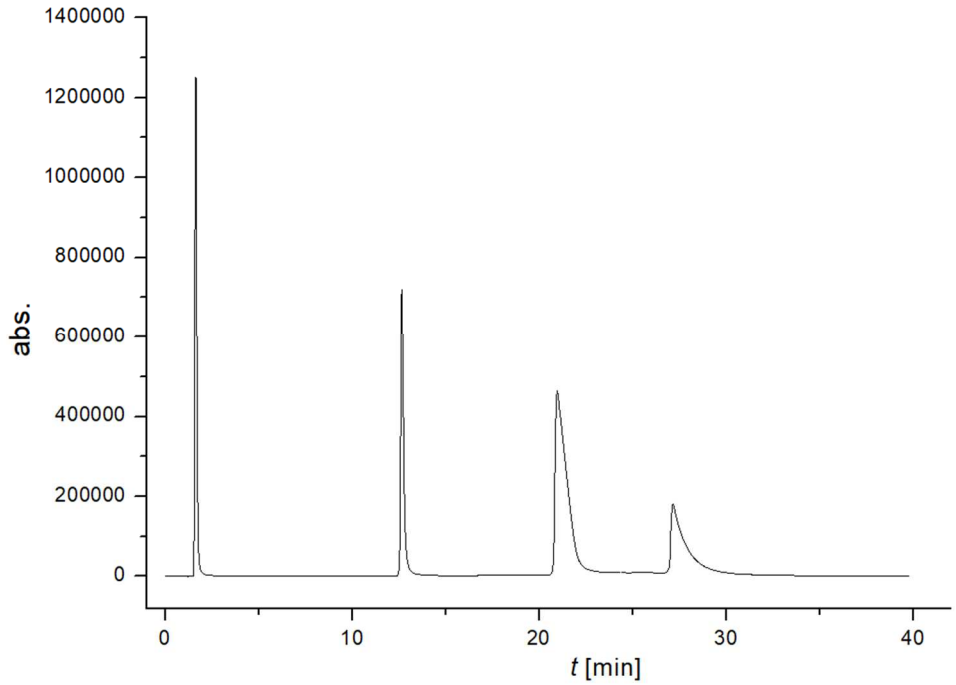

Figure 4.8 Chromatogram of each 5 mM Adenosine t_R = 2 min, AMP t_R = 12 min, ADP t_R = 21 min and ATP t_R = 27 min on SAX column (Dionex PA-200 anion exchange 250 x 4.0 mm) and detected at λ = 254 nm and 260 nm. Flow rate 1 mL/min and gradient 5 → 70 % B (100 mM (Na^+/NH_4^+) Acetate, pH 8). With increasing charge of the compounds, the interaction with the solid phase of the SAX column is stronger and leads to higher retention times.

In Figure 4.8 was observed that the compounds adenosine, AMP, ADP and ATP are sequentially eluted according to the charge. Uncharged adenosine did not interact with the solid phase and eluted after 2 min from column. Two-fold charged AMP interacts with the SAX column and eluted therefore after t_R = 12 min. Very strong interactions with the solid phase of the column are noticeable at three-fold charged ADP with t_R = 21 min and four-fold charged ATP with t_R = 27 min. As PP_i is equally charged to ATP and P_i to ADP it was expected that both eluate in the retention time areas of ATP or ADP respectively. After SAX chromatography of a test mixture (100 mM P_i/10 mM PP_i) the collected aliquots were screened whether the separation from P_i and PP_i succeeded. This was determined by adding $CaCl_2$ solution (1 M) to the fractions to precipitate insoluble calcium phosphate in the PP_i containing aliquots. However, it did not work out to yield significant amount of separated PP_i for a meaningful quantification.

The main reason for the failure of the P_i / PP_i separation with SAX chromatography was the absence of a signal in the chromatogram and therefore the fractions were collected blind. Furthermore, the interactions of four-fold charged PP_i with the solid phase of the column were possibly too strong and PP_i eluted over a larger timescale or did not elute completely from column at all. Since high concentrated PP_i (10 mM) in the test mixture could not be separated and quantified by HPLC, it would not make sense to try the SAX purification with reaction sample, in which the PP_i concentration is expected far below 10 mM.

Further approaches to separate P_i from PP_i *via* strong anion exchange chromatography on MonoQ column (HiTrap® Q Fast Flow, *Sigma Aldrich*, bed size 16 mm × 25 mm) based on a robust, 6% highly cross-linked beaded agarose matrix with good flow properties and high loading capacities, were successful and contributed to a robust qualitative interpretation of PP_i in the reaction samples.

The purification was performed first for a test mixture of 100 mM P_i / 2 mM PP_i and afterwards for a crude reaction sample. Each sample (5 mL) was 10-fold diluted with 10 mM TRIS (pH 8) and applied on anion-exchange MonoQ column. The compounds were eluted sequentially according to Figure 4.11 with increasing concentrations of NaCl solution (0.04-1 M). ^{31}P-NMR analysis was used to detect P_i and PP_i in the eluted fractions. For the test mixture 100 mM P_i/2 mM PP_i a satisfactory separation of Pi and PPi was achieved (Figure 4.10). The signals at ~2.5 ppm was attributed to P_i and for at -6.7 ppm to PP_i. The ^{31}P-NMR spectra from the fractions demonstrated that only in two fractions both P_i and PP_i were present (Figure 4.10). The remaining fractions contain only one compound.

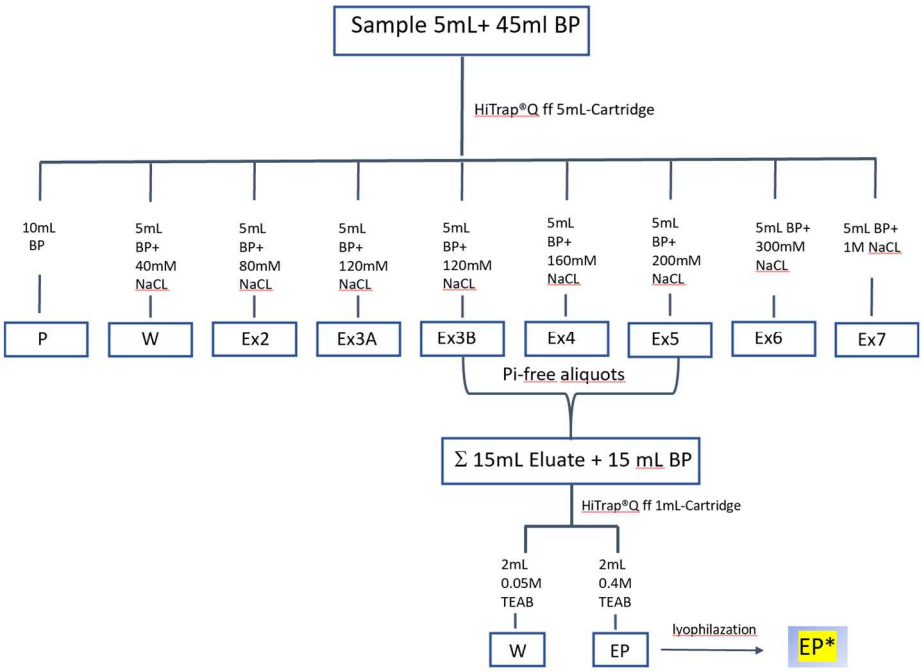

Figure 4.9 P_i -free sample preparation on strong anion exchange column (HiTrap® Q Fast Flow, 5 mL). 5 mL of a crude reaction sample was diluted with 45 mL basis-buffer *BP* (10mM TRIS/HCl, pH 8). The sample was eluted with increasing NaCl-concentrations and collected aliquots were analysed with ^{31}P-NMR. The P_i -free fractions were merged, diluted with *BP* and applied again on a smaller strong anion exchange column (HiTrap® Q Fast Flow, 1 mL). The sample was eluted with 0.4 M triethyl ammonia bicarbonate buffer (TEAB) and lyophilized multiple times to obtain the eluted product (EP*).

Since the results from the test mixture were very promising, attempts to separate Pi and PPi in the reaction sample with the described procedure (4.9) on anion-exchange MonoQ column were carried out. It was obtained that the elution of the Pi-containg fractions was comparable to the results from the test mixture, but a PPi signal was not detected in any fraction. This was not surprising, concentrations up to 1 mM are needed to detect ^{31}P-NMR signals in the spectra.

However, the results from the fractions of the test mixture (Figure 4.10) were attributed to the reaction samples. Therefore, P_i -free fractions were merged, eluted once more from strong anion exchange column with the volatile triethyl ammonium bicarbonate buffer (TEAB) and lyophilized multiple times. Thereafter, lyophilized samples were analysed by PP_i -specific bioluminescence assay (see Experimental Section). The results are shown in Figure 4.11.

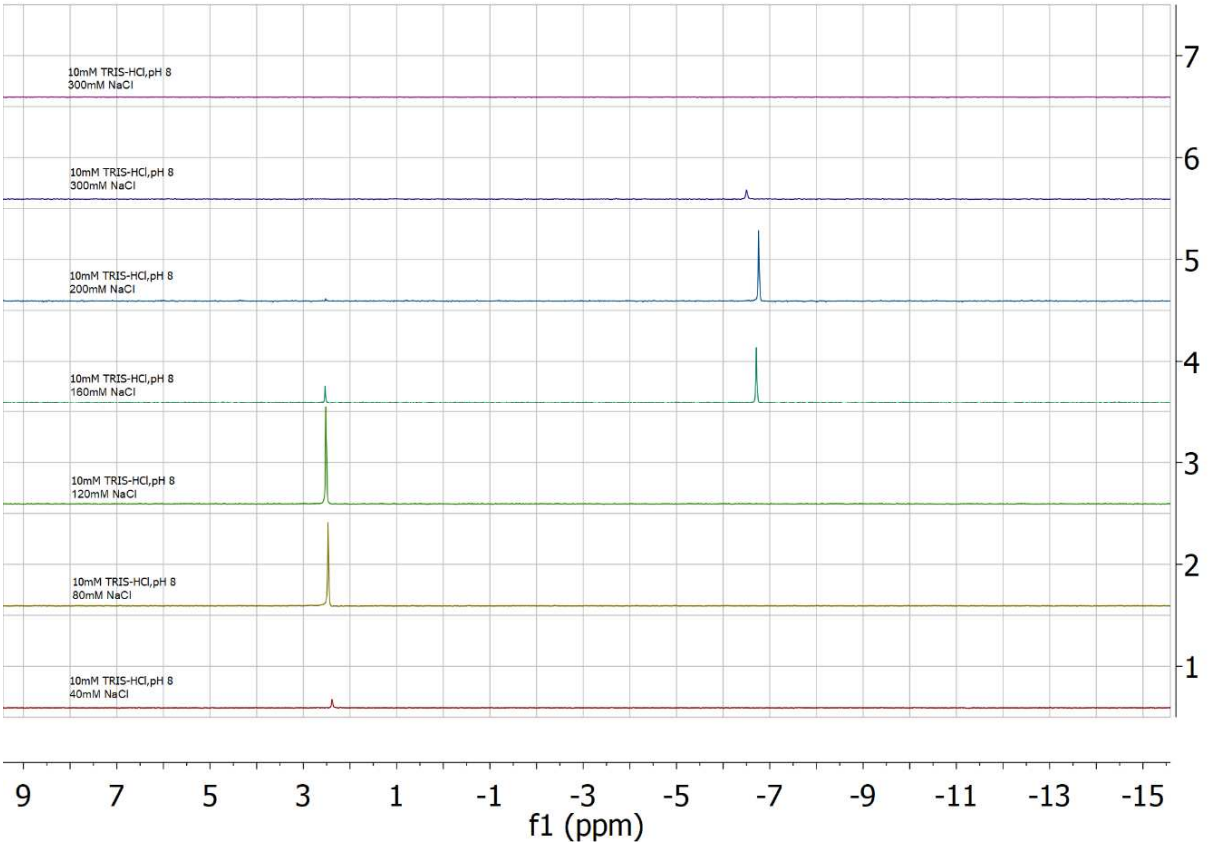

Figure 4.10 P_i (100 mM) and PP_i (2 mM) Reference mixture separation on anion exchange column (HiTrap® Q Fast Flow). The P_i signal is located at 2.5 ppm and the PP_i signal at -6.7 ppm. Except a mix fraction after the elution with 10 mM TRIS-HCl, pH 8 and 160 mM NaCl, in sample present P_i and PP_i are almost separated.

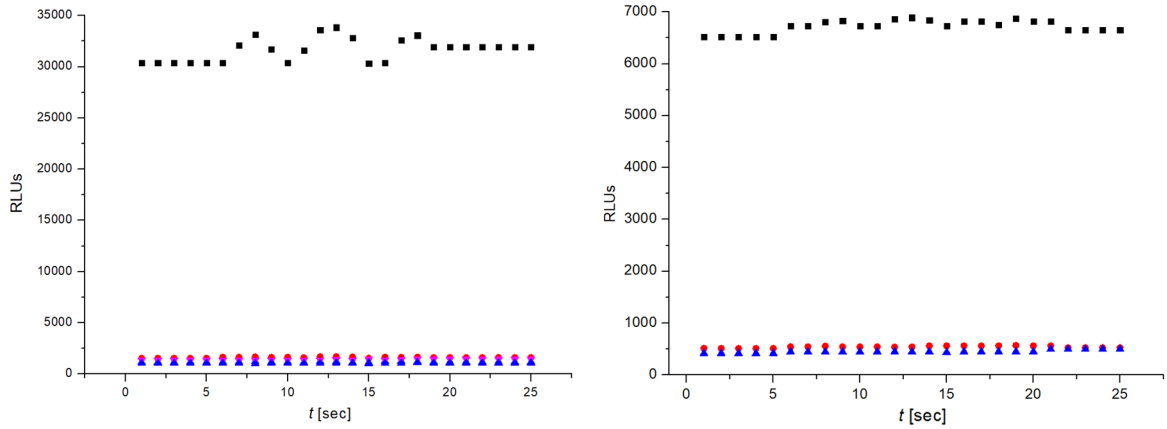

Figure 4.11 Luminescence measurements of lyophilized "P_i -free" (left) and crude reaction samples. Data points were measured in 1 s intervals over 25 s time period in *Area scan* mode (5x5). Black squares: Both soluble $NaHPO_4$ and insoluble $Ca_3(PO_4)_2$ present in the reaction mixture. Samples with only $NaHPO_4$ (red circles) or $Ca_3(PO_4)_2$ (blue triangles) present in the reaction mixture.

The illustrated results in Figure 4.11 show luminescence measurements of crude reaction sample and of lyophilized "Pi-free" sample purified by anion-exchange chromatography (Figure 4.11, left). It was noticed that the reaction mixture containing only soluble (red circles) or insoluble P_i (blue squares) shows no significant luminescence signal and thus were comparable with the obtained results from the fluorescence spectra (Figure 4.6, A and B). However, the reaction mixture containing both soluble and insoluble P_i, yield significant luminescence signal caused by formed PP_i. These results from the bioluminescence assay agree with those from the fluorescent measurements (Figure 4.6).

Although, the bioluminescence assay is more sensitive to small amounts of PP_i than fluorescent PP_i -sensor, it was not possible to quantify formed PP_i in the reaction mixture. Reasons could be that synthesized PP_i, which is anyway formed in low yields is further reduced by the several chromatography steps (Figure 4.9), although impeding P_i was separated. Luminescence measurements of the crude reaction samples show even less RLUs compared to the "P_i -free" samples, because of present P_i, which impede the luminescence of PP_i.

From the obtained measurements can be concluded that the results from the bioluminescence assay (Figure 4.11) indicated PP_i formation in the reaction mixture containing

soluble and insoluble P_i (Figure 4.11, black squares) and goes along with the results obtained by fluorescent PP_i -sensor (Figure 4.6, Panel C and D).

The PP_i -formation experiment can be understood as bridge between the findings from HUBER and WÄCHTERSHÄUSER to synthesize on the one hand prebiotically plausible an activated catalyst-bound acetyl group, which is able to acetylate compounds such as P_i to AcP and on the other hand with the results from WEBER and VIEYRA, who have shown that AcP and P_i react to PP_i. [3,8,103] This occur in a coherent chain of reactions with the result of a plausible procedure for PP_i condensation in hydrothermal fluids.

4.2 The Nature of the Active Species

In the fluorescence measurements (chapter 4.1, Figure 4.6, Panel D) was noticed that the PP_i synthesis is not constant during 8 h reaction time. Therefore, the original C/C-bond formation reaction was performed to observe product formation in a reaction time of 12 h. The approach was monitoring the kinetics of N-acetylaniline formation as product from catalyst bound acetyl group and in reaction present aniline. From the kinetic studies it was expected to draw conclusions about the catalytic activity in the reaction.

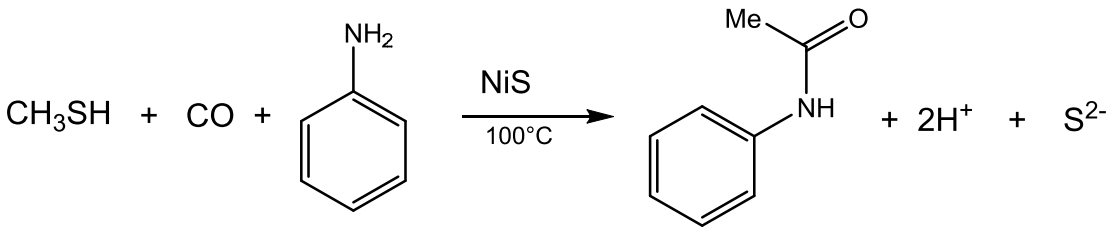

Scheme 4.3 Reaction scheme of N-acetylaniline formation from aniline and CH_3SH under CO atmosphere on NiS in aqueous suspesion at 100°C reaction temperature.

Aniline and N-acetylaniline have no prebiotic meaning and are just used as proxy for the synthesized acetic acid and methyl thioester, which were in very low yield present and therefore hardly to detect and quantified at all. But with present aniline as nucleophile in the

reaction mixture N-acetylaniline (Figure 4.1. IV) is synthesized and easily detected by HPLC due to an existing chromophor group (Scheme 4.3). The formation of N-acetylaniline requires the preliminary stage of activated catalyst-bound acetyl group (Figure 4.1, I) and is therefore an indirect proof for its existence.

4.2.1 Analytical Tools

Preliminary experiments were carried out to find an appropriate internal standard for quantitation of the formed N-acetylaniline and to ensure that the product is not concentrated due to evaporation at 100°C reaction temperature. The demands for the internal standard are stability under reaction conditions, significant but not too high affinity to the HPLC *reversed phase* (rp) and a high UV-absorption in the wavelength range, where the product is detected. Adenosine and tyrosine were chosen as possible internal standards, since they have an absorption maximum in the range of the product N-acetylaniline (Tab. 4.1.). Towards hydrolytic stability experiments at various reaction times from 0-64 h and constant pH 8, it has been found that adenosine was a suitable internal standard (Figure 4.12).

Tab.4.1. Absorption maxima of the incubated samples adenosine, tyrosine and N-acetylaniline.

Compound	**Absorption maximum** [106] λ_{max} **[nm]**
Adenosine	260
Aniline/Tyrosine	280
N-acetylaniline	240-250

In Figure 4.12 (C) was indicated, that the product N-acetylaniline and adenosine are hydrolytically stable at long term incubations experiments (Figure 4.12., C, blue squares) at 100°C. From this it can be concluded that adenosine is stable under reaction conditions and can be used as internal standard in the reaction.

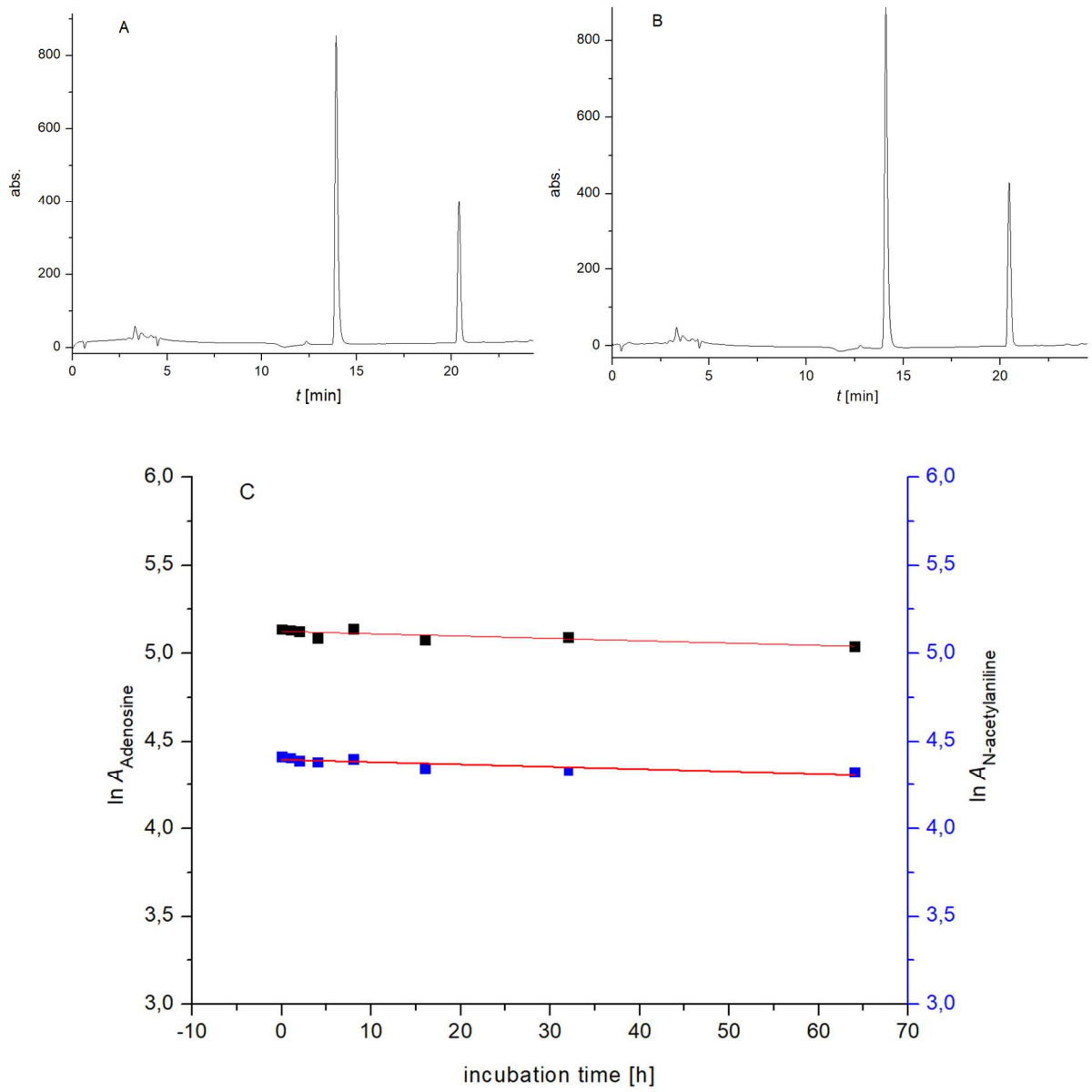

Figure 4.12 HPLC-Traces of adenosine and N-acetylaniline mixture at 100 °C after 0 h (A) and after 64 h (B). HPLC conditions: A: 0.1 M ammonium acetate, B: acetonitrile (MeCN), grad: 0 → 80 % B in 25 min on C18-column (MN Nucleodur®100 5, 250 x 4.6 mm, 5 µm), λ = 254 nm. C) Integrated peaks for adenosine (internal standard, black squares) and N-acetylaniline (product, blue squares) at each incubation time from 0 to 65 h.

Next was to determine suitable conditions for the HPLC analysis of the reaction mixture, containing the relevant compounds aniline, adenosine and N-acetylaniline. Therefore,

individual, and co-injected reference chromatograms (Figure 4.13) were measured to analyse the signals and retention times (t_R) of these compounds.

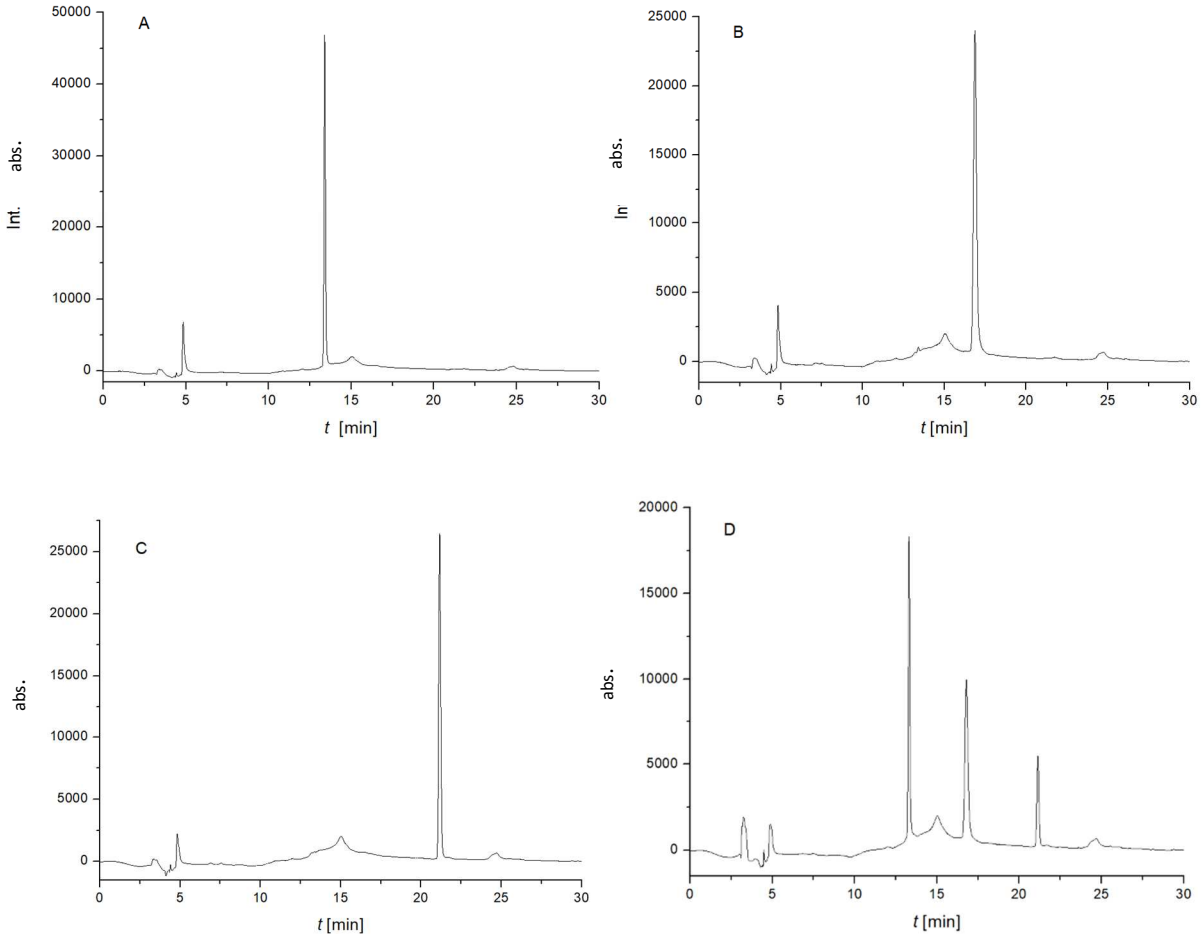

Figure 4.13 HPLC chromatograms of reference samples of adenosine (A), aniline (B), N-acetylaniline (C) and a co-injection of all three compounds (D). HPLC conditions were A: 0.05 M Trietyl ammonium citrate buffer (TEAC, pH 4.5), B: MeCN, gradient: 5 → 60% B in 25 min. on a C18-column (MN Nucleodur®100 5, 250 x 4.6 mm, 5 µm) λ = 254 nm.

To avoid overlapping signals of aniline and N-acetylaniline, it was necessary to protonate the amino group of aniline to reach faster elution than N-acetylaniline from column. Therefore a 0.05 M triethyl ammonia citrate buffer (TEAC, pH 4.5) was prepared as elution solvent, which was acidic enough to protonate the amino group of the aniline, but not too acidic to hydrolyse the adenosine's N-glycosidic bond. Adenosine eluted after t_R = 13.5 min, aniline after

t_R = 16.9 min and N-acetylaniline after 21.2 min from column (Figure 4.13). Thus, the preliminary experiments for the prebiotic reaction were finished and the kinetical experiments were described in the following.

4.2.2 Kinetical studies

The scale (Tab.2) of the prebiotic reaction was calculated and carried out as described in experimental section. Insoluble nickel sulfide (NiS) was precipitate from nickel sulfate ($NiSO_4 \cdot 6\ H_2O$) and disodium sulfide ($Na_2S \cdot 9\ H_2O$). The CO-atmosphere was created by passing CO-gas through the suspension. For the purpose of binding liberated protons to keep the pH constant during the reaction progress calcium carbonate ($CaCO_3$) was added (Scheme 4.3). Adenosine, aniline and methanethiol (CH_3SH) were added to the suspension and the reaction mixture was heated up

Tab.4.2. Reaction scale for kinetical studies of the prebiotic reaction.

#	compound	m [mg]	n [mmol]
1	$NiSO_4 \cdot 6\ H_2O$	786	3
2	$Na_2S \cdot 9\ H_2O$	600	2.5
3	Aniline	0.05	0.5
4	Adenosine	53	0.2
5	$CaCO_3$	150	1.5
6	25 mM TRIS · HCl buffer, pH 8		
	Total reaction volume		30 mL

to 100°C. Aliquots (1 mL) were taken hourly from the suspension, filtered, cooled down to room temperature (rt) and analysed by analytical HPLC to detect in reaction formed N-acetylaniline during the reaction time (Figure 4.14).

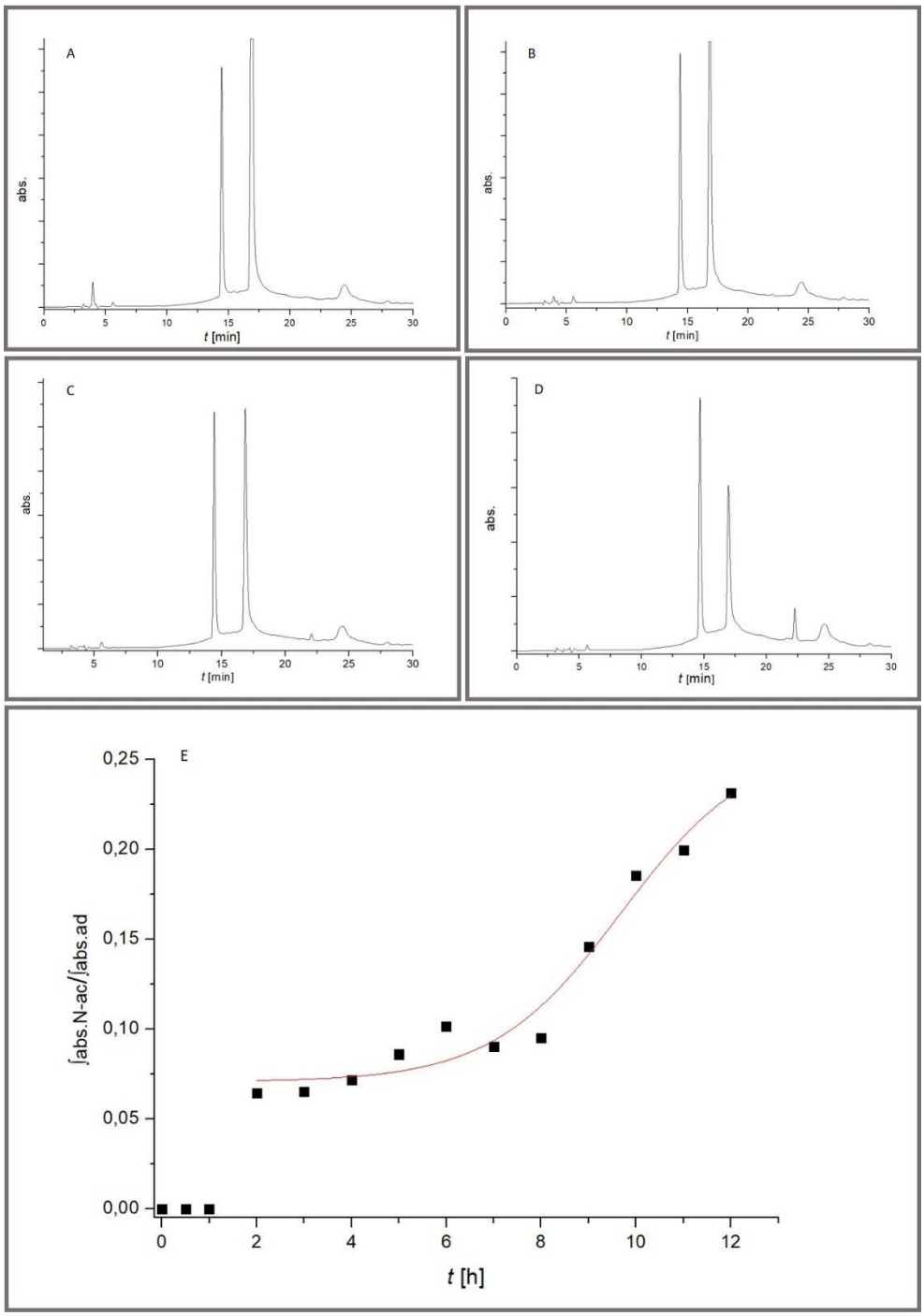

Figure 4.14 Aliquots after 0.5 (A), 3 (B), 6 (C) and 12 hours (D) from reaction mixture were analyzed by HPLC to detect N-acetylaniline formation from aniline, CO and methanethiol at detection wavelength of 254 nm. Adenosine was the internal standard for quantitation. In panel E the absorbance of integrated N-acetylaniline signal relative to integrated adenosine signal was plotted against time.

In the demonstrated time courses of N-acetylaniline formation (Figure 4.14, A-D) the signals at t_R = 13.8 min can be attributed to adenosine and the t_R = 14.4 min to aniline. During ongoing reaction progress a new peak arises with an t_R = 22.1 min (Figure 4.14, B-D). This peak was further analysed with mass spectrometry to confirm formed N-acetylaniline in the reaction. The time course of the reaction progress (Figure 4.14, E) illustrated the absorbance integral of N-acetylaniline relative to the absorbance integral of the internal standard adenosine against the time and shows the amount of formed product in 12 hours reaction time. The results between 0 to 6 hours can be interpretated as lag phase, in which no significant amount of N-acetylaniline is formed. After 8 hours reaction progress an exponential increase of product formation can be observed (Figure 4.14, E).

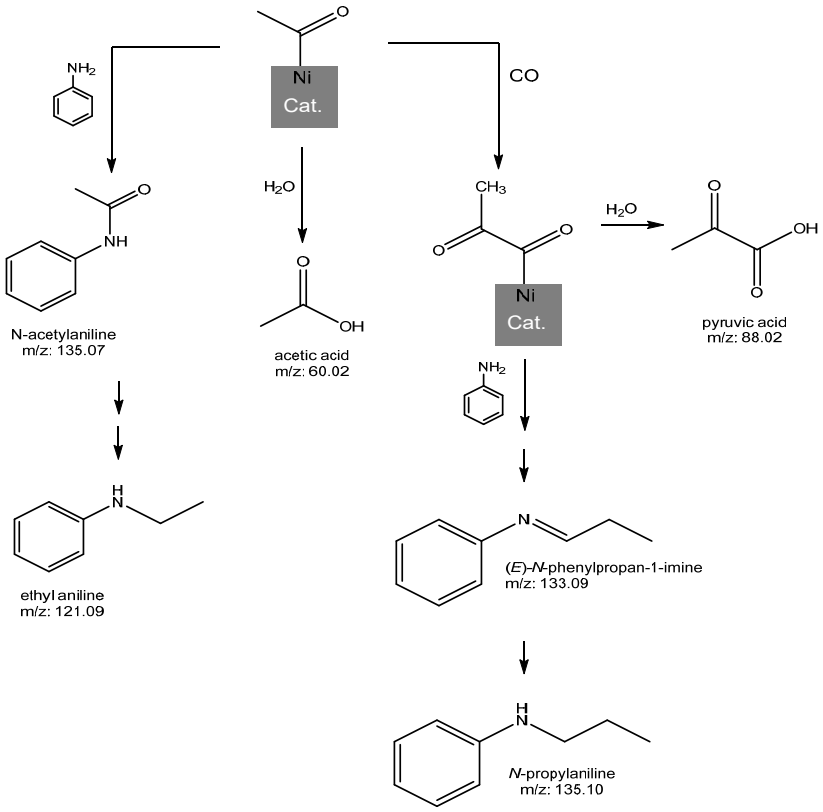

Figure 4.15 Structures of possible side products in the prebiotic reaction next to N-acetylaniline, which can be synthesized starting from aniline. Signals in the ESI-MS indicated the formation of ethyl aniline and N-propylaniline. The formation of biochemical important pyruvic acid under reaction conditions could be possible.

However, it was also noticed in Figure 4.14 that the aniline concentration decreased faster than N-acetylaniline was formed. An explanation for that could be possibly formed side products in the prebiotic reaction next to N-acetylaniline (Figure 4.15). Some proposed structures have been derived from signals in performed ESI-MS such as ethyl aniline or N-propylaniline. Another side product would also be conceivable under reaction conditions like pyruvic acid, which is an important compound in biochemistry.

Attempts to understand the kinetics of the C/C-bond forming prebiotic reaction were initially promising, but with the noticed aniline-leak the interpretation gets more complicated. It cannot be assumed that N-acetylaniline is under reaction conditions stable enough to accumulate in the reaction medium and therefore no clear conclusions about the active catalyst can be drawn.

4.2.3 Nickel mobilization

Even though the kinetical studies did not provide to the expected understanding of the catalyst forming process, a lag-phase between ca. 0-6 h in the time course (Figure 4.14, E) was noticed.

This finding lead to the hypothesis that freshly precipitated NiS may not be the active catalyst of the prebiotic reaction as assumed from the authors HUBER and WÄCHTERSHÄUSER [8]. From the time course it could be considered that NiS undergoes some slow chemical conversions (lag phase) in the presence of the reaction components carbon monoxide (CO) and methanethiol (CH_3SH) to form the active species. As soon as a steady state concentration of the active species would be reached fast catalysis leads to exponential N-acetylaniline formation (Figure 4.14, E).

The nature of the active species is of great interest and would contribute to a better understanding of the prebiotic reaction. As possible alternative to the hypothetical mechanism from HUBER and WÄCHTERSHÄUSER (Figure 2.9) an *in situ* reduction of nickel (II) to nanoparticles of elemental nickel (0) with regard of the sulfides and carbon monoxide in the reaction mixture is considered. In this context, a similar experiment was carried out from

HUBER and co-worker, in which Ni-particles embedded in a matrix from coprecipitated $Na(OH)_2$ and $CaSO_4$ were observed after exposure to CO (55 bar, 160 °C).[107]

For the reaction considered here, nanoparticles could subsequently mobilize from the heterogeneous phase to form an active Ni-based species. Under the prevailing reaction conditions and CO-atmosphere, the volatile tetracarbonyl nickel ($Ni(CO)_4$, TB = 43°C) is expected to be formed [108]. $Ni(CO)_4$ catalysts are known from the industrial *Monsanto acetic acid process* by carbonylation of methanol, where nickel-based homogeneous catalysts are used as low-priced alternative to rhodium-complexes. [109]

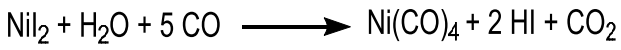

Scheme 4.4 Formation of active $Ni(CO)_4$ from NiI_2 under CO atmosphere in industrial processes. [109] The starting materials and implementation of the reaction are similar to the geochemical redox reaction.[8]

The active catalyst in this industrial acetic acid production is soluble $Ni(CO)_4$ and is synthesized *in situ* at 150°C (Scheme 4.4). The synthesis of the active species is comparable to the conditions in the geochemical redox reaction reaction (CO-atmosphere, 100 °C) and it seems probable that nickel-based complex is formed *in situ* from NiS. [109]

Since the mobilization of Ni(II) is conceivable, it is required to synthesize $Ni(CO)_4$ and investigate the catalytic activity of this compound under prebiotic reaction conditions.

MOND discovered coincidentally $Ni(CO)_4$ as he extracted and purified elemental nickel with carbon monoxide at high temperatures [110]. During the different purification steps the reaction temperatures also varied and at 130°C the present elemental nickel reacted under CO atmosphere to a volatile complex, which was afterwards analysed as $Ni(CO)_4$. MOND described that as soon as the gas phase was enriched with $Ni(CO)_4$, a highly luminous flame was observed at the *Bunsen burner*.

Under consideration of the results from MOND et al., the approach of this part of the project was to mobilize nickel (II) under prebiotic conditions and then to characterize the compound

with the flame test. The first step was to reduce Ni(II) to Ni (0) under reaction conditions to identify the volatile *in situ* formed nickel species as active catalyst. Alternative analysis method for $Ni(CO)_4$ beside the flame test was found in the publication of HIEBER [111] in which he described that reacting $Ni(CO)_4$ with pyridine gives a yellow pyridine tricarbonyl nickel complex (Scheme 4.5).

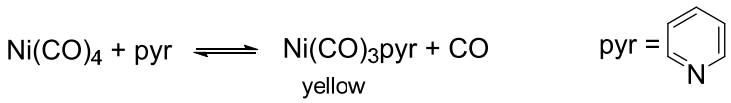

Scheme 4.5 $Ni(CO)_4$ reacts with pyridine to a yellow $Ni(CO)_3pyr$ complex. [111]

Therefore, $NiSO_4 \cdot 6H_2O$ was filled in a combustion boat and transferred to a glass tube (Figure 4.16). CO-stream (1 bar) was passed through the glass tube and heated up to 130°C in a tube furnace. The glass tube was connected to a bubbler filled with pyridine to identify formed volatile $Ni(CO)_4$ by colouring the pyridine solution yellow. [111]

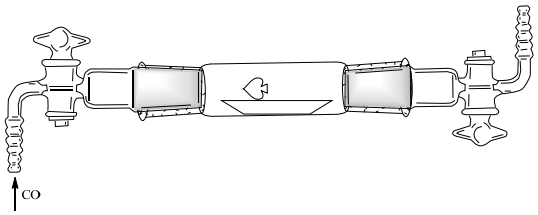

Figure 4.16 Glass tube with $NiSO_4 \cdot 6H_2O$ or elemental Ni (H_2O slurry) filled combustion boat and heated up to 130°C in a tube furnace. CO-gas is passed (1 bar) through the glass tube and afterwards through pyridine containing bubbler.

But neither the pyridine solution coloured yellow, nor the apparatus passed gas-exhaust showed a highly luminous flame in the burner. It seemed that CO is not reductive enough to reduce Ni(II) compounds to Ni(0) particles and to mobilize them to $Ni(CO)_4$. Therefore, $NiSO_4 \cdot 6H_2O$ was replaced by Ni (0) powder to skip the reduction process of Ni(II) with CO and the experiment was repeated. But also, in this attempt $Ni(CO)_4$ could not be qualitatively detected neither as pyridine tricarbonyl nickel, nor in the flame test. The reason for that could be a passivated surface of elemental nickel, which leads to inactivity. In a third reaction

execution elemental nickel powder was replaced by Raney®-Nickel (slurry in H_2O, *Sigma Aldrich*) and the rest of the implementation was retained. This approach led to a positive flame test for $Ni(CO)_4$ after 60 min reaction time (Figure 4.17).

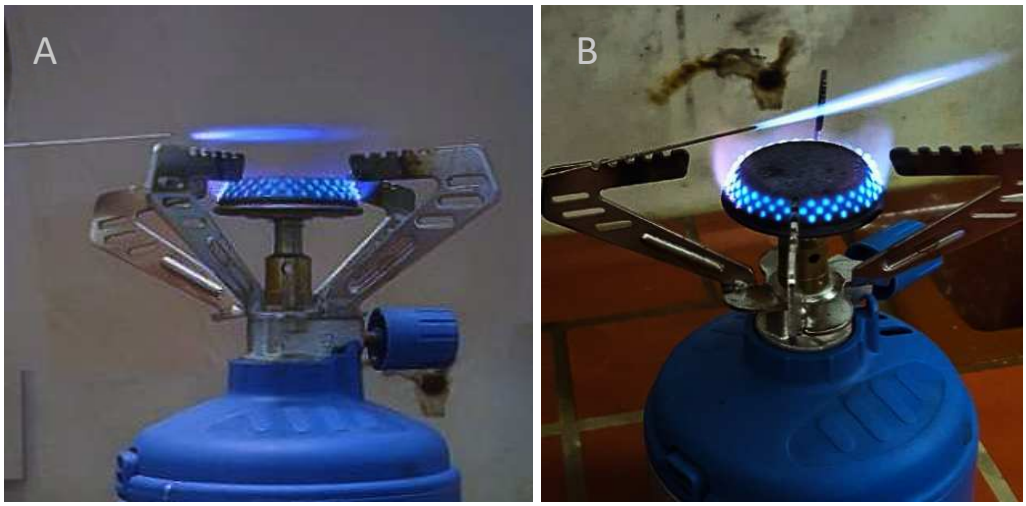

Figure 4.17 CO-stream (1 bar) passed through the glass tube, which is heated up to 130 °C in a tube furnace and the exhaust was led into the burner flame. A: The CO-stream passed into the flame after 5 min reaction time is not luminous. But after 60 min the exhaust was again led into the burner flame and a highly luminous flame could be observed (B).

The colour or luminosity of the burner flame in Panel A did not differ from the flame, when pure CO-stream was led in. During ongoing reaction time, enough nickel particles were mobilized to form volatile $Ni(CO)_4$ (T_B = 43°C), which can accumulate in the CO-gas phase to give the characteristic highly luminous flame illustrated in figure 4.17 (B). However, approaches to detect $Ni(CO)_4$ in the prebiotic reaction with the flame test weren't successful. It must be considered that the flame test is an uncomplicated method to analyse volatile compounds but has difficulties to detect small amounts of compounds and relies on subjective perception. Spectroscopic techniques can be used for a robust compound characterization, which can resolve small amounts much better. Hence, *gasphase-infrared spectroscopy* (G-IR) was chosen to detect *in situ* formed $Ni(CO)_4$ but first in a reaction, which is known to produce significant amounts of $Ni(CO)_4$.[112]

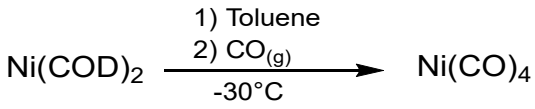

Scheme 4.6 In toluene dissolved $Ni(COD)_2$ reacts immediately to $Ni(CO)_4$ under CO atmosphere.

Therefore, *zero-valent* bis(cyclooctadiene)nickel(0) ($Ni(COD)_2$) was reacted with CO to form $Ni(CO)_4$. After 30 min ongoing reaction the gas phase was collected in a cylindrical vessel and was analysed by gasphase -infrared (G-IR) spectroscopy to observe characteristic IR-bands for $Ni(CO)_4$.

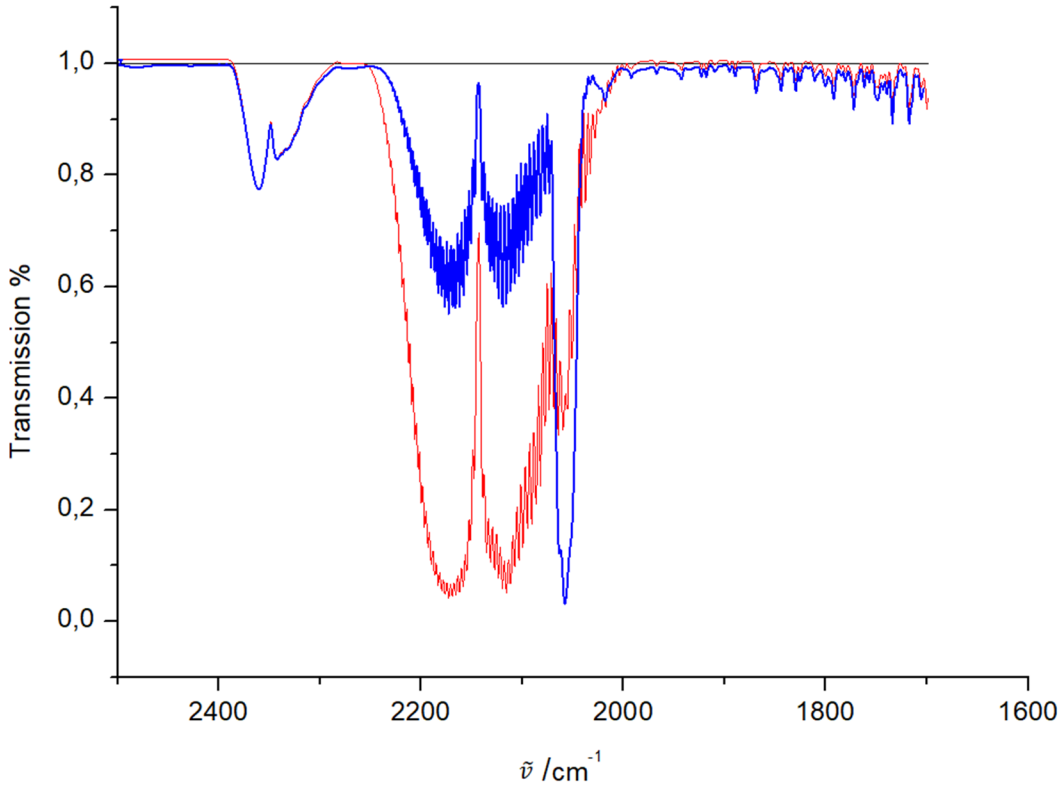

Figure 4.18 Gasphase-IR spectra of gaseous $Ni(CO)_4$ in CO atmosphere (red course) and in N_2 atmosphere (blue course). The fundamental of $Ni(CO)_4$ is obtained at 2059 cm^{-1} in both spectra, but with a stronger band in IR-inactive N_2 atmosphere.

In Figure 4.18 the gasphase-IR spectra from synthesized $Ni(CO)_4$ were measured in CO- and N_2 atmosphere to obtain the fundamental band of $Ni(CO)_4$ at 2059 cm^{-1} in accordance with literature values.[113] The spectrum under CO atmosphere (red course) is dominated by the CO-bands at 2170-2116 cm^{-1} interfering with $Ni(CO)_4$. Therefore, the CO-gas stream in the

reaction mixture was replaced for 5 min by IR-inactive nitrogen (N_2) to yield a stronger $Ni(CO)_4$ band (blue course) by reducing the strong CO-bands. The obtained results about the synthesis and analysis method for $Ni(CO)_4$ can be used for further investigation of the active species in the geochemical redox reaction. As volatile $Ni(CO)_4$ is assumed as probably *in situ* formed active species, an experiment could provide further results about it. In fact, if the reaction vessel, where the active species is synthesized (Scheme 4.7, eq.1) was separated from the reaction vessel, where it should catalysis the reaction (Scheme 4.7, eq.2).

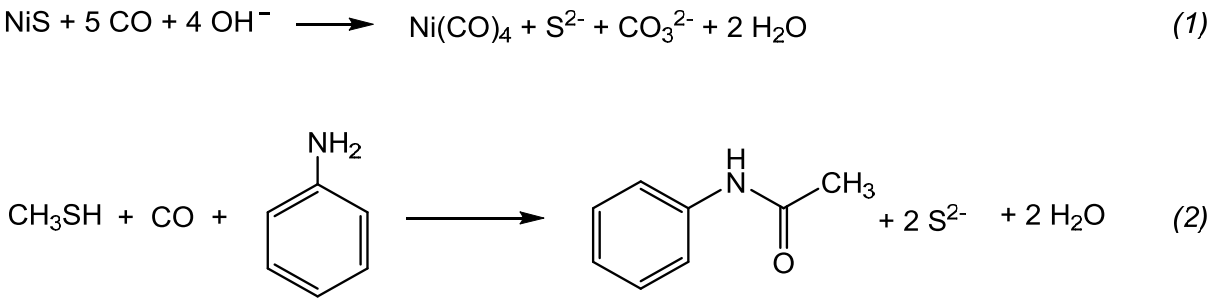

Scheme 4.7 Proposed reaction to $Ni(CO)_4$ in vessel 1 (eq. *1,* Figure 4.19) and subsequent enrichment of $Ni(CO)_4$ in connected vessel 2 (eq. *2*, Figure 4.19) to catalyse the reaction from aniline to N-acetylaniline under CO and CH_3SH atmosphere.

In a modified two-vessels experimental set up of the prebiotic reaction, it was tried to synthesize the assumed volatile catalyst in the high temperature vessel 1, which can then enrich in a connected vessel 2 to catalyse there the formation of N-acetylaniline (Figure 4.19). In vessel 1 nickel could be mobilized from NiS and CO at 70 °C to form $Ni(CO)_4$, which could be the active species of the reaction. As $Ni(CO)_4$ is known to be volatile (T_B = 43°C) it can accumulate in the connected vessel 2. In vessel 2 aniline is present, as well as CH_3SH at room temperature (rt) and if mobilized active species from vessel 1 is the catalyst of the reaction (Figure 4.19), then it would be expected that N-acetylaniline is formed in vessel 2. But neither by HPLC, nor by mass spectrometry N-acetylaniline was detected in the reaction samples. Different temperatures in both vessels were adjusted, but still no N-acetylaniline

could be monitored. The reasons why the experiment did not work out could be that NiS cannot be easily mobilized under the reaction conditions or $Ni(CO)_4$ is not or just an intermediate of the active species.

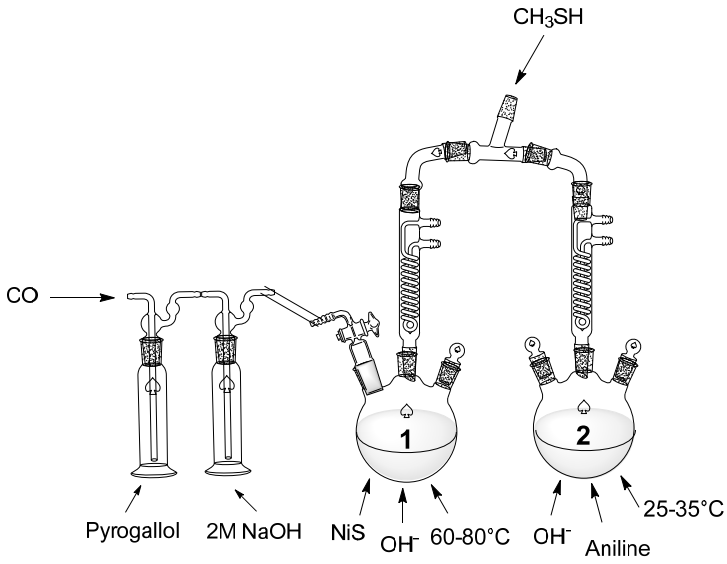

Figure 4.19 Modified two-vessel experimental set up of the prebiotic reaction. CO-stream was purified by initiating through pyrogallol and NaOH solutions. In vessel 1 NiS, OH- at 60-80°C are present and in vessel 2 aniline, OH- at 25-35°C are present. The intention was to separate the place, where the catalyst is formed (vessel 1) and the place, where it catalyses the reaction (vessel 2).

In a second experimental approach the confirmed $Ni(CO)_4$ producing reaction (Scheme 4.6) was carried out [112] in vessel 1 and vessel 2 remains unchanged. However, the detection of N-acetylaniline was still negative, what could mean that $Ni(CO)_4$ is not the active species at least under the described modified experimental conditions (Figure 4.19).

4.3 Hydrolytic Stabilities of PP_i and AcP

For energy storing compounds (“energy currency”), especially compounds that were considered as prebiotic energy currency similar to present ATP, metastability is required. In this regard the energy-bearing bond must be kinetically stable enough in aqueous solution, not hydrolyse too fast, but at the same time to be reactive enough to undergo reactions to

pass the energy to other molecules. In this context AcP [88] and PP_i[1] were considered as plausible energy storing compounds on early Earth. To evaluate, which compound is more stable, the hydrolysis rate was measured under various conditions.

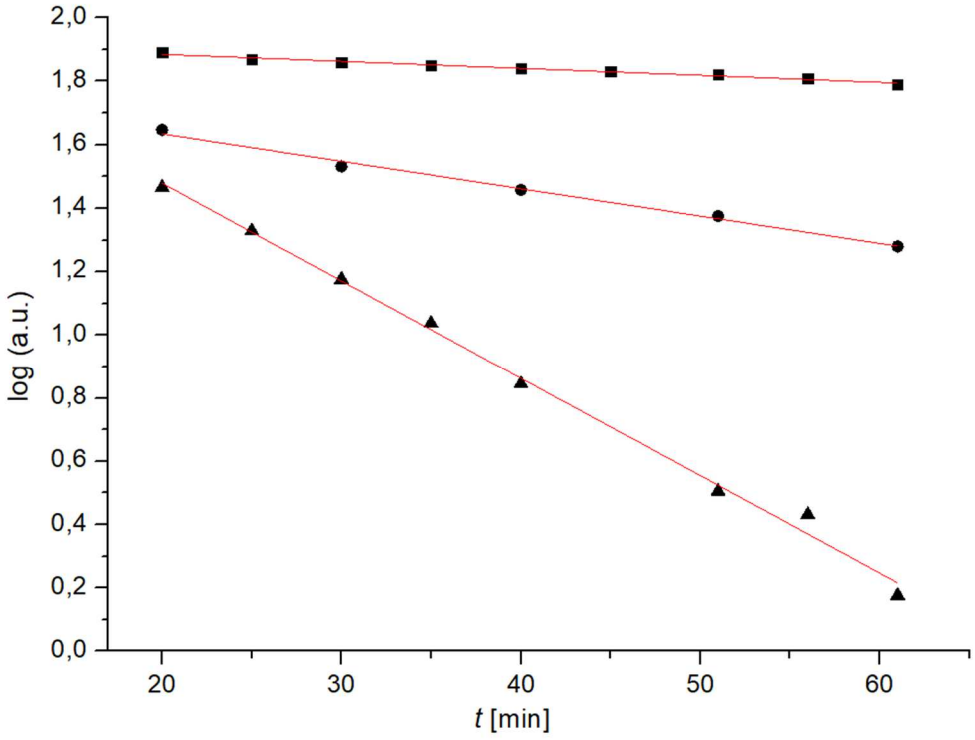

Figure 4.20 AcP hydrolysis kinetics at 40°C (squares), at 50°C (circles) and at 60 °C (triangles). The spectra show the decrease of the ^{31}P-NMR AcP integrated signal over the time. At increasing temperatures, faster hydrolysis of AcP is noticeable.

The hydrolysis kinetics from 20 mM AcP at different temperatures was measured wit ^{31}P-NMR-spectroscopy (Figure 4.20). In 5-10 minute intervals, spectra were recorded for 60 minutes to analyse the decrease of the integrated AcP signal and calculate the half-life-time of AcP at the respective temperature. The spectra show that the reaction follows a pseudo-first order kinetics with half-life-times for AcP at 40 °C of 150 min, for 50 °C of 88 min and for 60 °C of 40 min.

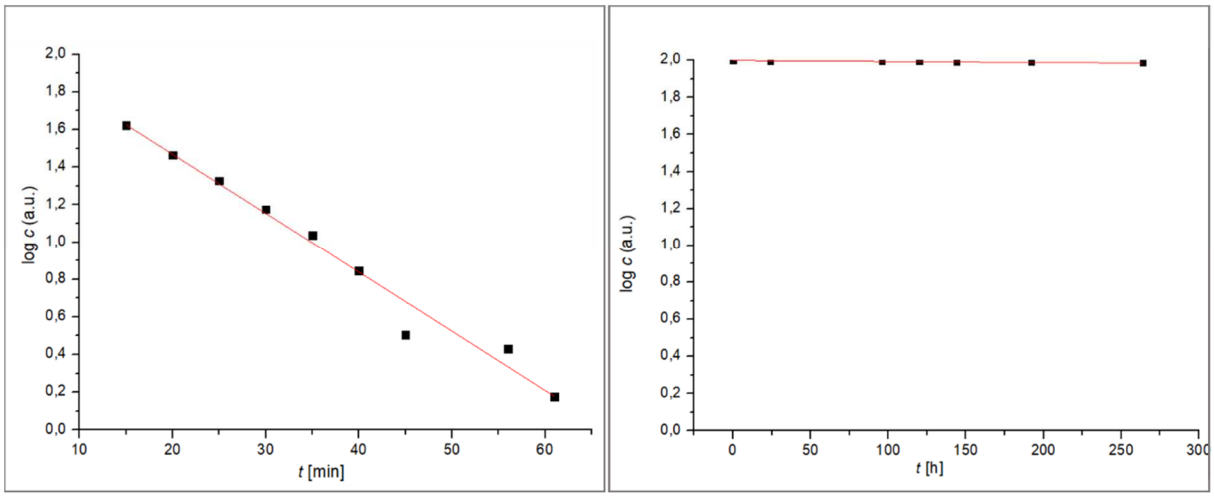

Figure 4.21 Hydrolysis kinetics from AcP (left) and PP_i (right) at 60°C. Both reactions follow pseudo-first order kinetics. The illustration pointed out that PPi is much more stable than AcP.

It can be concluded that AcP is not too labile to hydrolysis but may not stable enough to serve as primordial energy storing molecule. Comparing the hydrolysis rates of AcP and PP_i at 60 °C (Figure 4.21), it is evident that PP_i with a half-life time of 310 days compared to 40 min of AcP is more stable and therefore plausible to be considered as long-term energy storing compound on prebiotic Earth.

4.4 Experiments towards Peptidic Minimal Model of Acetyl coenzyme A Synthase

4.4.1. Ni-Oligo Peptide Complex

The solid emissions from hydrothermal vents of *black smoker* type consists mainly of transition metal sulfides. Among other compounds, CO, H_2S and various intermediates are dissolved in the *fluid*.

The evolution of the acetyl CoA synthase enzyme (ACS, see Wood-Ljundahl Pathway) could have started from inorganic nickel compounds e.g. NiS to reduced $Ni(CO)_4$ and to gradual exchange of the inorganic ligands by peptides. This could have led to a heteroleptic complex,

which could catalyse reactions of CO and thiol to thioester similar to the reaction on the active site of ACS.

The idea is that Ni (II) is selectively mobilized from the sulfides by reduction to Ni (0) and subsequent complexation to $Ni(CO)_4$. The latter is either the catalyst for the C-C-bond linkage of CO and methanethiol or it is the intermediate for the formation of catalytically active, heteroleptic complexes. As soon as small peptides were present in the fluids they could have served as ligands and contributed to complex formation. Such nickel-peptide complexes, which have occupied at least one coordination site with CO are the best candidates for being the earliest evolutionary precursors of the enzyme acetyl-CoA synthase (ACS). ACS, for example, from the anaerobic bacterium *Moorella thermoacetica* [114] is a $\alpha_2\beta_2$ quaternary protein and consists four different metal clusters.[115][116]

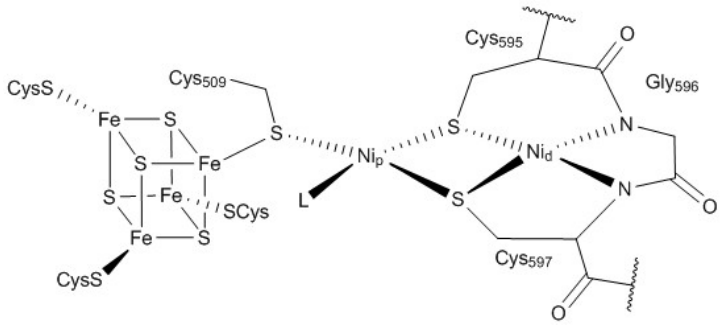

Figure 4.22 A cluster of acetyl coenzyme A synthase (ACS) containing a cuboidal Fe_4S_4 unit, a peptide coordinated distal Ni_d and a proximal metal (M_p), which appears to be Ni_p in the active site.[98]

The A-Cluster is the active site for ACS activity (Figure 4.22) and contains three components, a cuboidal Fe_4S_4 unit, a square planar distal Ni_d coordinated by two peptide amide nitrogens and two side Cysteine chain thiolates and a four coordinated proximal metal site (*M*p). The metal in the central site appears to be nickel in the active enzyme. [62,98]

To form heteroleptic nickel peptide complexes as predecessors of ACS, it is firstly required to synthesize an expedient peptide sequence of *Moorella Thermoacetica.* [117] Therefore, a short peptide sequence 594-598 from the A cluster of *Moorella Thermacetica* was synthesized by manual or automated *Solid Phase Peptide Synthesis* (SPPS, for details see Experimental

Section).[118] The peptide sequence 594-598 contains the amino acids serine (S), cysteine (C), glycine (G), cystein (C) and phenylalanine (F) (Figure 4.23).

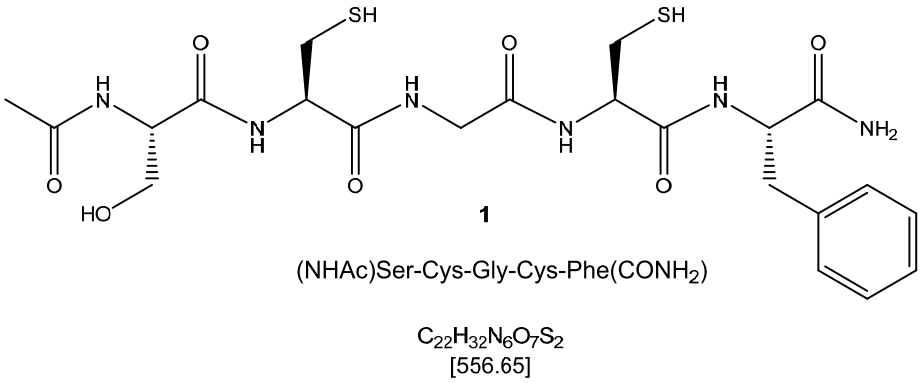

Figure 4.23 Peptide sequence 594-598 from *Moorella Thermoacetica* [62,117], synthesized by *Solid Phase Peptide Synthesis* (SPPS).

The protected amino acids were firstly deprotected with piperidine (20 %) in DMF and then linked activator assisted, sequentially on an insoluble solid phase. Polystyrene based MBHA rink amide was chosen as resin for the synthesis of the peptide **1** (Figure 4.23) due to higher swelling properties and low load density (0.38 mmol/g), which reduces aggregation of the peptide. The activator reagent *N*, *N* diisopropylcarbodiimid (DIC), HATU to impede racemization and DIPEA to reduce precipitation of the reagents were used. All amino acids were coupled twice, in which coupling methods were chosen by the nature of the amino acid and if the coupling process was manually or automated accomplished. The finished peptide sequence still bound on resin was capped with acetanhydride to block residual free amino functionalities. After cleavage from resin with TFA/H_2O/EDT/TIS (94 : 2.5 : 2.5 : 1) the crude peptide (Figure 4.23) was purified *via* HPLC (Figure 4.24) and analysed with ESI-MS to result the pure peptide for nickel complexation.[119]

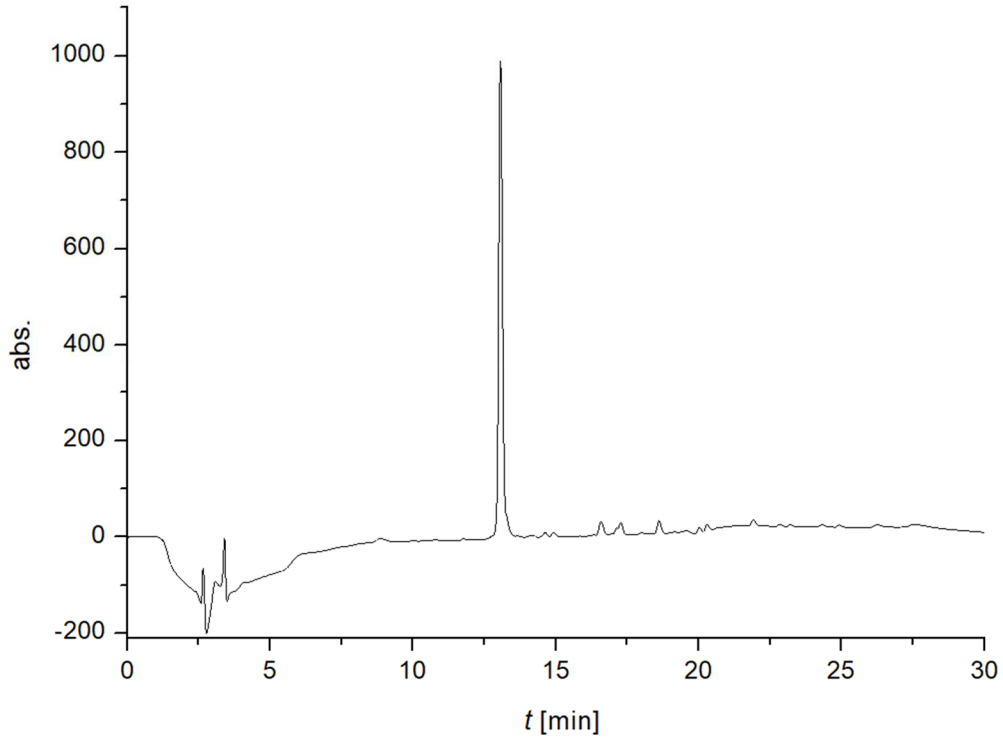

Figure 4.24 Chromatogram of peptide (**1**) with a retention time of 13.1 min after manual SPPS. Eluent A: H_2O + 0.1 % TFA, B: MeOH and the gradient was 5 → 80 % B in 30 min, flow rate: 10 mL/min, column specification: C18, size: 250 x 21 mm. Detection wavelength λ = 215 nm.

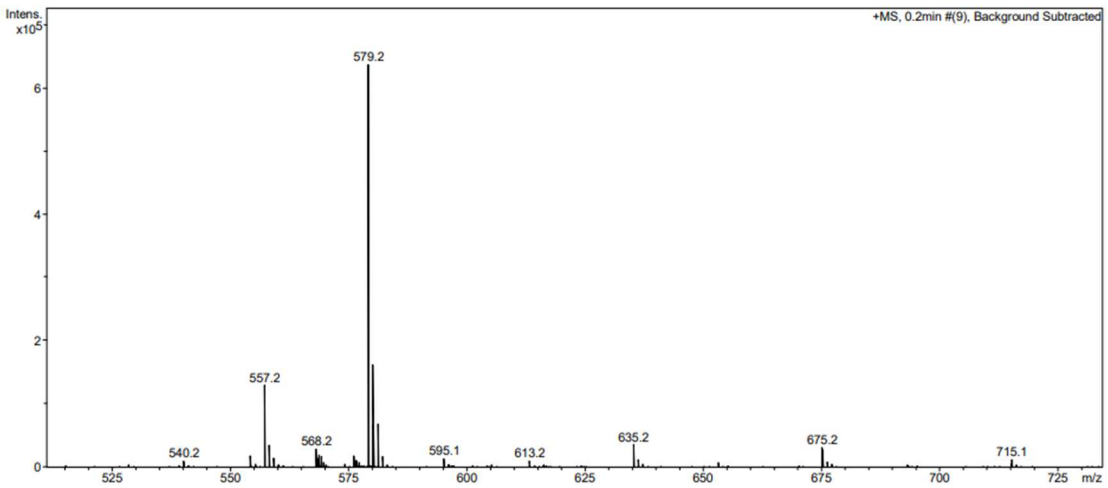

Figure 4.25 ESI-MS of the peptide **1**. The signal for the synthesized peptide **1** as sodium adduct $[M+Na]^+$ was found at 579.2 m/z in the ESI-MS spectrum. The signal for the protonated molecule ion peak of **1** was found at $[M+H]^+$: 557.2 m/z.

The synthesized peptide sequence (Figure 4.32) was dissolved in DMF and reacted with an $Ni(acac)_2$ under alkaline conditions in analogy to experiments of Riordan et al. [98] to form the square planar Ni-center coordinated by two peptide amide nitrogens and two Cysteine side chain thiolates (Scheme 4.8).

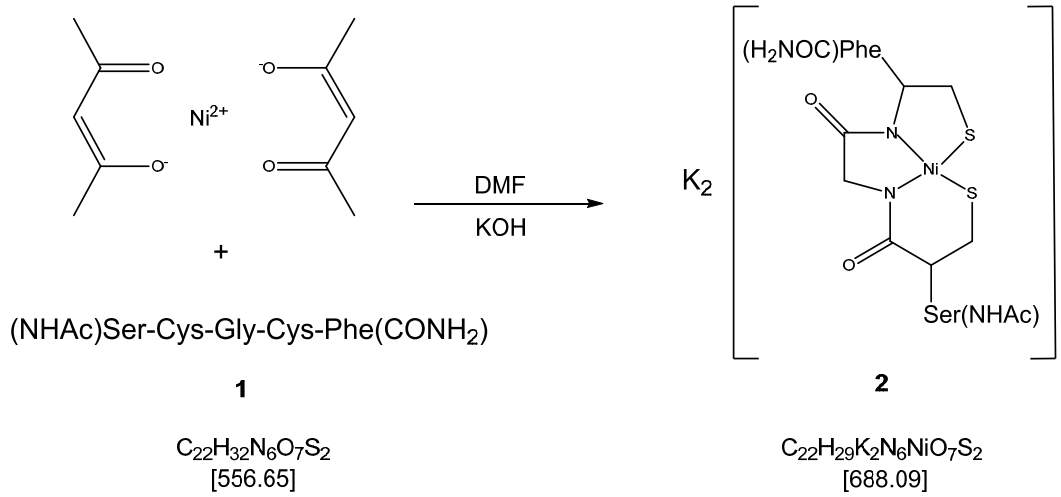

Scheme 4.26 Pentapeptide **1** reacted with $Ni(acac)_2$ to form a square planar Ni-center coordinated by the peptide K_2[Ni(SCGCF)] (**2**).

In presence of molecular oxygen formation of disulfide bridges between the cysteins is very likely, therefore the reaction was carried out under N_2 atmosphere in a glovebox and the product was stored under exclusion of oxygen. The formed complex **2** was confirmed by ESI-MS, HR-MS (Figure 4.26) and also analysed by UV-spectroscopy (Figure 4.27).

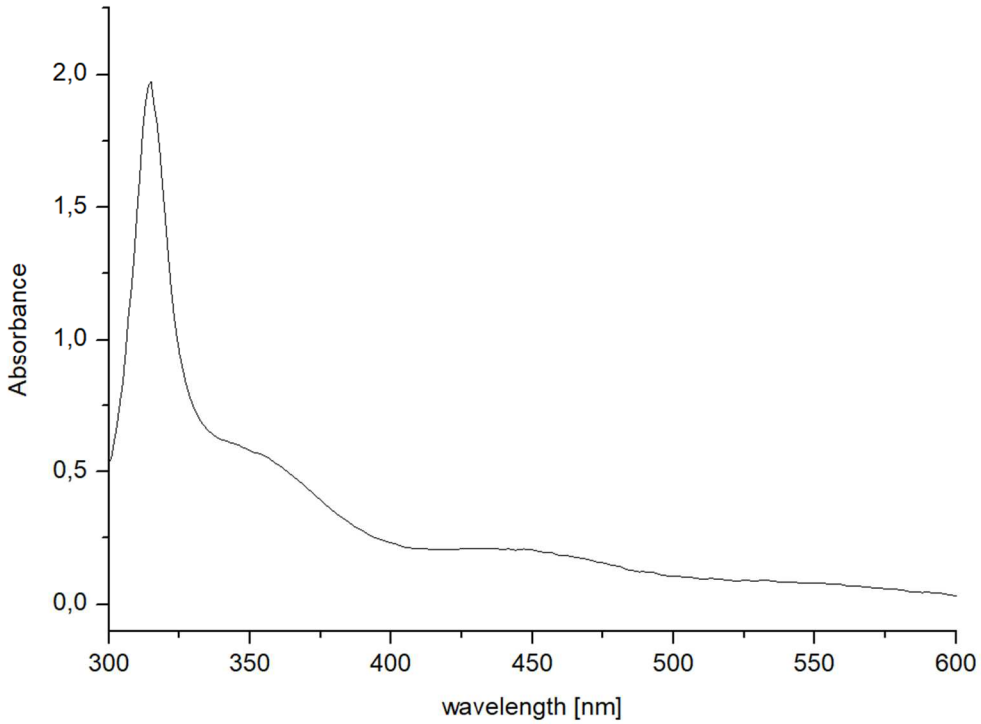

Figure 4.27 UV-spectrum of K_2[Ni(SCGCF)] (**2**) in MeOH with maxima at 450 nm, 350 nm and 320 nm.

The transitions at 450 nm can be assigned to N → Ni attributed to ligand-metal-charge-transfer (LMCT) and the band at 350 nm to S→Ni LMCT. Transitions around 320 nm can be expected for π-π* transitions of aromatic rings and n-π* of C=N groups respectively. d-d transitions at 500-550 nm of the Ni-ion are very weak and indicates square planar geometry around the Ni-center.[120]

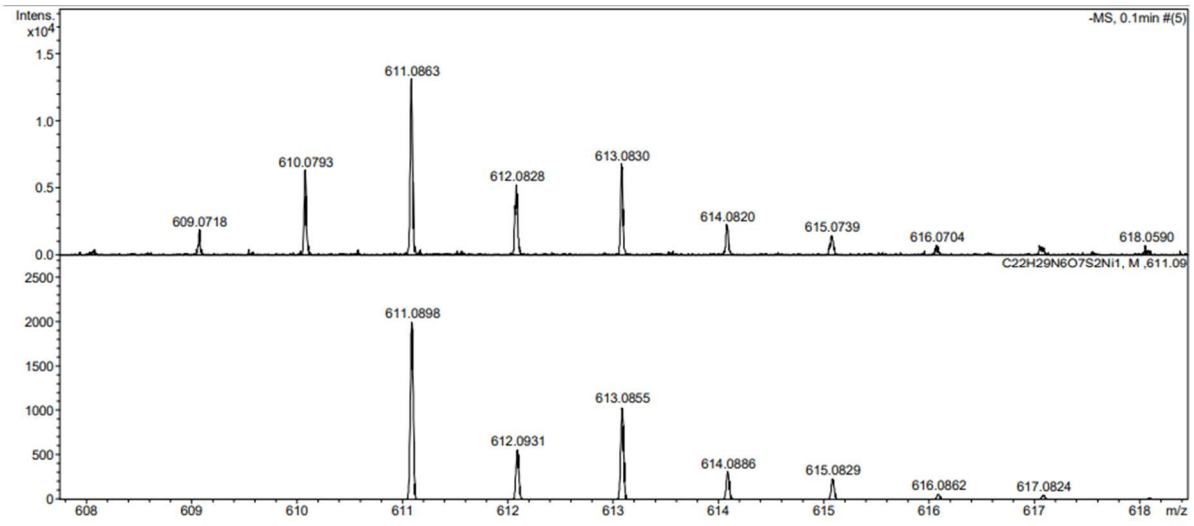

Figure 4.28 Experimental (top) and calculated (bottom) HR-MS-spectra of synthesized nickel peptide complex **2** in DMF. For calculated $C_{22}H_{29}N_6O_7S_2Ni$ [M]: 611.0887 was found m/z: 611.0863 and the isotopic pattern of compound **2**.

Compound **2** was elongated by introducing a second nickel center with 1,2-bis(diphenylbosphino)ethane nickel(II) chloride ($Ni(dppe)Cl_2$) (Figure 4.29). Therefore, to the solution of **2** in DMF the reactant $Ni(dppe)Cl_2$ was added an stirred for 12 h under exclusion of oxygen (Scheme 4.9).

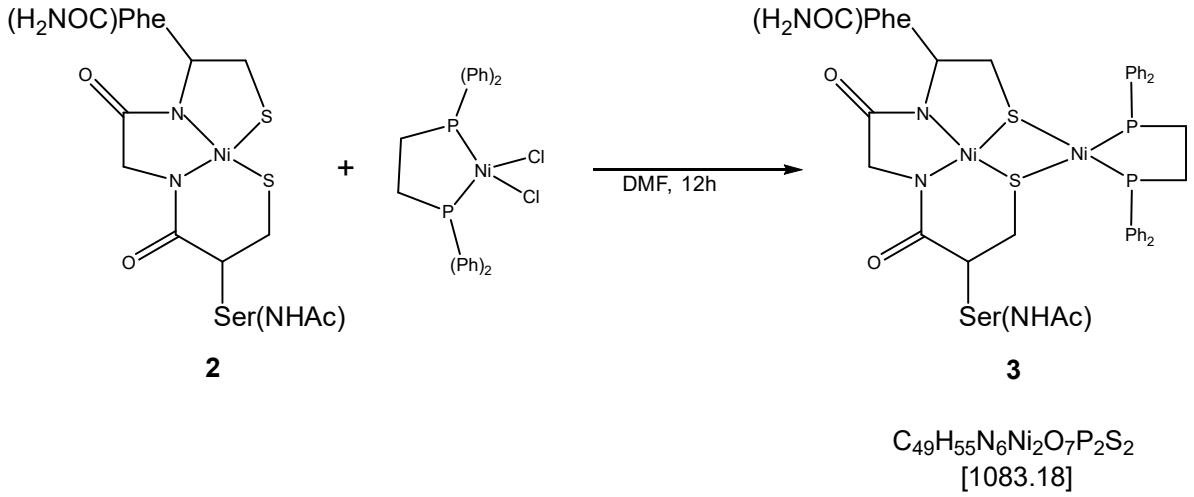

Scheme 4.29 Reaction of **2** and 1,2-bis(diphenylbosphino)ethane nickel(II) chloride ($Ni(dppe)Cl_2$) to form the second Ni-center in the heteroleptic complex.

The product **3** was analysed and confirmed by ESI-MS and HR-MS (Figure 4.30).

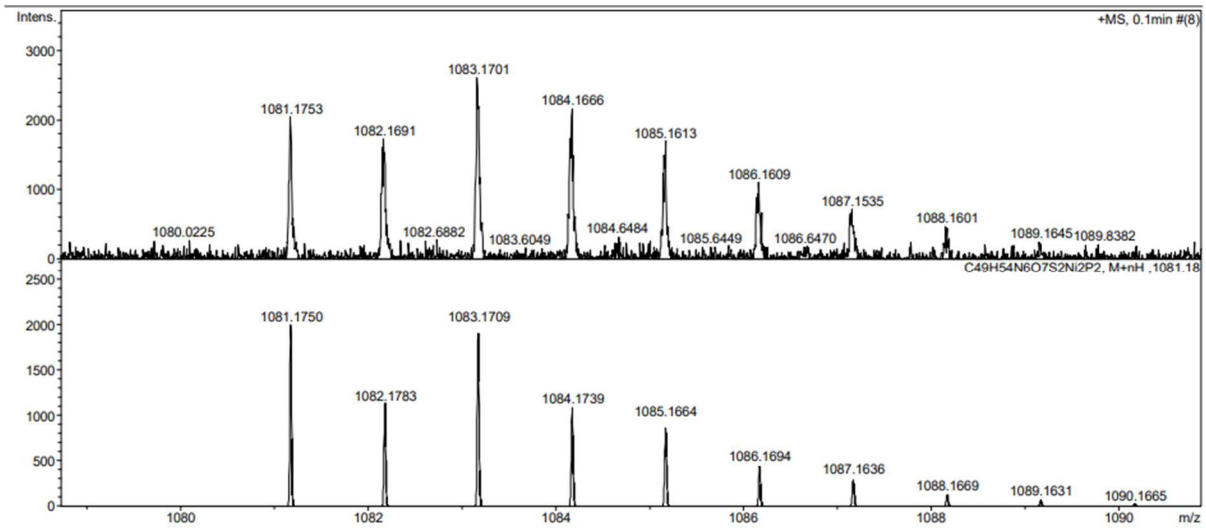

Figure 4.30 Experimental (top) and calculated (bottom) HR-MS-spectra of synthesized nickel peptide complex **3** in DMF. For calculated $C_{49}H_{55}N_6O_7S_2Ni_2P_2$ [M]: 1083.1709 was found m/z: 1083.1701 and the isotopic pattern of compound **3**.

The experimental results indicated that it was possible to develop a heteroleptic complex **3** containing two nickel centers. The first complex **2** contained one Ni-center, which was square planare coordinated by synthesized peptide sequence **1** (594-598) from *Morella Thermoacetica*. This complex **2** was expanded in a further reaction by another Ni-center to complex **3**. The experimental procedure was carried out according to RIORDIAN [98], but with a pentapeptide instead of a tripeptide. The next synthesis step of modelling compound **3** would be an Fe-S-cluster in analogy to ACS A-cluster (4.22). The final heteroleptic complex could be used to check whether it can catalyse the reaction of inorganic compounds like CO and CH_3SH to methyl thioester.

The final nickel complexes connected to an Fe-S-cluster could be understood as probable precursor of the binuclear complex of the A-cluster in ACS on prebiotic Earth.

5. Conclusions

5.1 Prebiotic PP_i Synthesis

In this thesis, a prebiotically plausible synthesis for inorganic pyrophosphate (PP_i) condensation by coupling the Pi dimerization to a geochemical redox reaction was demonstrated. For this approach the geochemical C/C-bond formation experiment containing carbon monoxide (CO), methanethiol (CH_3SH) on the surface of hydrothermal fluids containing metal sulfides e.g. NiS was utilized.[8] Adding soluble orthophosphate (P_i) and insoluble $Ca_3(PO_4)_2$ to the reaction mixture led after 8 h reaction time to PP_i formation, which was detected with fluorescence spectroscopic measurements by using fluorescent PP_i -sensor (see Chapter 4, Figure 4.6). PP_i formation was indicated by increased fluorescence signal after 8 h reaction progress, but not if one of the compounds P_i or $Ca_3(PO_4)_2$ was absent in the suspension.

Since the yield of PP_i was low, an alternative more sensitive bioluminescence assay was used to confirm the PP_i formation with a further independent method. PP_i formation in the prebiotic reaction with present soluble P_i and insoluble $Ca_3(PO_4)_2$ was also detected with the luminescence measurement method (Figure 4.11). In these measurements too, it was observed that no significant increasing of the luminescence signal was detected in absence of P_i or $Ca_3(PO_4)_2$.

Attempts to quantify formed PP_i in the reaction samples with the assays was complicated since it was detected that present P_i in the samples impede the fluorescence and luminescence intensity. Efforts to separate P_i from PP_i with strong anion exchange chromatography (SAX) were complicated and did not yield the expected results (Figure 4.11).

Summarized, can be concluded that PP_i synthesis under prebiotic conditions at 60°C, pH 8 and without using condensing agents was indicated (Chapter 4.1). These results demonstrated that there is no need to postulate a thioester world (DeDuve) as a distinct phase of prebiotic

evolution preceding phosphoanhydride bioenergetics, since thioester and PP_i could have been synthesized simultaneously on prebiotic Earth.

5.2 The Nature of the Active Species

It was noticed that PP_i formation in 8 h reaction time was not constant (Figure 4.8, D) and therefore an explanation for that was researched in the original C/C-bond formation experiment. From the kinetical studies it was noticed that between 0-8 h reaction time no significant amount of product formation was detected, but after 8 h an exponential increase of product formation was observed (Figure 5.1).

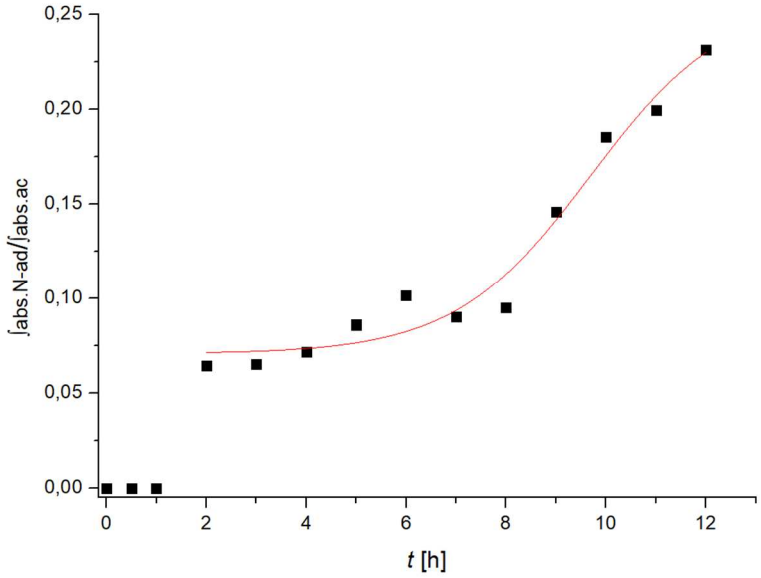

Figure 5.3 The absorbance of integrated adenosine relative to integrated N-acetylanilne plotted against the reaction time. After a lag phase (0-7 hours) no significant amounts of N-acetylaniline is formed. But after 8 hours an increase of product formation can be observed.

These results indicated that NiS is may not the active catalyst as assumed, but rather NiS undergoes some slow chemical conversions (lag phase) to form the active species, which catalyses then fast the reaction as soon as a steady state concentration is reached. Under the prevailing reaction conditions NiS, CO atmosphere, 60 °C and a mobilization of Ni to a Ni(0)-compound e.g. nickel tetra carbonyle ($Ni(CO)_4$) was considered.

Attempts to detect hypothesized $Ni(CO)_4$ in the reaction mixture were not effective. However, the nature of the active species, the acetyl group transferring catalyst of the prebiotic reaction remained open. Investigation of the mobilization of the nickel-compound in the reaction process would contribute to a understanding, whether nickel is being mobilized or the reaction occur on the surface of precipitated NiS.

5.3 Hydrolytic Stabilities of PP_i and AcP

In the literature PP_i and AcP were both considered as plausible prebiotic energy storing compounds similar to present day ATP. For this circumstance metastability in aqueous solutions is required and the hydrolytic stability of both compounds was determined with ^{31}P - NMR-spectroscopy (Figure 4.20). The signals from AcP and PP_i were integrated and the half-life-time at the respective temperature was determined. The processed data from the ^{31}P - NMR-measurements have shown that the reaction follows a pseudo-first order kinetics.

From the hydrolysis kinetics at 60°C a half-life-time for AcP of 40 min was determined and 310 days for PP_i. Therefore, it can be concluded that PP_i is more stable than AcP and plausible to be considered as long-time energy storing compound on prebiotic Earth.

5.4 Experiments towards Peptidic Minimal Models of Acetyl coenzyme A Synthase (ACS)

The key enzyme ACS in the ancient WOOD-LJUNDAHL pathway catalyses the formation of acetyl-CoA from CoA, CO and CH_3 in bacteria and archaea. The active site for this reaction is the A-cluster which consists a peptide coordinated Ni-center, which is thiolate bridged to a second Ni-center and connected to a cuboidal Fe_4S_4-unit. Since ACS was unlikely on early Earth heteroleptic Ni-complexes could be considered as prebiotic precursor of ACS.

Modelling a complex containing two Ni-centers in analogy to the A-cluster of ACS was achieved. First, a peptide sequence from thermophilic acetogen *Moorella Thermoacetica* (594-598) containing the amino acids serine (S), cysteine (C), glycine (G), cystein (C) and phenylalanine (F) was synthesized. Afterwards the distal Ni-center (**2**) was coordinated square

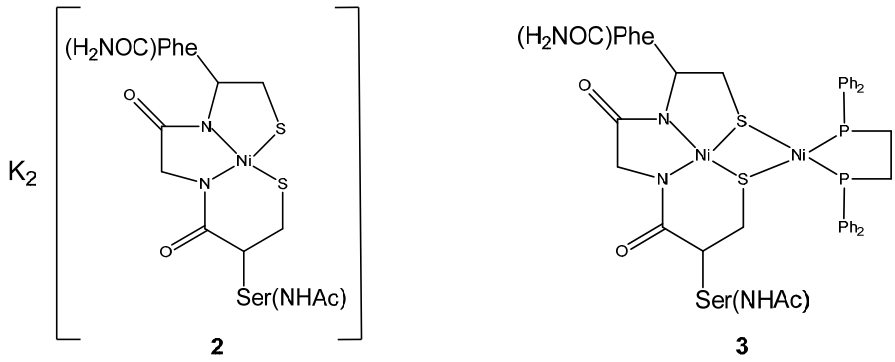

Scheme 5.1 Square planar coordinated distal Ni-center (**2**) by peptide. Ni-complex **2** was extended by a second Ni-center in analogy to the A-cluster in ACS.[98]

planar by the peptide (Figure 5.5), which was indicated due to UV-spectroscopy. Then the peptide coordinated Ni-complex was extended by a second Ni-center (**3**), which was detected with ESI-MS method.

The next synthesis step of complex **3** would be the connection to a synthesized Fe-S-cluster in analogy to the A-cluster of ACS. The modelled complex would be then finalized and the catalytic activity could be examined by reacting CO and methanethiol in aqueous solution to thioester to investigate whether this complex could be considered as precursor of ACS on prebiotic Earth.

6. Experimental Section

6.1. General Equipment and Methods

6.1.1 Solvents, Chemicals and Gases

Solvents used were either analytical *("p.a.")* or HPLC grade. Ultrapure water was prepared by passing standard demineralized water through an *arium mini lab* water system (Sartorius, Göttingen, Germany). Nickel chloride hexahydrate (≥99.999 %) was from *Chempur* (Karlsruhe, Germany), sodium sulfide nonahydrate (≥98.0 %) from *Fluorochem* (Hadfield,UK), disodium hydrogen phosphate heptahydrate (≥98.0 %) from *Alfa Aesar* (Kandel, Germany) and Calcium chloride (anhydrous) from *Grüssing* (Filsum, Germany). Tris base (99.9 %) was from *ROTH* (Karlsruhe, Germany). Carbon monoxide (99.9 %) and methanethiol (>98 %) were purchased from *Linde AG* (Pullach, Germany) and *Sigma-Aldrich* (St. Louis, MO, USA), respectively.

6.1.2 General Procedures

Experiments were carried out under nitrogen atmosphere in ultrapure water, deoxygenized by bubbling a stream of nitrogen through it for 45 min. Glassware was heat-dried under reduced pressure and flushed with nitrogen prior to use. Freeze-drying was performed using an *Alpha-2-4-LD plus* benchtop freeze-dryer from *Christ* (Osterode am Harz, Germany) at pressures < 1 mbar. Small sample amounts (< 2 mL) were freeze-dried in a *RVC 2-18 CD plus* vacuum centrifuge by *Christ*.

6.1.3 Software

Chemical structures and Schemes were drawn with *ChemBioDraw* (version 20). ^{31}P-NMR spectra were processed with *MestReNova* (version 10). Graphs were plotted with *OriginPro* (version 8.5G).

6.2 Analytical Methods

6.2.1 Mass Spectrometry

For sample preparation aqueous or freeze-dried samples were filtered or dissolved in ultrapure water and mixed with MeOH (HPLC grade) up to a 1:1 ratio. A few drops 10 % formic acid were added to samples prior to injection into the spectrometer. Electrospray ionization (ESI) was applied to obtain mass sepectra with a *maXis* or *MicroTOF* spectrometer from *Bruker Daltonik GmbH* (Bremen, Germany). For detection of ionizable derivatives of phosphoric acid, the instrument was set to negative mode. Data were processed with *Compass DataAnalysis* (version 4.0) software by *Bruker*. Selected peaks of high-resolution spectra (HR-MS) were compared to masses calculated for particular molecular species (all values stated as m/z).

6.2.2 High Performance Liquid Chromatography (HPLC)

For kinetical studies an analytical HPLC system by *JASCO* (Tokio, Japan) was used, equipped with an *MD-2010* diode array detector, *PU-2085* pumps, *a CO-2060* column thermostat and a *AS-2055* autosampler. For purification preparative HPLC systems by *JASCO* were used, equipped with *UV-4075* detector, PU-4086 pumps, a column oven *CO-4060*, *LC-NetII/ADC* interface and a fraction collector *Fraction Collector Controller*. Data were processed with *ChromNav 2.01.06* provided by the manufacturer. The compounds were detected, if not otherwise indicated at wavelengths of 220 nm, 254 nm and 280 nm. Used columns with *Nucleodur* phase were from *Machery-Nagel* and those with *Spherisorb SAX* phases were from *Waters*.

Tab. 6.1 List of used columns for HPLC chromatography.

Column Name	Specification	Flow rate
MN Nucleodur, C18	C18, 250 x 4.6 mm, 100 Å, 5 µm	1 mL/min
MN Nucleodur, C18	C18, 250 x 10.0 mm, 100 Å, 5 µm	5 mL/min
Spherisorb SAX OBD	250 x 10 mm, 80 Å, 5 µm	5 mL/min
MN Nucleodur, C18	C18, 250 x 21 mm, 100 Å, 5 µm	10 mL/min

The flow rates with 1mL/min for analytical, 5 mL/min for semi-preparative and 10 mL/min for preparative runs were adjusted. The gradients for each measurement were indicated at each case. Used solvents for HPLC analysis were listed below (Tab 6.2).

Tab. 6.2 Solvent systems used for HPLC analysis and purification.

Solvent A	Solvent B
H_2O	MeCN
0.05 M Triethyl ammonium citrate buffer, pH 4.5 (0.05 M TEAC)	MeOH
H_2O + 0.1 % TFA	MeOH

The 0.05 mM TEAC-buffer was prepared as described in the following. 1000 mL of TEAC-buffer was prepared from citric acid monohydrate (10.5 g, 0.05 mol) and triethyl amine (7.6 g, 0.075 mol). All solvents were degassed prior to use.

For purification of the crude peptides preparative HPLC system from *Jasco* equipped with *PU-4086* pumps, *UV-4075* detector, column oven *CO-4060* and a fraction collector *CHF122SC* (Advantec) was used.

The compounds were detected at 215 nm and 220 nm. Used columns with *Nucleodur* phase were from *Machery-Nagel* (Tab. 6.1).

The gradients for each measurement were indicated at each case.

6.2.3 Liquid Chromatography Mass Spectrometry (LC-MS)

LC-MS analysis was performed at *UltiMate 3000* system from *Thermo Fischer Scientific* (Waltham, USA), equipped with 3000 series pumps, autosampler, column oven and diode array detector. The chromatographic system was coupled to the mass system *LTQ XL* from *Thermo Fischer Scientific*.

6.2.4 Nuclear Magnetic Resonance Spectroscopy (NMR)

For 31P-NMR measurements Acetyl phosphate (AcP) and pyrophosphate (PP_i) were prepared as described in the following.
The samples of acetyl phosphate (3.7 mg, 20 mmol) dissolved in 100 mM TRIS·HCl buffer (10 % D_2O, 1 mL) were transferred to NMR-Tubes and measured at different temperatures (22-60°C) over a time period between 20-180 minutes.
Samples of pyrophosphate (20 mM) were incubated for 0 to 11 days at 60°C. The pH value of all samples was tested before and after measurement to be constantly pH 8.

Spectra were recorded using an *AV 401* spectrometer by *Bruker* (Billerica, Massachusetts, USA) equipped with a heater for setting variable temperatures. The spectrometer was field frequency locked on the deuterium resonance of deuterium oxide (D_2O) used as a solvent. The spectra are referenced to external 85% phosphoric acid (H_3PO_4), which accomplished electronically using the lock signal without running the spectrum of the standard sample every time. All spectra were broadband ^1H-decoupled, and the chemical shifts are given in parts per million (ppm). All FIDs are processed with an exponential multiplication prior to Fourier transform. Spectra are baseline- and phase corrected before they are fitted with the T_1/T_2 relaxation module of the software *TopSpin* (version 3.6.2).

6.2.5 Fluorescence Spectroscopy

Spectra were recorded using a *FP-6200* spectrophotometer from *Jasco* (Tokyo, Japan) at 20 °C, controlled by an *ETC-272T* Peltier thermostat (*Jasco)* connected to a *Thermo Haake WKL26* water recirculator of *Thermo Fisher Scientific* (Waltham, MA, USA). Samples were kept in *Hellma Quartz SUPRASIL QS* fluorescence cuvette of 1.0 cm path length from *Hellma Analytics* (Müllheim, Germany) under a continuous stream of nitrogen. Settings were as follows. Excitation wavelength: 316 nm; recording range for emission: 350 nm - 550 nm; bandwidth: 5 nm; response: 0.5 s; scanning speed: 200 nm/min; data pitch: 1.0 nm; sensitivity: 'high'. Raw data were processed with *Spectra Manager* software (version 1.54.03) provided by the manufacturer.

6.2.6 UV Absorption Spectroscopy

The sample was dissolved in MeOH and transferred to a cuvette (10 mm, 500 µL) from *Hellman Analytics* (Mühlheim, Germany). UV absorption was measured with *V-550* spectrometer from *JASCO* (Tokio, Japan) and the data were processed with *Spectra Manager* software (1.54.03) provided by the manufacturer.

6.2.7 Gasphase- Infrared Spectroscopy (Gasphase-IR)

Aliquots of gaseous phase was collected in a cylindrical vessel to analyse with Gasphase Infrared (Gasphase-IR) Spectroscopy. The spectra were recorded with a *Bruker Vertex 70* (Billerica, Massachusetts) spectrometer and processed with the associated program *OPUS 7.5*.

6.2.8 Luminescence Spectroscopy

The luminescence spectra were recorded on a *Cytation 3* plate reader from *BioTek Instruments* (Winooski, Vermont, USA). Samples were read (0.1 s integrated reading) with *area scan mode* (5x5) over the entire area of the well. The crude data were given as *excel* files and processed with the software program *Origin* (Northampton, Massachusetts, USA).

6.3 N-Acetylaniline Synthesis

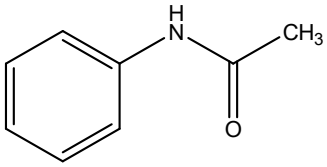

C_8H_9NO
135.17 g/mol

Caution: Carbon monoxide (**CO**) is an odorless, colourless and **toxic gas** and therefore it is necessary to work under a good ventilated fume hood.

Hazard symbols

TLV (threshold limit value)**:** 40 ppm 2 min

6.3.1 Synthesis of N-Acetylaniline at 100 °C

Reactions were carried out in a 100 mL three-necked flask equipped with a reflux condenser, a gas inlet tube, a rubber septum and a magnetic stirring bar. Carbon monoxide (CO) and methanethiol (CH_3SH) were individually passed through bubblers filled with silicon oil and united in a Y-junction between bubblers and gas inlet tube. A solution of $Na_2S{\cdot}9\ H_2O$ (600 mg, 2.5 mmol) in 2 mL water was added dropwise to $NiSO_4 \cdot 6H_2O$ (786 mg, 3.00 mmol) in 3 mL water. Carbon monoxide was bubbled through the resulting suspension in which aniline (46 µL, 0.5 mmol) was given to the mixture. Afterwards CH_3SH was initiated and the reaction mixture was filled up to 30 mL with 25 mM TRIS·HCl buffer (pH 8). Then the suspension was heated up to 100 °C over 12 hours and a sample (1 mL) was hourly withdrawn by syringe through the rubber septum. After filtered through a syringe filter (regenerated cellulose, 0.45 µm pore size), 25 µL of the sample was analysed by analytical HPLC. The signal with the retention time (t_R) 22.1 min was collected and analysed with ESI-MS.

Analytical Data

HPLC (analytical) on C18-column (MN Nucleodur®100 5 C18, 250 x 4.6 mm, 5 µm), solvent A: 0.05 M trietyl ammonium citrate buffer (TEAC, pH 4.5) and solvent B: MeCN, gradient: 5 → 60% B in 25 min. The absorption was recorded at λ = 254 nm, t_R = 22.2 min.

ESI-MS: (MeOH) *m/z* (rel %) = 136.1 (100) $[M+H]^+$.

6.3.2 Synthesis of N-acetylaniline at 60 °C

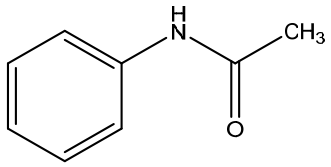

C_8H_9NO
135.17 g/mol

Reactions were carried out in a 100 mL three-necked flask equipped with a reflux condenser, a gas inlet tube, a rubber septum and a magnetic stirring bar. Carbon monoxide (CO) and methanethiol (CH_3SH) were individually passed through bubblers filled with silicon oil and united in a Y-junction between bubblers and gas inlet tube. A solution of $Na_2S{\cdot}9\ H_2O$ (600 mg, 2.5 mmol) in 2 mL water was added dropwise to $NiSO_4 \cdot 6H_2O$ (786 mg, 3.00 mmol) in 3 mL water. Carbon monoxide was bubbled through the resulting suspension in which aniline (46 µL, 0.5 mmol) was given to the mixture. Afterwards CH_3SH was introduced and the reaction mixture was filled up to 30 mL with 25 mM TRIS·HCl buffer (pH 8). Then the suspension was heated up to 60 °C over 12 hours and a sample (1 mL) was hourly withdrawn by syringe through the rubber septum. After filtered through a syringe filter (regenerated cellulose, 0.45 µm pore size), 25 µL of the sample was analysed by analytical HPLC. The signal with the retention time (t_R) 22.1 min was collected and analysed with ESI-MS.

Analytical Data

HPLC (analytical) on C18-column (MN Nucleodur®100 5 C18, 250 x 4.6 mm, 5 µm), solvent A: 0.05 M trietyl ammonium citrate buffer (TEAC, pH 4.5) and solvent B: MeCN, gradient: 5 → 60% B in 25 min. The absorption was recorded at λ = 254 nm, t_R = 22.2 min.

ESI-MS: (MeOH) *m/z* (rel %) = 136.1 (100) $[M+H]^+$.

6.3.3 N-acetylaniline Synthesis with Modified Experimental Set Up

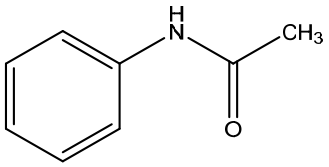

C_8H_9NO
135.17 g/mol

Experimental Set Up

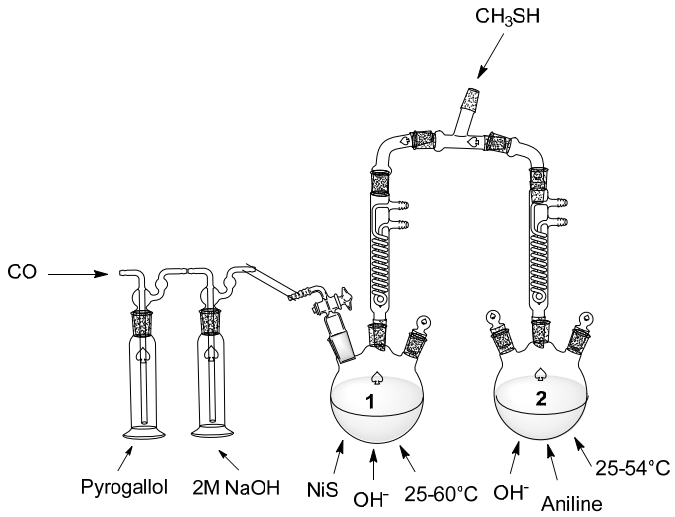

Figure 6.1: Modified two-vessel experimental set up of the prebiotic reaction. CO-stream was purified by initiating through pyrogallol and NaOH solutions. In vessel 1 NiS, OH- at 60-80°C are present and in vessel 2 aniline, OH- at 25-35°C are present. The intention was to separate the place, where the catalyst is formed (vessel 1) and the place, where it catalyses the reaction (vessel 2).

Reactions were carried out in two 100 mL three-necked flask equipped with a reflux condenser, a gas inlet tube, a rubber septum, and a magnetic stirring bar. In reaction flask 1 NiS was precipitated from $Na_2S{\cdot}9\ H_2O$ (600 mg, 2.5 mmol) in 2 mL water and $NiSO_4 \cdot 6H_2O$ (786 mg, 3.00 mmol) in 3 mL water. Carbon monoxide (CO) passed through a pyrogallol solution and sodium hydroxide solution (2 M) was introduced through a Y-junction with a gas inlet tube to the reaction mixture in flask 1. In a TRIS-HCl containing three neck-flask 2 aniline (46 µL, 0.5 mmol) is added and methanethiol is passed through a tap into the reaction mixture. Both flasks are connected through the condenser of flask 1 and a gas inlet tube in flask 2. Then the suspension in flask 1 was heated up to 70 °C and flask 2 was held at room temperature. A sample (1 mL) was hourly withdrawn by syringe through the rubber septum from flask 2. After filtered through a syringe filter (regenerated cellulose, 0.45 µm pore size), 25 µL of the sample was analysed by analytical HPLC. The signal with the retention time (t_R) 22.1 min was not detected.

6.4 Ni (II) Reduction and Tetracarbonyle Nickel ($NiCO_4$) Synthesis

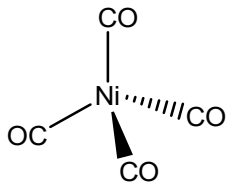

C_4NiO_4
170.73 g/mol

Caution: The **$Ni(CO)_4$** compound is volatile (43°C), **very toxic** and therefore it is necessary to work under a good ventilated fume hood.

Hazard symbols

TLV: 0.05 ppm

Lethal concentration [121]: 2 ppm

6.4.1 Reduction of Ni (II)

NiS was precipitated from $NiSO_4 \cdot 6H_2O$ (524 mg, 2 mmol) and $Na_2S \cdot 9H_2O$ (600 mg, 2.5 mmol). Afterwards 1 M NaOH (20 ml) was added to the suspension and CO-gas stream was passed through the mixture [122]. The suspension was heated up to 100°C and hydrazine acetate was added after 100 min ongoing reaction. During 5 h reaction time the gas exhaust was led in 10 min intervals into the burner flame.
The from MOND et al. described characteristically, highly luminous flame [110] was not observed.

6.4.2 Reduction of Ni (II) with CO in water

$NiSO_4 \cdot 6H_2O$ (262 mg, 1 mmol) was dissolved in ultrapure water (10 mL). CO (~1 bar) was passed through the solution (pH 7) and the solution was heated up to 100 °C.
No nickel (0) particles could be observed in the solution.

6.4.3 Reduction of Ni (II) with CO in 100 mM $NaHCO_3$

$NiSO_4 \cdot 6H_2O$ (262 mg, 1 mmol) was dissolved in 100 mM $NaHCO_3$ solution (10 mL). CO (~1 bar) was passed through the solution (pH 9-10) and heated up to 100 °C.
No nickel (0) particles could be observed in the solution.

6.4.4 Reduction of Ni (II) with CO in 100 mM $NaCO_3$

$NiSO_4 \cdot 6H_2O$ (262 mg, 1 mmol) was dissolved in 100 mM $NaCO_3$ solution (10 mL). CO (~1 bar) was passed through the solution (pH 11) and heated up to 100 °C.
No nickel (0) particle could be observed in the solution.

6.4.5 Reduction of Ni (II) with CO in NH_3

$NiSO_4 \cdot 6H_2O$ (262 mg, 1 mmol) was dissolved in NH_3 solution (25 %, 10 mL). CO (~1 bar) was passed through the solution and heated up to 100 °C.
No nickel (0) particle could be observed in the solution.

6.4.6 Reduction of Ni (II) with CO in tube furnance

$NiSO_4 \cdot 6H_2O$ (0.5 g, 2 mmol) was filled in a combustion boat and transferred to a glass tube. After evacuation of the solid, a carbon monoxide (CO) stream (~1 bar) passed through the glass tube, which was heated up to 130°C in a tube furnace *HTM Reetz* (Berlin, Germany) for 6 h. The glass tube was connected to a pyridine filled bubbler, which was passed from the gas stream. The exhaust leaves through the fume hood shaft. At certain times the exhaust was led into the burner flame.

Neither pyridine solution, nor the burner flame indicated $Ni(CO)_4$ formation due to mobilization of nickel.

6.4.7 Ni(0) compounds in a Tube Furnance

Solid Ni-powder (325 Mesh) (0.5 g, 8.5 mmol) was filled in a combustion boat and transferred to a glass tube. After evacuation of the solid, a carbon monoxide (CO) stream (1 bar) passed through the glass tube, which was heated up to 130°C in a tube furnace (HTM Reetz, Berlin) for 6 h. The glass tube was connected to a pyridine filled bubbler, which was passed from the gas stream. The exhaust leaves through the fume hood shaft. At certain times the exhaust was led into the burner flame.

Neither pyridine solution, nor the burner flame indicated $Ni(CO)_4$ formation.

6.4.8 Urushibara Nickel Synthesis

$NiCl_2 \cdot 6H_2O$ (2 g, 8.5 mmol) was dissolved in HCl (conc.) (3 mL) and heated up to 90°C. The solution was added to zinc powder (100 Mesh) (1.3 g, 20 mmol) a precipitation was observed. After gas formation finished the precipitated compound was filtered under oxygen-free conditions and washed with degassed ultrapure water (2 x 25 mL). Thereafter, the precipitate was transferred to 100 mL acetic acid solution (15 %), which was again filtered under oxygen-free conditions after gas formation finished. Then it was washed with ultrapure water (2 x 25 mL), ethanol (2 x 10 mL) and was stored in ethanol. [123]

The synthesized Urushibara Nickel (0.5 g) was transferred in a combustion boat and transferred to a glass tube. After evacuation of the solid, a carbon monoxide (CO) stream (~1 bar) passed through the glass tube, which was heated up to 130°C in a tube furnace *HTM Reetz* (Berlin, Germany) for 6 h. The glass tube was connected to a pyridine filled bubbler, which was passed from the gas stream. The exhaust leaves through the fume hood shaft. At certain times the exhaust was led into the burner flame.

Neither pyridine solution, nor the burner flame indicated $Ni(CO)_4$ formation.

6.4.9 Raney-Nickel

Raney®-Nickel (2 g, slurry in H_2O, *Sigma Aldrich*) in a combustion boat was transferred to a glass tube and degassed. CO-stream (~1 bar) was passed through the glass tube and an heated up to 130°C in a tube furnace type *LOSA* from *HTM Reetz* (Berlin, Germany). The exhaust was held in a gas flame and the characteristical $Ni(CO)_4$ flame was observed, which was highly luminous and greenish. [110,124]

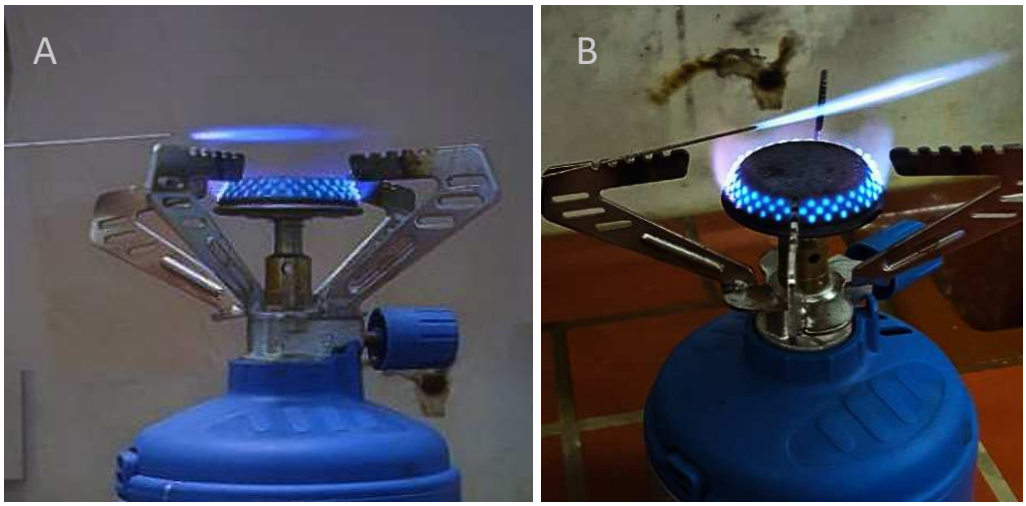

Figure 6.2 CO-stream (1 bar) passed through the glass tube, which is heated up to 130 °C in a tube furnace and the exhaust was led into the burner flame. A: The CO-stream passed into the flame after 5 min reaction time is not luminous. But after 60 min the exhaust was again led into the burner flame and a highly luminous flame could be observed (B).

6.4.10. $Ni(CO)_4$ Synthesis

The preparation and experimental part was carried out under nitrogen atmosphere due to highly air sensitive bis(cyclooctadiene)nickel(0) ($Ni(COD)_2$) educt.

$$Ni(COD)_2 \xrightarrow[-30°C]{\text{1) Toluene, 2) } CO_{(g)}} Ni(CO)_4$$

$Ni(COD)_2$ (200 mg, 0.7 mmol) was dissolved in dry toluol (17 mg, 20 mL, 0.2 mmol) and cooled down to -20 °C with a dry ice/acetone mixture. Through a pyrogallol solution (2 M) passed CO stream (~ 1 bar) was introduced to the reaction solution.[112] After 30 min. aliquots of synthesized gaseous $Ni(CO)_4$ was collected in a cylindric vessel for gasphase-IR analysis and the rest was quenched passing the gas stream through aqueous HNO_3-solution (2 M).

Analytical Data

Gasphase-IR: $\tilde{\nu}/cm^{-1}$ = 2059 (s, CO)

6.5 Synthesis and Detection of Inorganic Pyrophosphate (PP_i)

6.5.1 Detection of PP_i with fluorescent *Pyrophosphate Sensor Assay*

Accumulation of PP_i in synthesis reactions was monitored using the pyrophosphate (PPi) assay kit MAK168 of *Sigma-Aldrich* (St. Louis, MO, USA). The assay is based on enhanced fluorecence (λ_{Ex} = 316 nm, λ_{Em} = 456 nm) upon binding of PP_i to a sensor fluorophore. Assay mixtures were prepared as described in the *Technical Bulletin* provided by the manufacturer. Briefly, 50 µL aliquots of samples taken from a reaction mixture, diluted 5-fold with Tris·HCl (pH 8), were mixed with 50 µL of 200x PP_i sensor stock solution. Prior to recording fluorescence spectra, mixtures were incubated at room temperature for 20 min.

Reference spectra were recorded to examine the sensitivity for low PP_i yields and how other compounds in the sample influence the fluorescence intensity of the sensor.

6.5.1.1 Unloaded “free” fluorescent sensor

The sensor shows fluorescence intensity without present PP_i in solution (“True Backround”) at the excitation wavelength 316 nm and 304 nm.

Tab. 6.3 Data from fluorescence measurements of unloades fluorescent sensor in 100 mM TRIS-buffer (pH 8) and H_2O (Spectra see Appendix).

	λ_{Ex} **[nm]**	λ_{Em} **[nm]**	$\lambda_{Em,max}$ [nm]	$\lambda_{Em,max\ /Int.}$ **[nm]**
„True Background“ (sensor without PP_i)				
100mM TRIS, pH8	316	350-550	435	1334.9
H_2O (ultrapure)	316	350-550	437	1282.3
100mM TRIS, pH8	304	350-550	436	1439.6
H_2O (ultrapure)	304	350-550	438	1400.3

6.5.1.2 Fluorescence Sensor + PP_i

With increasing PP_i concentrations the fluorescent PP_i sensort shows increasing fluorescent intensity and a shift of $\lambda_{Em,max}$ to higher wavelength.

Tab. 6.4 Data from fluorescence measurements for various PP_i concentrations (Spectra see Appendix.

	λ_{Ex} [nm]	λ_{Em} [nm]	$\lambda_{Em,max}$ [nm]	$\lambda_{Em,max\ /Int.}$ [nm]
		PP_i, pH 8		
0.5 µM	304	350-550	439	1721.6
1 µM	304	350-550	440	1710.4
5 µM	304	350-550	452	5135.9
10 µM	304	350-550	454	6390.0
0.5 µM	316	350-550	438	1557.1
1 µM	316	350-550	443	1709.1
5 µM	316	350-550	453	5761.3
10 µM	316	350-550	454	7950.0

6.5.1.3 Fluorescent sensor + P_i

Though the fluorescent sensor is highly sensitive to PP_i, it responds also to high P_i concentrations.

Tab. 6.5 Data from fluorescence measurements for various P_i concentrations (see spectra in Appendix).

	λ_{Ex} [nm]	λ_{Em} [nm]	$\lambda_{Em,max}$ [nm]	$\lambda_{Em,max\ /Int.}$ [nm]
		P_i, pH 8		
10 mM	304	350-550	443	1547.1
20 mM	304	350-550	444	1548.1
50 mM	304	350-550	448	2537.3
100 mM	304	350-550	450	2992.9
10 mM	316	350-550	442	1415.7
20 mM	316	350-550	444	1620.0
50 mM	316	350-550	449	2507.2
100 mM	316	350-550	450	3390.7

6.5.2 PP_i Light™ inorganic pyrophosphate assay

A 5 mL sample from the crude reaction mixture was filtered, 10-fold diluted with 10 mM TRIS (pH 8), and purified over a strong anion exchange column (HiTrap® Q Fast Flow, *Sigma Aldrich*, bed size 16 mm × 25 mm) based on a robust, 6% highly cross-linked beaded agarose matrix with good flow properties and high loading capacities. The P_i -free fractions Ex3B, Ex4 an Ex5 (Figure 6.4) were merged, applied again on an anion exchange column (HiTrap® Q Fast Flow,

Sigma Aldrich, bed size 7 mm × 25 mm) and eluted with triethyl ammonia bicarbonate buffer (TEAB, 0.4 M, 2 mL). Afterwards the eluate was lyophilized multiple times, dissolved in ultrapure water (500 µL) and further processed with the PP_i Light™ inorganic pyrophosphate assay for luminescence measurements.

The converting and detecting reagents where prepared as in the PP_i *Light™ inorganic pyrophosphate assay* instruction described. Converting reagent (20 µL) was added to the sample (40 µL) in the 96-well F-bottom plate from *Greiner Bio-One* (Frickenhausen, Germany)

and incubated at room temperature for 30 minutes. Then detecting reagent (20 µL) was added to the mixture and incubated again for 30 minutes. Afterwards the luminescence of the samples was read (0,1 s integrated reading) at the plate reader *Cytation 3* from *BioTek* (Winooski, USA).

Before measuring the samples, the assay was calibrated with varying PP_i concentrations and P_i / PP_i mixtures.

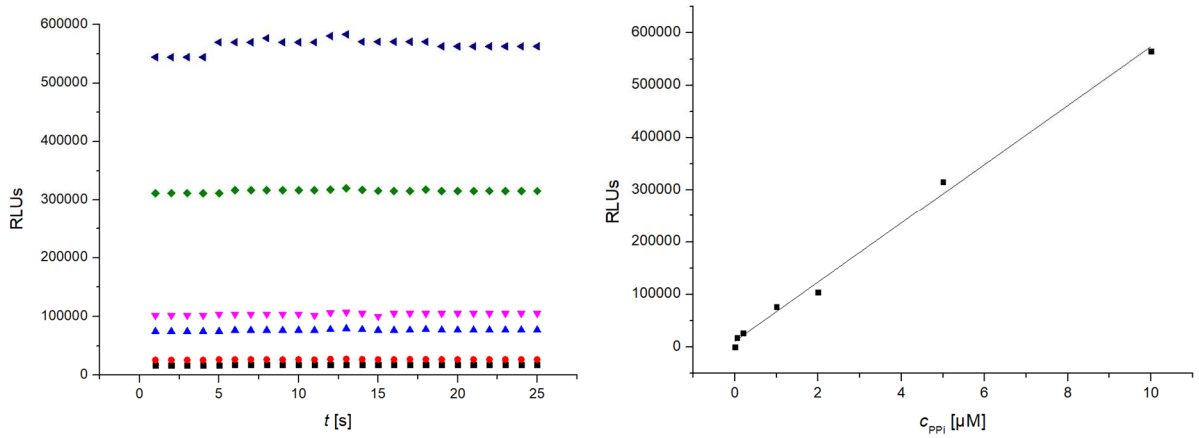

Figure 6.3 Luminescence signal of varying PP_i concentrations from 0.05 µM (blacksquares, 0.2 µM (red circles), 1 µM (blue triangles), 2 µM (pink triangles) 5 µM (green diamond) to 10 µM (blue triangles) in 25 s.

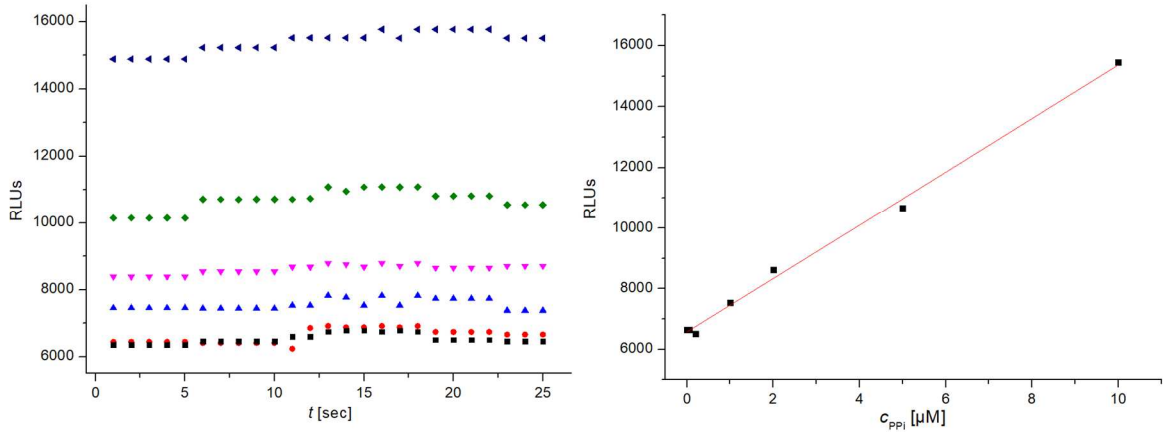

Figure 6.4 Luminescence signal of a mixture of constant 100 mM P_i and varying PP_i concentrations from 0.05 µM (blacksquares, 0.2 µM (red circles), 1 µM (blue triangles), 2 µM (pink triangles) 5 µM (green diamond) to 10 µM (blue triangles) in 25 s.

The luminescence intensity increases proportional to the PP_i concentration in the range of 0.05 – 10 µM as described from the manufacturer.

6.5.3 Prebiotic PP_i Synthesis

Reactions were carried out in a 100 mL three-necked flask equipped with a reflux condenser, a gas inlet tube, a rubber septum and a magnetic stirring bar. Carbon monoxide and methanethiol were individually passed through bubblers filled with silicon oil and united in a Y-junction between bubblers and gas inlet tube. The experiment was carried out as follows. A solution of $Na_2S{\cdot}9\ H_2O$ (600 mg, 2.5 mmol) in 2 mL water was added dropwise to $NiCl_2{\cdot}6\ H_2O$ (713 mg, 3 mmol) in 3 mL water. Carbon monoxide was bubbled through the resulting suspension and Na_2HPO_4 (15 mL) of a 120 mM aqueous solution, adjusted to pH 8 by addition of HCl was added. In a separate flask, 5 ml 600 mM Na_2HPO_4 (3 mmol) were added dropwise to 5 mL 300 mM $CaCl_2$. The suspension of precipitated calcium orthophosphate was stirred for 30 min, allowed to settle, washed with 3 x 5 mL 100 mM Na_2HPO_4, then taken up in another 10 mL 100 mM Na_2HPO_4 and added to the reaction mixture to give 3 mmol of insoluble orthophosphate corresponding to a formal concentration of 100 mM in the total volume of 30 mL. Concentration of soluble orthophosphate was 93.3 mM. Thereafter, the

methanethiol gas stream was turned on and the suspension was stirred at 60 °C. At various time points, samples of 1 mL each were withdrawn from the reaction mixture by syringe through the rubber septum and analysed with fluorescent *Pyrophosphate Sensor*.

Analytical: With both soluble and insoluble P_i present in the mixture the formation of PP_i was indicated through increasing of fluorescence intensity in the measurements.

6.5.4 PP_i synthesis without insoluble $Ca_3(PO_4)_2$

Reactions were carried out in a 100 mL three-necked flask equipped with a reflux condenser, a gas inlet tube, a rubber septum and a magnetic stirring bar. Carbon monoxide and methanethiol were individually passed through bubblers filled with silicon oil and united in a Y-junction between bubblers and gas inlet tube. The experiment was carried out as follows. A solution of $Na_2S{\cdot}9\ H_2O$ (600 mg, 2.5 mmol) in 2 mL water was added dropwise to $NiCl_2{\cdot}6\ H_2O$ (713 mg, 3 mmol) in 3 mL water. Carbon monoxide was bubbled through the resulting suspension and Na_2HPO_4 (25 mL) of a 120 mM aqueous solution, adjusted to pH 8 by addition of HCl was added. Thereafter, the methanethiol gas stream was turned on and the suspension was stirred at 60 °C. At various time points, samples of 1 mL each were withdrawn from the reaction mixture by syringe through the rubber septum and analysed with fluorescent *Pyrophosphate Sensor*.

Analytical: Without insoluble P_i no increasing fluorescent signal could be observed between 0- and 8-hours reaction time.

6.5.5 With insoluble 100 mM $Ca_3(PO_4)_2$ and without soluble Na_2HPO_4

Reactions were carried out in a 100 mL three-necked flask equipped with a reflux condenser, a gas inlet tube, a rubber septum and a magnetic stirring bar. Carbon monoxide and methanethiol were individually passed through bubblers filled with silicon oil and united in a Y-junction between bubblers and gas inlet tube. The experiment was carried out as following described. A solution of $Na_2S{\cdot}9\ H_2O$ (600 mg, 2.5 mmol) in 2 mL water was added dropwise to $NiCl_2{\cdot}6\ H_2O$ (713 mg, 3 mmol) in 3 mL water. In a separate flask, 10 ml 600 mM Na_2HPO_4 (3 mmol) were added dropwise to 10 mL 300 mM $CaCl_2$. The suspension of precipitated calcium

orthophosphate was stirred for 30 min, allowed to settle, washed with 3 x 10 mL 100 mM Na_2HPO_4, then taken up in another 10 mL 100 mM Na_2HPO_4 and added to the reaction mixture to give 3 mmol of insoluble orthophosphate corresponding to a formal concentration of 100 mM in the total volume of 30 mL adjusted with ultrapure water. Thereafter, the methanethiol gas stream was turned on and the suspension was stirred at 60 °C. At various time points, samples of 1 mL each were withdrawn from the reaction mixture by syringe through the rubber septum and analysed with fluorescent *Pyrophosphate Sensor*.

Analytical: Without insoluble P_i no increasing fluorescent signal could be observed between 0- and 8-hours reaction time.

6.5.6 With soluble 10 mM Na_2HPO_4 and insoluble $Ca_3(PO_4)_2$

The prebiotic synthesis reaction of PP_i was exactly carried out as described in 6.5.1, but the concentration of soluble ortho phosphate was decreased from 93.3 mM to 10 mM P_i.

Analytical: With decreased soluble P_i from 93.3 mM to 10 mM P_i no increasing fluorescent signal could be observed between 0- and 8-hours reaction time.

6.6. Purification with Anion Exchange Chromatography

6.6.1. Separation of adenosine, AMP, ADP and ATP by HPLC

In sample present P_i impede the PP_i signal in fluorescent and bioluminescent assay. Therefore, P_i / PP_i containing samples were purified on HPLC at strong anion exchange (SAX) column. Purification attempts on HPLC were carried out with assistance of reference chromatograms of the nucleotides AMP, ADP, ATP and Adenosine due to missing chromophores in P_i and PP_i. The retention time of P_i and PP_i could be estimated from the retention times of the equally charged nucleotides.

A mixture of each 5 mM Adenosine, AMP, ADP and ATP was prepared and applied on SAX column *Spherisorb SAX* phases from *Waters*. The sample was analysed with analytical HPLC system by *JASCO* (see Experimental Section 6.2), purified with a preparative HPLC system from *Jasco* and detected at λ = 254 nm and 260 nm.

The flow rates with 1mL/min for analytical and 8 mL/min for preparative runs were adjusted. Used solvents for HPLC analysis was listed below.

Tab. 6.6 Solvent systems used for HPLC analysis of adenosine, AMP, ADP and ATP.

Solvent A	Solvent B
H_2O	100 mM (Na^+/NH_4^+) Acetate, pH 8
H_2O + 0.1 % TFA	MeOH

Analytical Data

HPLC (JASCO): Gradient: 5 → 70 % B in 30 min. Retention times (t_R): Adenosine t_R = 2 min, AMP t_R = 12 min, ADP t_R = 21 min and ATP t_R = 27 min.

6.6.2 Mono Q Chromatography

A 5 mL sample from the crude reaction mixture (Experimental Section 6.6.1) was filtered, 10-fold diluted with 10 mM TRIS (pH 8), and purified over a strong anion exchange column (HiTrap® Q Fast Flow, *Sigma Aldrich*, bed size 16 mm × 25 mm) based on a robust, 6% highly cross-linked beaded agarose matrix with good flow properties and high loading capacities. The compounds were eluted sequentially with increasing concentrations of NaCl solution (0.04-1 M). The eluted aliquots were analysed with 31P-NMR to discover in which fractions P_i and P P_i were present. Afterwards the P_i -free fractions were merged, applied again on an anion exchange column (HiTrap® Q Fast Flow, *Sigma Aldrich*, bed size 7 mm × 25 mm) and eluted with triethyl ammonia bicarbonate buffer (TEAB, 0.4 M, 2 mL). Then the eluate was lyophilized multiple times, dissolved in ultrapure water (500 µL) and further processed with the PP_i Light™ inorganic pyrophosphate assay for luminescence measurements.

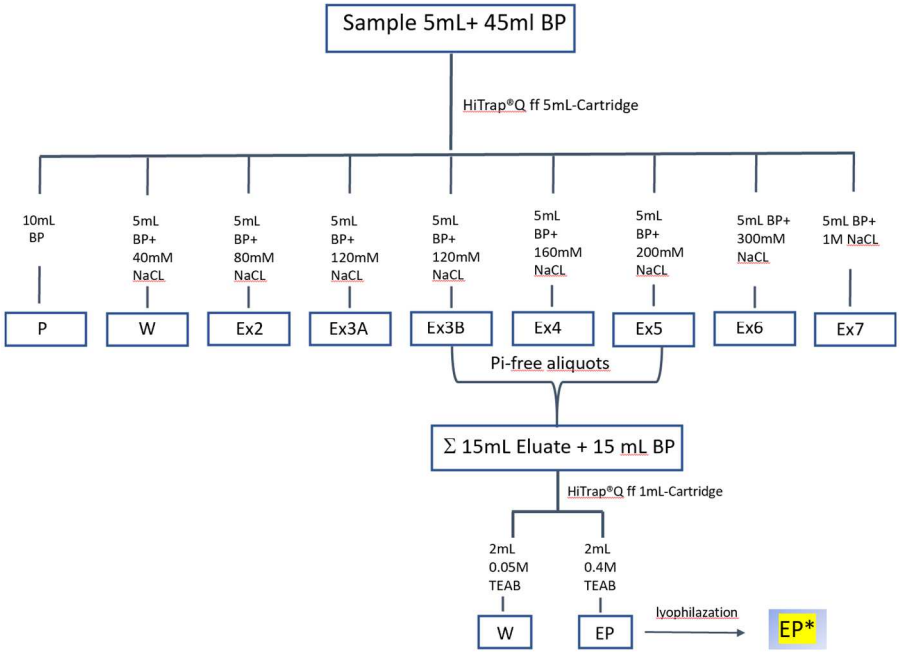

Figure 6.5 P_i -free sample preparation on strong anion exchange column (HiTrap® Q Fast Flow, 5 mL). 5 mL of a crude reaction sample was diluted with 45 mL Basis-Buffer *BP* (10mM TRIS/HCl, pH 8). The sample was eluted with increasing NaCl-concentrations and collected aliquots were analysed with ^{31}P-NMR. The P_i -free fractions were merged, diluted with *BP* and applied again on a smaller strong anion exchange column (HiTrap® Q Fast Flow, 1 mL). The sample was eluted with 0.4 M Triethyl ammonia bicarbonate buffer (TEAB) and lyophilized multiple times to obtain the eluted product (EP*)

6.7 Hydrolysis Kinetics

6.7.1 Acetyl Phosphate (AcP) Hydrolysis Kinetics

Spectra were recorded using an *AV 401* spectrometer by *Bruker* (Billerica, Massachusetts, USA) equipped with a heater for setting variable temperatures. The spectrometer was field frequency locked on the deuterium resonance of deuterium oxide (D_2O) used as a solvent. The spectra are referenced to external 85% phosphoric acid (H_3PO_4), which accomplished electronically using the lock signal without running the spectrum of the standard sample every time. All Spectra were broadband ^1H-decoupled, and the chemical shifts are given in parts per million (ppm). All FIDs are processed with an exponential multiplication prior to Fourier transform. Spectra are baseline- and phase corrected before they are fitted with the T_1/T_2 relaxation module of the software *TopSpin* (version 3.6.2).

Sample Preparation

Samples of acetyle phosphate (3.7 mg, 20 mmol) and pyrophosphate (8.92 mg, 20 mM) were dissolved in 100 mM TRIS·HCl buffer (pH 8, 10 % D_2O, 1 mL) and transferred to NMR-Tubes. For acetyl phosphate ^{31}P-NMR spectra were recorded in 5-minute intervals at *room temperature*, 30°C, 40°C, 50°C and 60°C in 60 minutes (Figure 4.27). Samples of pyrophosphate were incubated from 0-11 d at 60°C and analysed with ^{31}P-NMR spectroscopy (Figure 4.28). The pH-value of all samples (pH 8) were monitored and did not change before and after the measurements.

The samples of acetyl phosphate (3.7 mg, 20 mmol) dissolved in 100 mM TRIS·HCl buffer (10 % D_2O, 1 mL) were transferred to NMR-Tubes and measured at different temperatures (22-60°C) over a time period between 20-180 minutes.^{31}P-NMR spectra were recorded at *AV 401* spectrometer by *Bruker* (Billerica, Massachusetts, USA) equipped with a heater for setting variable temperatures. The spectrometer was field frequency locked on the deuterium resonance of deuterium oxide (D_2O) used as a solvent. The spectra are referenced to external 85% phosphoric acid (H_3PO_4), which accomplished electronically using the lock signal without running the spectrum of the standard sample every time. All Spectra were broadband ^1H-decoupled, and the chemical shifts are given in parts per million (ppm). All FIDs are processed with an exponential multiplication prior to Fourier transform. Spectra are

baseline- and phase corrected before they are fitted with the T_1/T_2 relaxation module of the software *TopSpin* (version 3.6.2) (see spectra in Appendix).

6.7 Peptide Synthesis

The Peptide sequence was synthesized using manual or automated Solid Phase Peptide Synthesis (SPPS)

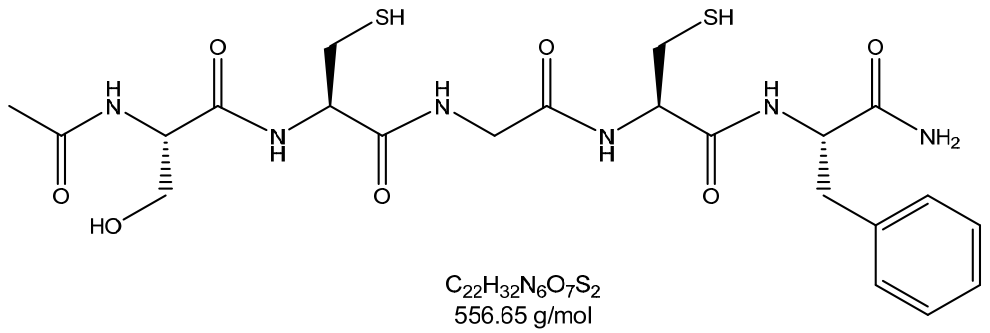

6.7.1. Manual SPPS

For 0.076 mmol scale 200 mg Rink amide resin MESH 200 (0.38 mmol/g) was swollen in DMF for 2 hours. Afterwards the swollen resin was transferred to a PE-frit BD syringe, washed (3 x DMF, 3 x NMP) and Fmoc deprotection was carried out with piperidine (20 %, in DMF, 1 mL, *v*/*v*) microwave assisted using a *Discover* microwave (MW) from *CEM* (Kamp-Lintford, Germany) at 50°C and 25 W for 300 s. Then Fmoc protected amino acids (3 eq., Tab.1) were added to a solution of HOBt (3 eq.) in DMF and dissolved with a sonicator. Then NMP (250 µL), DMF (250 µL) and DIC (58 µL) were added to the solution and directly transferred to the resin.

Tab.6.7 Initial weight of protected amino acids for peptide synthesis in a 0.076 mmol scale.

Amino Acid	*m* [mg]
Phe (Fmoc)	147.2
Cys (MMT)	233.07
Gly (Fmoc)	113.0
Cys (MMT)	233.7
Ser (But)	145.7

The double coupling process was started under microwave irradiation (50°C, 25 W, 10 min.). Afterwards the resin was washed (7 x DMF) and the double coupling process was repeated for

the residual amino acids. For the double coupling process of the amino acid *Cystein* (*MMT*) the temperature and microwave irradiation were decreased to 40 °C, 20 W for 10 min.
As soon as the peptide sequence was completed Ac_2O (1mL), DIPEA (1 ml) and NMP 80 ml) were added to the resin to block residual free amino functionalities and shaked for 10 min at room temperature. After thoroughly washing the resin with DMF (3 x 1 mL), DCM (3 x 1 mL) and MeOH (3 x 1 mL), it was dried under reduced pressure in the desiccator.

6.7.2. Automated SPPS

Peptide sequences were synthesized with automated *Liberty Blue* synthesizer by *CEM* (Matthews, North Carolina, USA) connected to a *Discover* microwave unit by *CEM*.
0.2 M amino acids solutions in DMF (Tab.6.8) were prepared. Phe (Fmoc) was filtered before use. The Rink-Amide LL (357 mg) was swollen for 1 h at room temperature and transferred to a reaction vessel.

Tab.6.8 Protected amino acids for automated peptide synthesis in a 0.25 mmol scale.

Amino Acid	***m* [mg]**
Phe (Fmoc)	360
Cys (MMT)	1540
Gly (Fmoc)	510
Ser (But)	630

For the deprotection of the protecting groups a solution of piperidine in DMF (20 %, *v*/*v*) was used. A solution of DIC (0.5 M in DMF) for amino acid activation and Oxyma (1 M in DMF) as activator base were prepared. After all solutions were set and placed at the designated positions, the synthesizer was started. The first step was the deprotection and removal of Fmoc protection group under microwave irradiation (i) 75°C, 90 W, 15s, ii) 90°C, 20 W, 50 s). After washing with DMF (4 x 4 mL) the amino acids (5 eq) were transferred together with DIC

(5eq.) and Oxyma (5 eq.) to the resin. Next the double coupling started under microwave irradiation (i) 75°C, 170 W, 15 s, ii) 90°C, 30 W, 110 s). For the attachment of Cys (MMT) the microwave conditions were reduced to 50°C, 30 W, 110 s. After the peptide sequence was finished, the resin was transferred to a PE-frit BD syringe, washed thoroughly with DCM (7 x 2 mL), MeOH (3 x 2 mL) and dried under reduced pressure in the desiccator.

6.7.3 Cleavage from Resin

The peptide sequence was cleaved from resin in an BD syringe equipped with PE-frit. A cleavage mixture containing TFA/H_2O/EDT/TIS (94 : 2.5 : 2.5 : 1) was prepared and added to the resin. Afterwards the resin shaked at least for 2 h, but not longer than 3 h at room temperature. After treated with the cleavage cocktail, the solution was filtered from the resin, washed with the cleavage mixture (2 x 3 mL), collected in a tube and concentrated in a nitrogen stream. Thereafter, the crude peptide was precipitated with icecold diethylether (or methyl *tert*-butyl ether) and centrifuged (9000 rpm, 30 min, -15°C). In the next step the pellet was separated from the solvent and dried under reduced pressure in desiccator. The crude peptide was stored under oxygenfree atmosphere to avoid disulfide bridge formation between the sulfides of the cysteins in the peptide.

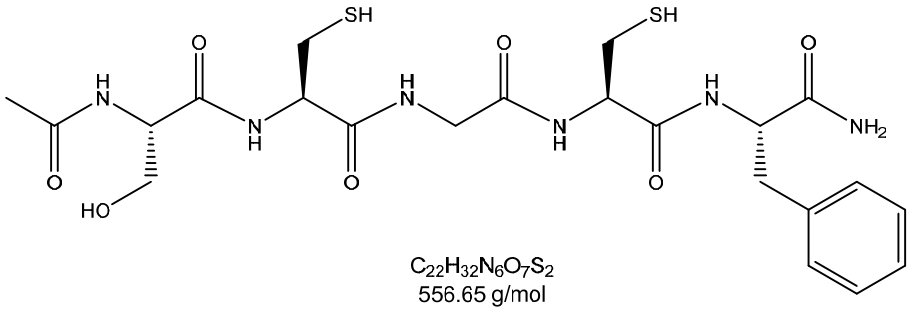

$C_{22}H_{32}N_6O_7S_2$
556.65 g/mol

The crude peptide was dissolved in MeOH and purified *via* HPLC. The HPLC conditions are described in the following:

Column:	MN Nucleodur, C18, 250 x 4.6 mm, 100 Å, 5 µm
Gradient:	10 → 90 % MeCN in 50 min

Solvent A: H_2O + 0.1 % TFA

Solvent B: MeCN

With a retention time (t_R) of 16 min the peptide eluated from column and was analysed further with ESI-MS.

Analytical data

MS (ESI): *m/z* (*%*) = 557.2 (21) $[M+H]^+$, 579.2 (99) $[M+Na]^+$.

HR-MS (ESI): calc. for $C_{22}H_{32}N_6O_7S_2$ $[M+H]^+$: 557.1847, found: 557.1843;

calc. for $C_{22}H_{32}N_6O_7S_2Na$ $[M+Na]^+$: 579.1666, found: 579.1667.

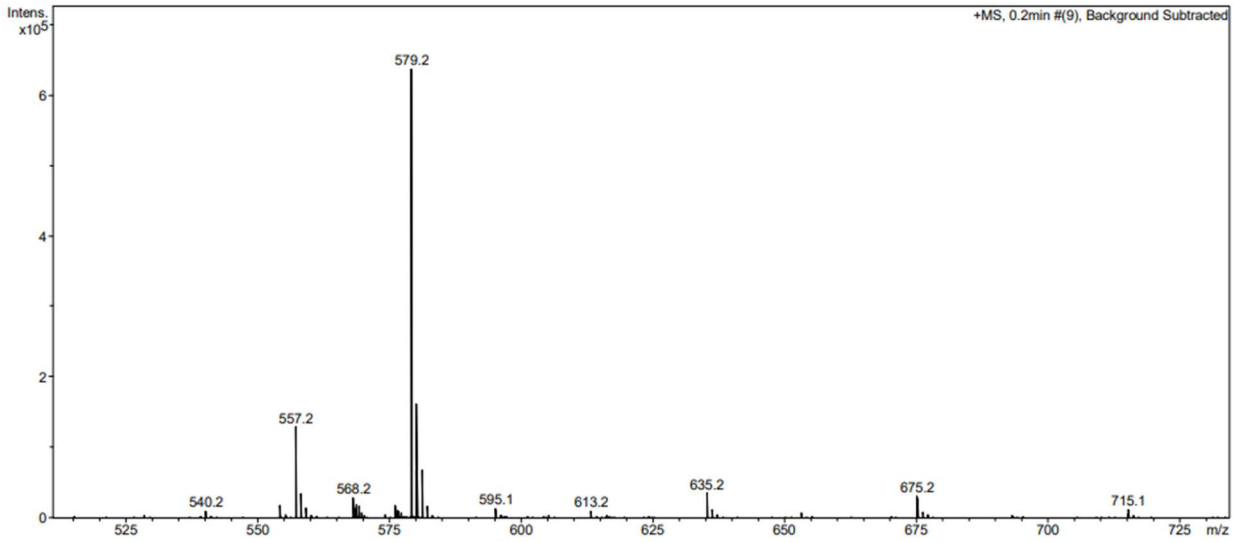

Figure 6.6 In the ESI-MS spectrum from the synthesized peptide the peaks for 579.2 $[M+Na]^+$ and 557.2 $[M+H]^+$ were detected.

6.8. Experiments towards Peptidic Minimal Models of Acetyl-CoA Synthase (ACS)

The synthesis of peptide coordinated products were highly sensitive to oxygen and therefore performed in a Glovebox.

1. Step

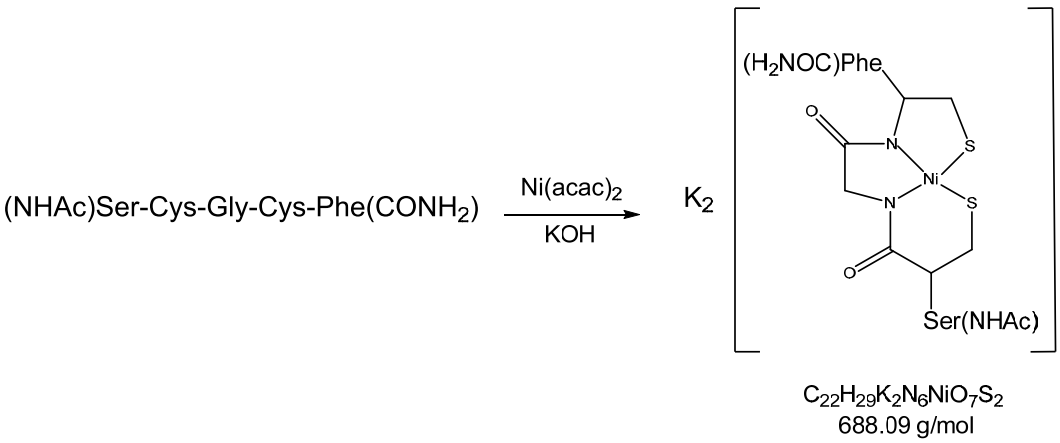

$C_{22}H_{29}K_2N_6NiO_7S_2$
688.09 g/mol

The synthesized and purified peptide (12 mg, 0.01 mol, see Experimental Section 6.7) was dissolved in dry toluol (1 mL). $Ni(acac)_2$ (5 mg, 0.02 mmol) was also dissolved in dry DMF (1 mL) and added to the peptide solution. The clear solution turned subsequently to red and after 30 min KOH (2.2 mg, 0.04 mol) was added to the solution. The mixture stirred for 12 h at room temperature in the Glovebox.

After separation of the solid KOH, dry diethylether was added to precipitate the product (5.5 mg, 0.008 mmol) as highly pink solid.

Analytical data

MS (ESI, negative mode): *m/z* (*%*) = 611.1 (11) $[M\text{-}K_2]^{2-}$.

HR-MS (ESI): calc. for $C_{22}H_{29}N_6O_7S_2Ni$ $[M\text{-}K_2]$: 611.0887, found: 611.0891.

UV-Vis: λ_{max} = 450 nm, 350 nm, 250 nm.

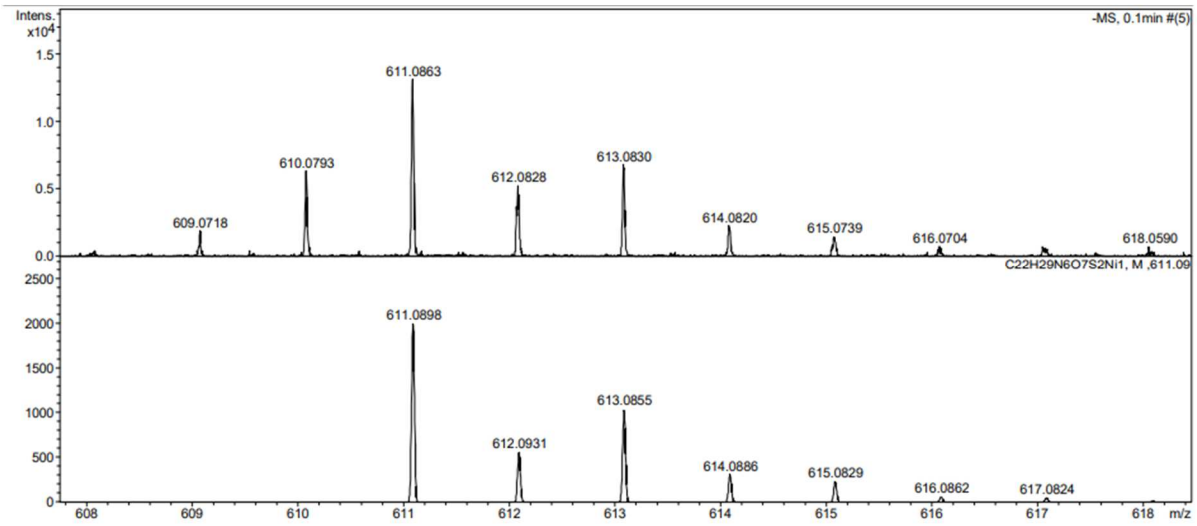

Figure 6.7 In the ESI-MS spectrum from the nickel complex the calculated peak for m/z $[M-K_2]^-$ 611.0863 was detected.

2. Step

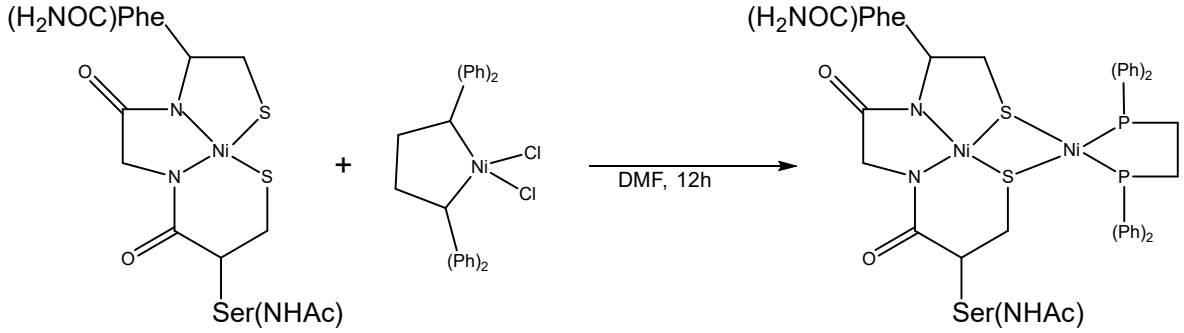

$C_{49}H_{55}N_6Ni_2O_7P_2S_2$
1083.18 g/mol

To K_2[Ni(SCGCF)] (5.5 mg, 0.008 mmol) dissolved in DMF (2 mL) was 1,2-Bis(diphenylbosphino)ethane nickel(II) chloride (4 mg, 0.007 mmol) dissolved in DMF (2 mL) added. The reaction mixture was stirred for 12 h at room temperature in the glovebox. Afterwards diethylether was added to precipitate the product, which was washed with MeCN and dried under reduced pressure in the desiccator.

Analytical data

MS (ESI): *m/z* (*%*) = 1083.2 (11) [M].

HR-MS (ESI): calc. for $C_{49}H_{55}N_6O_7S_2Ni_2P_2$ [M]: 1083.1709, found: 1083.1701.

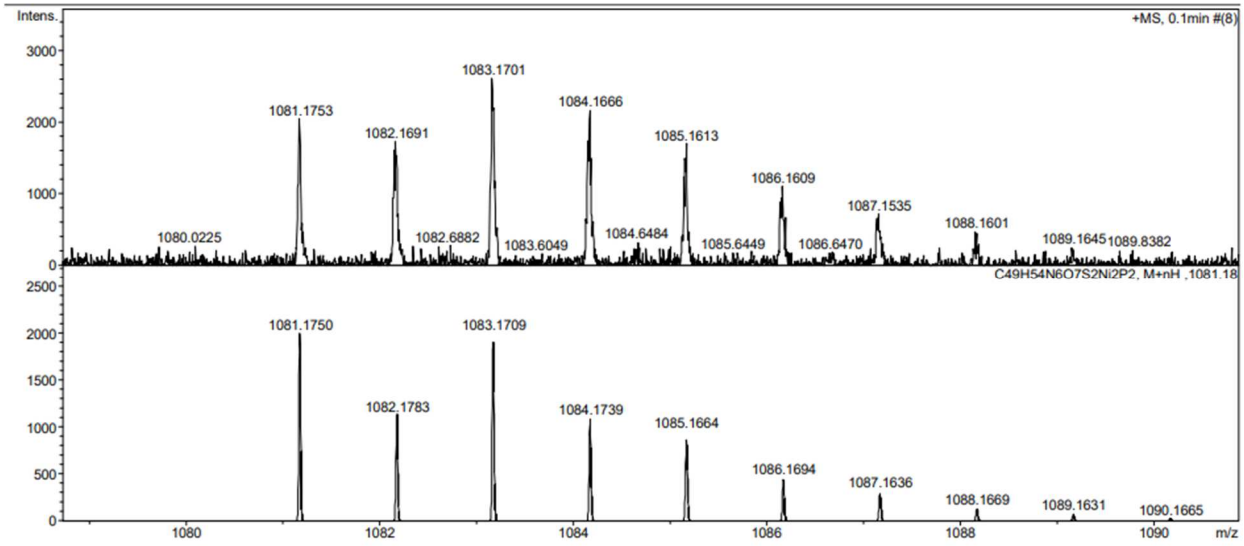

Figure 6.8 In the ESI-MS spectrum from the nickel complex the calculated peak for m/z [M] 1083.1701 was detected.

Appendix

A.1. Calibration measurements of fluorescent *Pyrophosphate Sensor Assay*

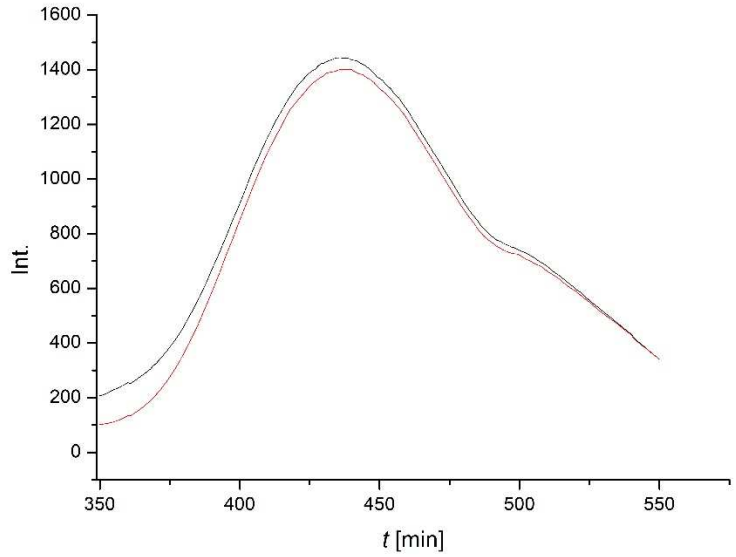

Figure A.1 Fluorescent PPi-sensor in water (red course) and in 100 mM TRIS (pH 8, black course) at λ_{EX} = 304 nm.

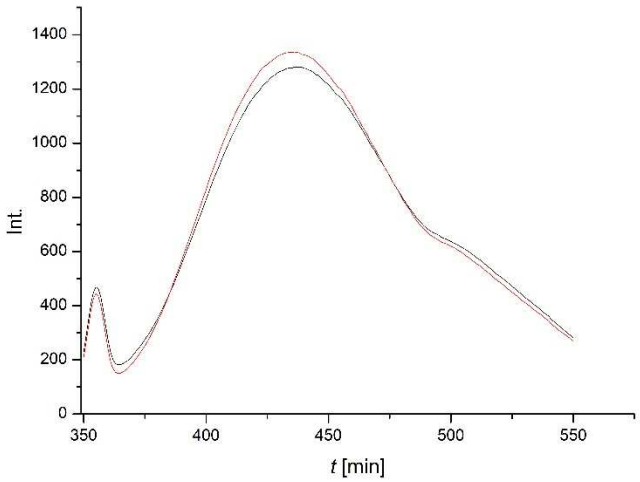

Figure A.2: Fluorescent PPi-sensor in water (red course) and in 100 mM TRIS (pH 8, black course) at λ_{EX} = 316 nm.

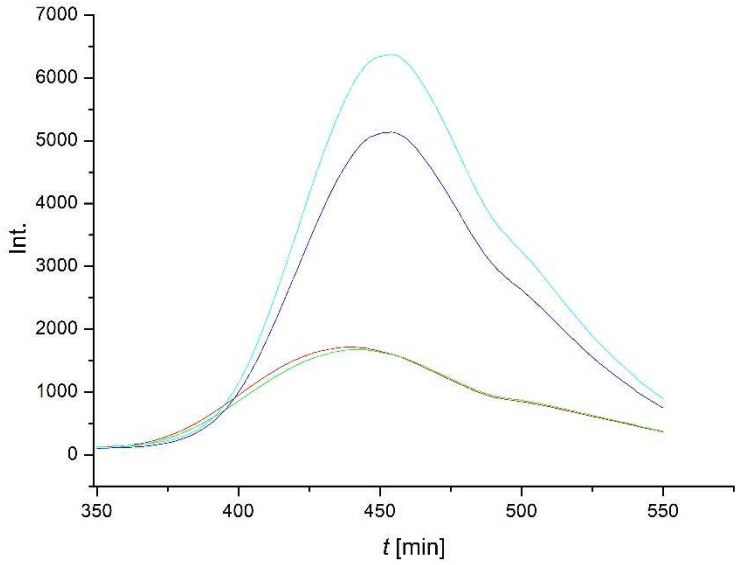

Figure A.3 PPi Fluorescent PPi-sensor + 0.5 µM PP_i (red course), 1 µM PP_i (green course), 5 µM PP_i (blue course) and 10 µM PP_i (light blue course at λ_{EX} = 304 nm, pH 8.

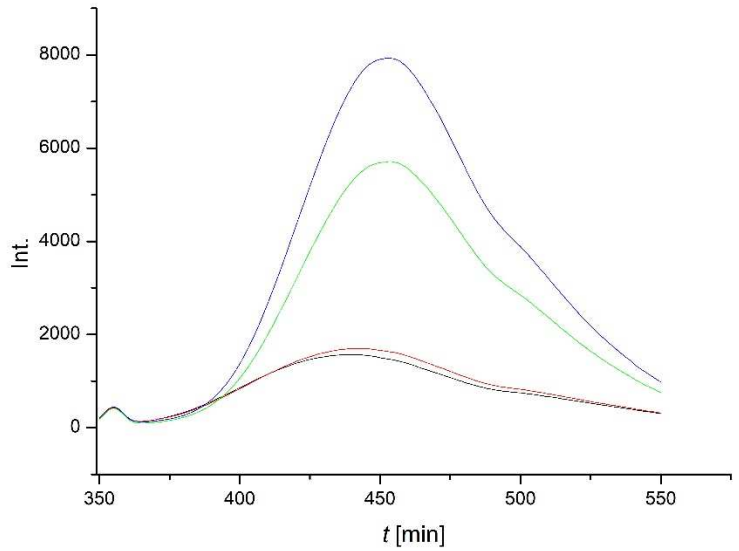

Figure A.4 PPi Fluorescent PPi-sensor + 0.5 µM PP_i (black course), 1 µM PP_i (red course), 5 µM PP_i (green course) and 10 µM PP_i (blue course at λ_{EX} = 316 nm.

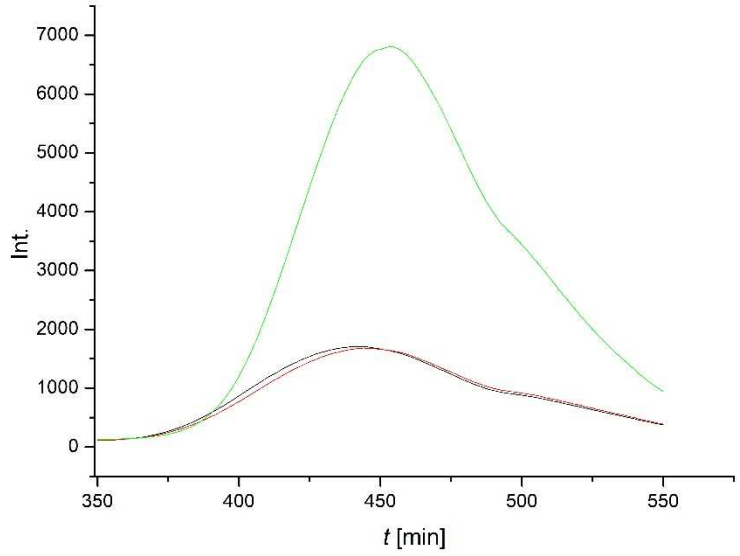

Figure A.5 PPi Fluorescent PPi-sensor + 0.5 µM PP_i (black course), 1 µM PP_i (red course), 10 µM PP_i (green course) and 10 µM PP_i (light blue course at λ_{EX} = 304 nm and pH 10.

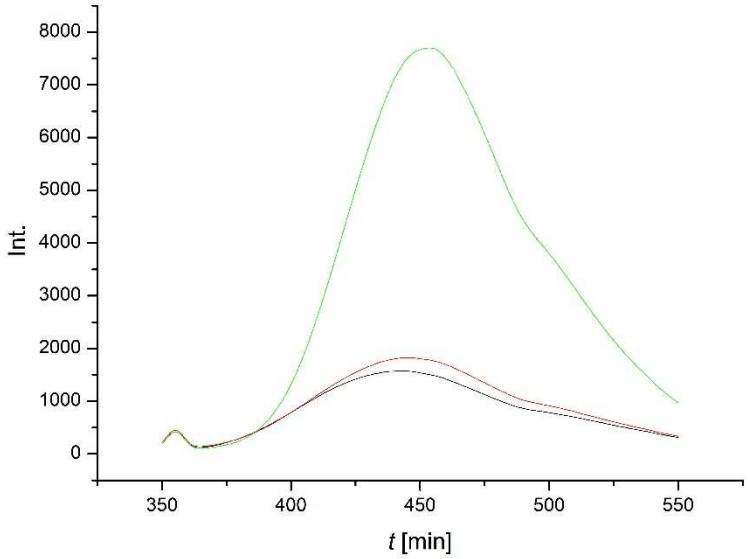

Figure A.6 Fluorescent PPi-sensor + 0.5 µM PP_i (black course), 1 µM PP_i (red course), 10 µM PP_i (green course) and 10 µM PP_i (light blue course at λ_{EX} = 316 nm and pH 10.

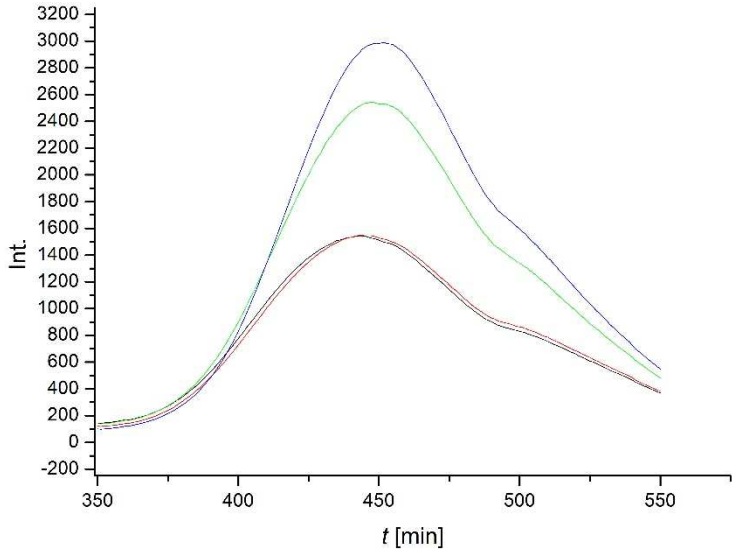

Figure A.6 Fluorescent PPi-sensor + 10 mM P_i (black course), 20 mM PP_i (red course), 50 mM PP_i (green course) and 100 mM PP_i (light blue course at λ_{EX} = 304 nm.

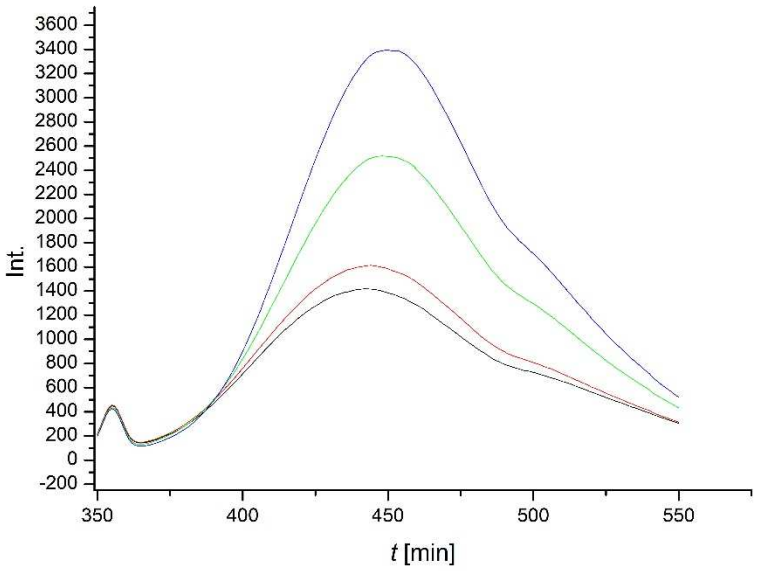

Figure A.7 Fluorescent PPi-sensor + 10 mM P_i (black course), 20 mM P_i (red course), 50 mM PP_i (green course) and 100 mM PP_i (light blue course at λ_{EX} = 316 nm

A.2 Further Kinetical measurements of prebiotic reaction

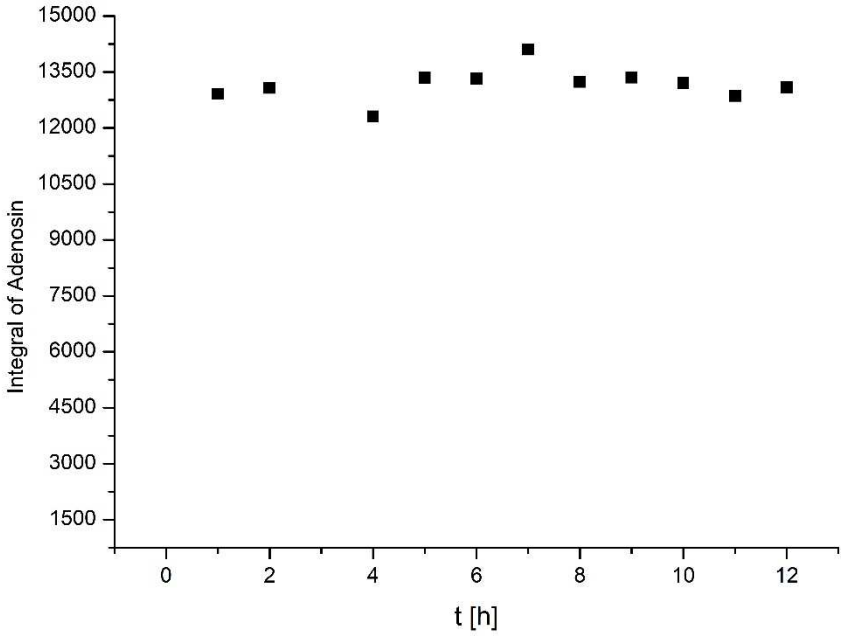

Figure A. 8 Absorbance integral of adenosine signals against time as a measure of reaction progress.

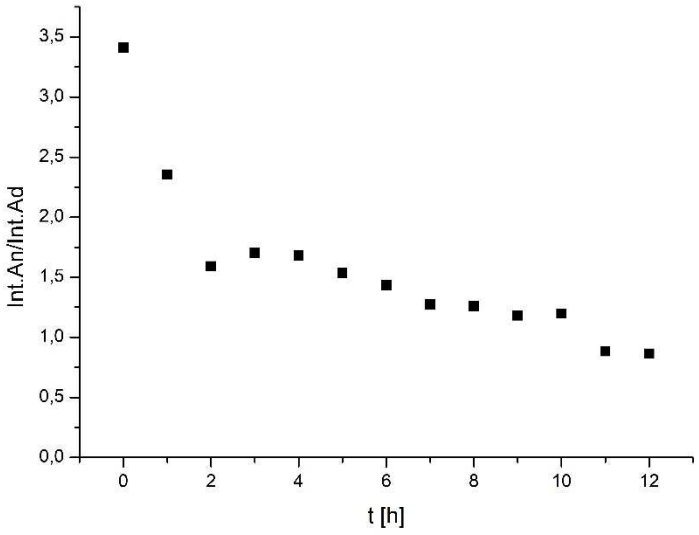

Figure A.9 Absorbance integral of adenosine signals against absorbance integral of aniline signals against time as a measure of reaction progress.

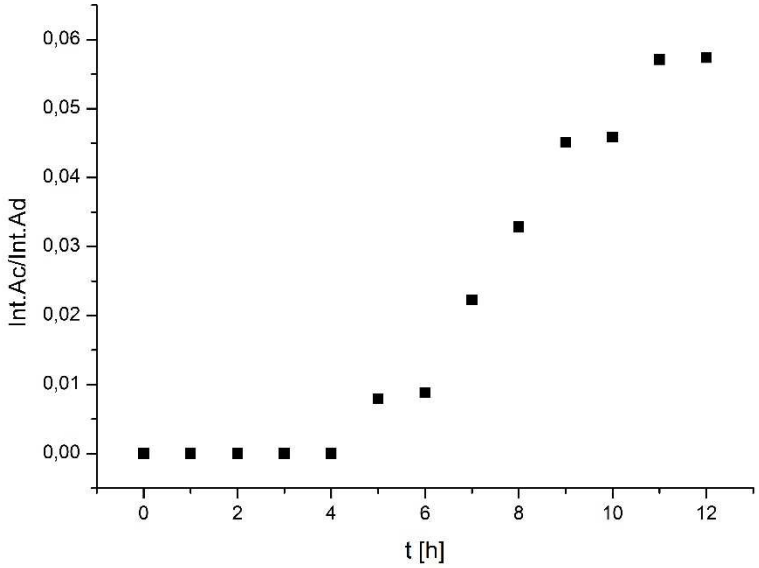

Figure A.10 Absorbance integral of adenosine signals against absorbance integral of N-acetylaniline signals against time as a measure of reaction progress

A.3 ^{31}P-NMR of PPi, Pi and AcP

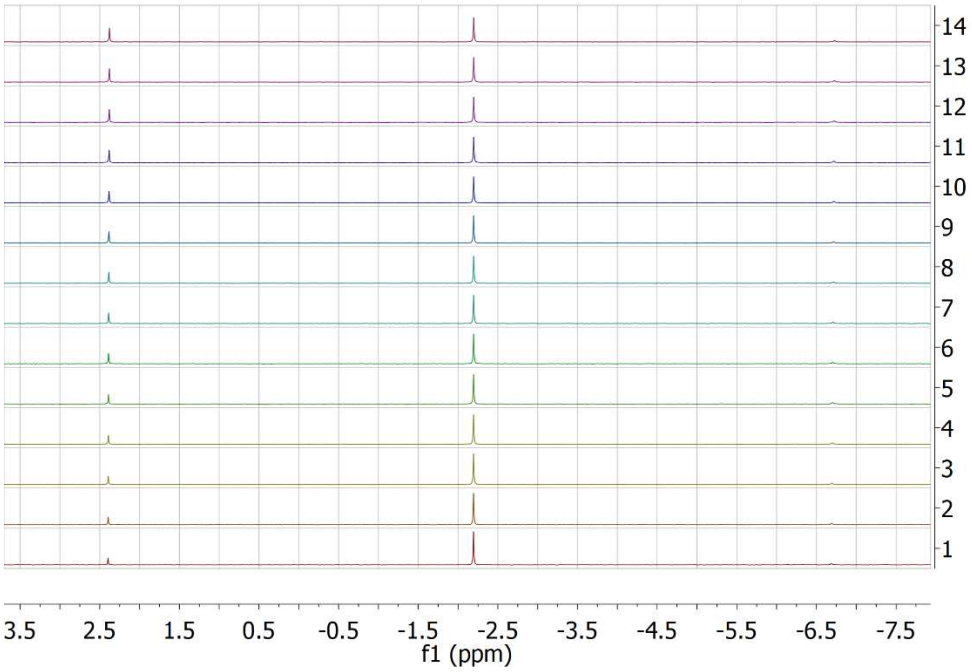

A.11 Stacked ^{31}P-NMR spectra from 20 mM AcP (in 25 mM TRIS, pH 8) at 30°C. In 5 min intervals spectra were recorded for 80 min. The signal at ~2.05 ppm is attributed to Pi, at ~1.8 ppm to AcP and at ~-6.95 ppm to PPi.

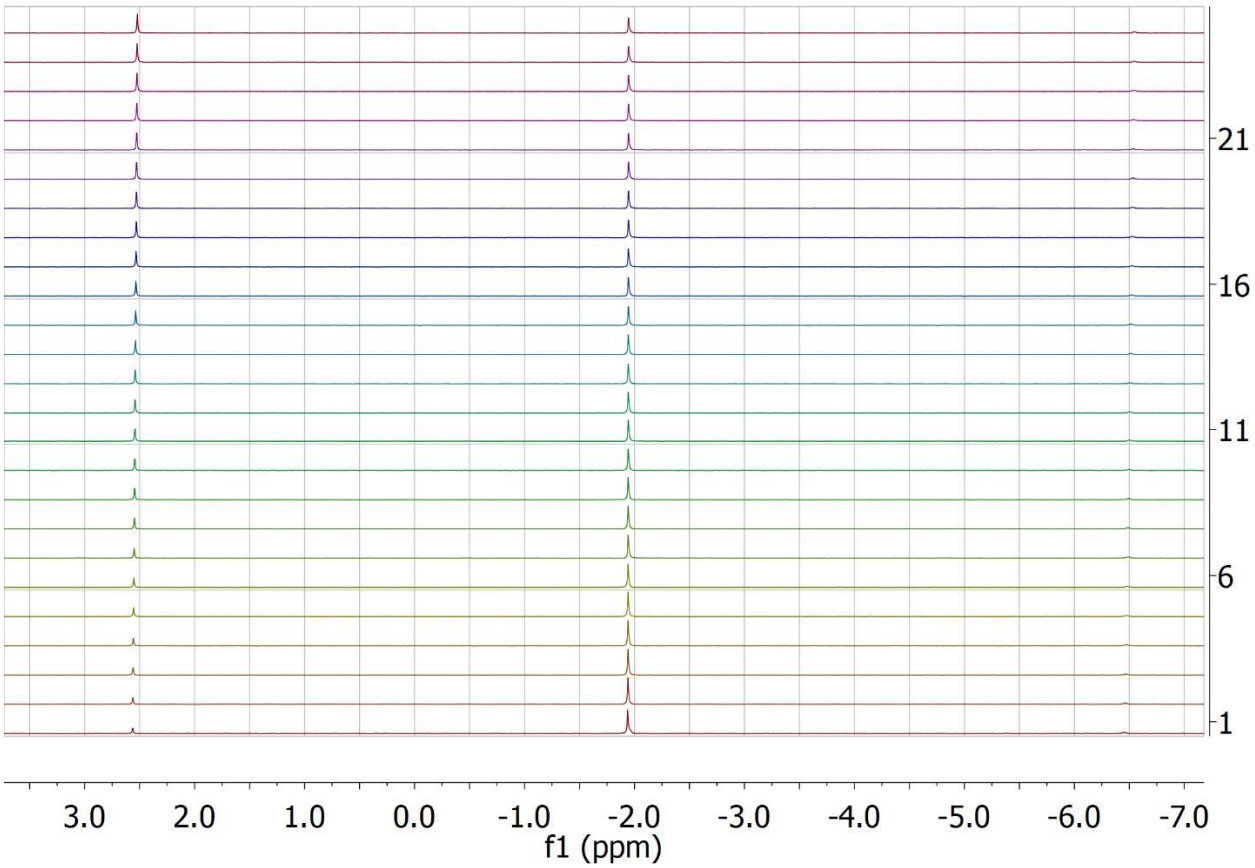

A.12 Stacked ^{31}P-NMR spectra from 20 mM AcP (in 25 mM TRIS, pH 8) at 60°C. In 5 min intervals spectra were recorded for 80 min. The signal at ~2.05 ppm is attributed to Pi, at ~1.8 ppm to AcP and at ~-6.95 ppm to PPi.

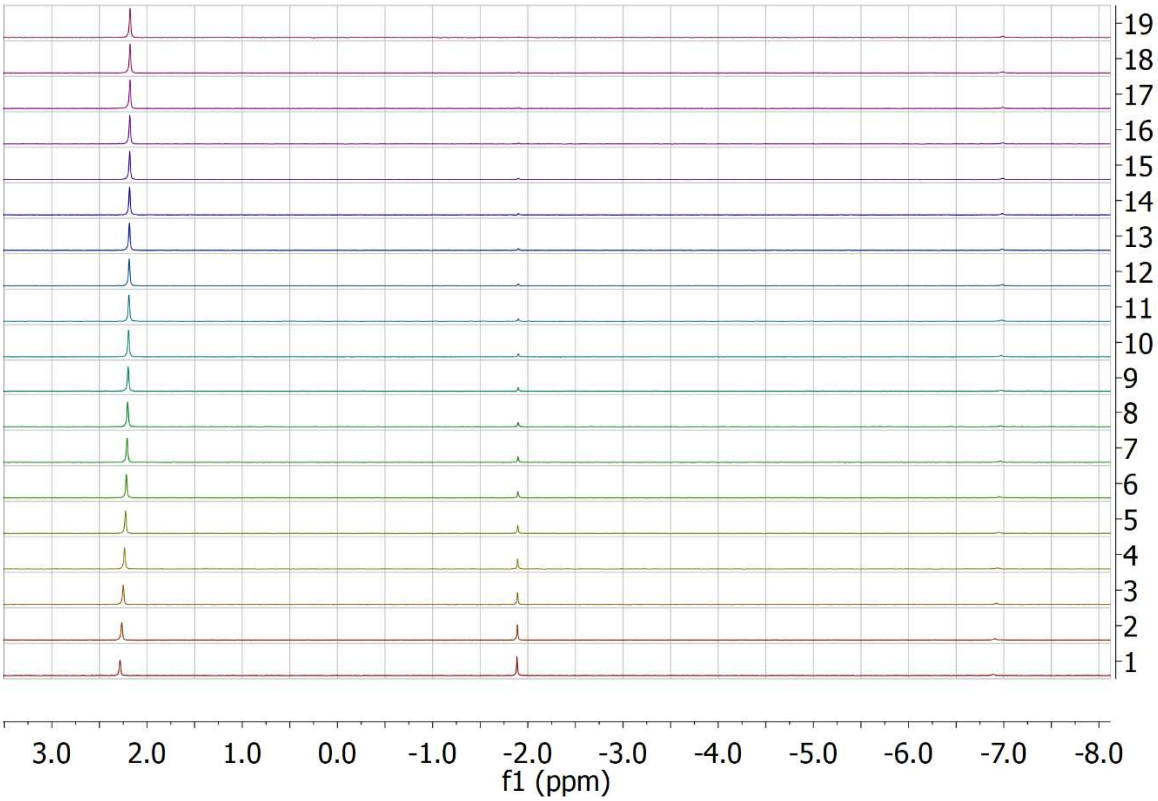

A.13 Stacked ^{31}P-NMR spectra from 20 mM AcP (in 25 mM TRIS, pH 8) at 50°C. In 5 min intervals spectra were recorded for 60 min. The signal at ~2.05 ppm is attributed to Pi, at ~1.8 ppm to AcP and at ~-6.95 ppm to PPi.

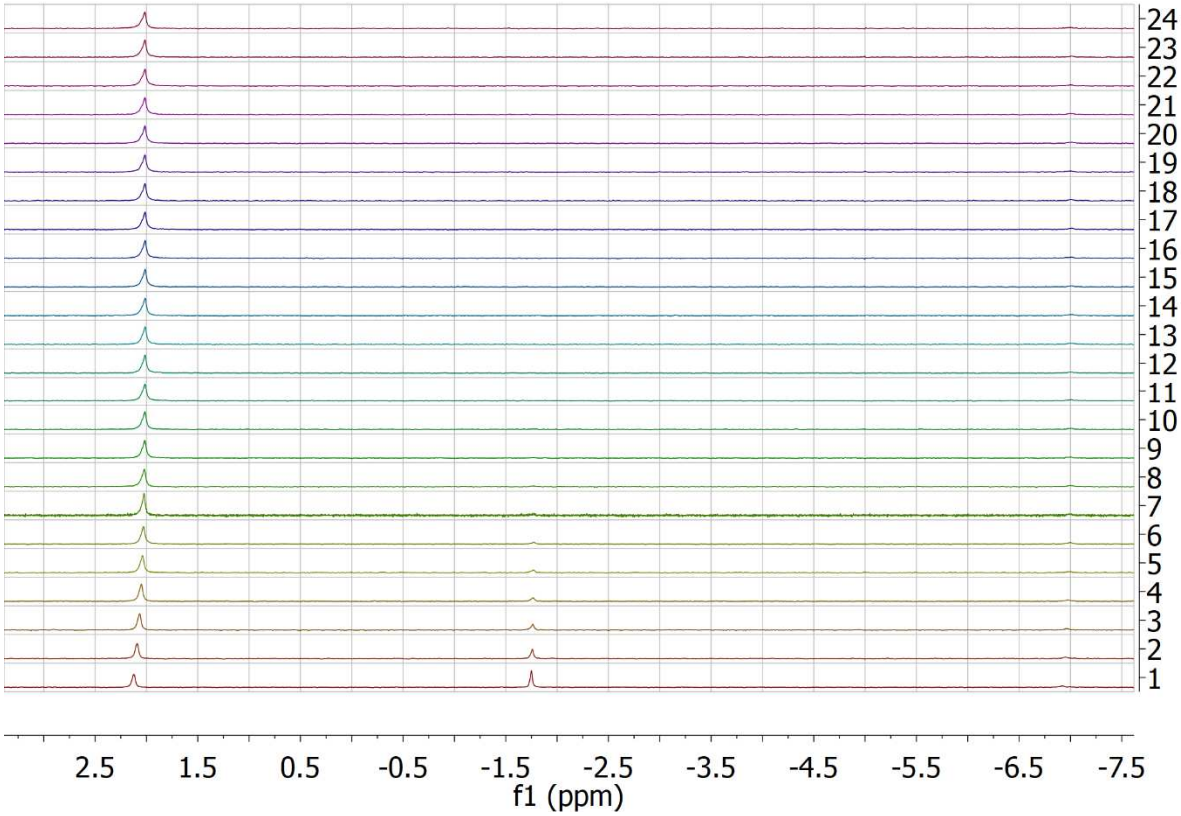

A.14 Stacked ^{31}P-NMR spectra from 20 mM AcP (in 25 mM TRIS, pH 8) at 60°C. In 5 min intervals spectra were recorded for 60 min. The signal at ~2.05 ppm is attributed to Pi, at ~1.8 ppm to AcP and at ~-6.95 ppm to PPi.

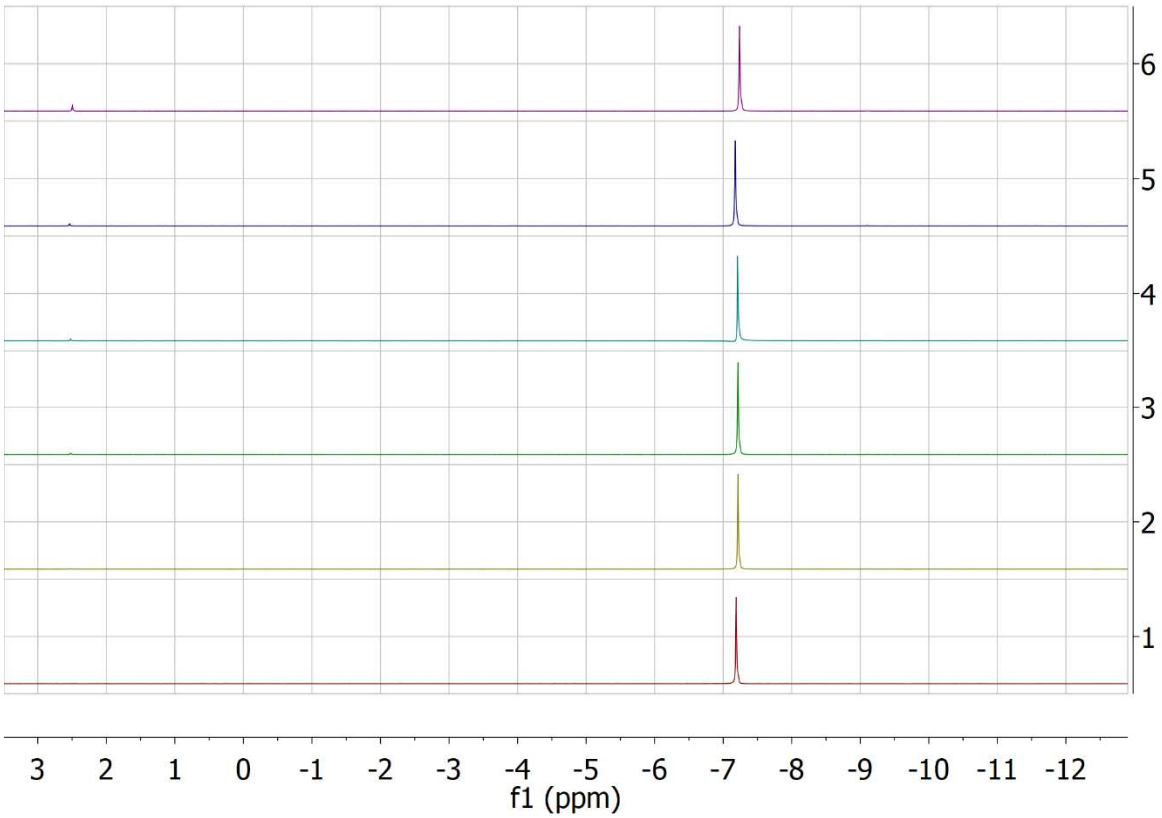

A.15 Stacked ^{31}P-NMR spectra from 20 mM PPi (H_2O, pH 7) at 60°C. The spectra were recorded after 0, 1, 3, 4, 5 and 10 days. The signal at ~2.5 ppm is attributed to Pi and at ~-7.21 ppm to PPi.

Abbreviations

AcP	acetyl phosphate
ACS	acetyl-CoA synthase
ADP	Adenosine diphosphate
AMP	Adenosine monophosphate
ATP	Adenosine triphosphate
CO	Carbon monoxide
CoA	Coenzyme A
CODH	carbon monoxide dehydrogenase
DCM	dichloromethane
DIC	N, N diisopropylcarbodiimid
DIPEA	N,N-diisopropylethylamine
DMF	dimethylformamide
EDT	1,2-ethanedithiole
ESI-MS	electrospray ionisation mass spectrometry
FeS	Iron sulfide
Fmoc	9-fluorenylmethoxycarbonyl protection group
Ga	"giga anum", billion years
gasphase-IR	Gasphasen Infrared Spectroscopy
HATU	1-(bis(dimethylamino)methylene)-1H-1,2,3-triazolo[4,5-b]
HOBt	1-Hydroxybenzotriazol
HPLC	high performance liquid chromatography
HR-MS	high resolution mass spectrometry
LC-MS)	Liquid Chromatography Mass Spectrometry
LMCT	ligand-metal-charge-transfer
LUCA	Last Universal Common Ancestor
MeCN	acetonitrile
MeOH	methanol

MMT	Monomethoxytrityl
Ni(COD)2	bis(cyclooctadiene)nickel(0)
Ni(dppe)Cl2	1,2-Bis(diphenylbosphino)ethane nickel(II)
NiS	Nickel sulfide
NMP	N-methylpyrrolidone
NMR	nuclear magnetic resonance
Pi	orthophosphate
PPi	inorganic Pyrophosphate
rp	reversed phase
rt	room temperature
SAX	strong anion exchange
SPPS	Solid Phase Peptide Synthesis
TEAB	triethyl ammonia bicarbonate
TEAC	trietyl ammonium citrate
TFA	trifluoroacetic acid
TIS	triisopropylsilane
TLV	threshold limit value
tR	retention times
TRIS	2-Amino-2-(hydroxymethyl)propane-1,3-diol
WLP	Wood-Ljungdahl pathway

References

[1] K. Matsuno, K. Dose, K. Harada, D. L. Rohlfing, *Molecular Evolution and Protobiology*, Springer US, Boston, MA, 1984.

[2] J. O. Nriagu, P. B. Moore (Eds.) *Phosphate Minerals*, Springer Berlin Heidelberg, Berlin, Heidelberg, s.l., **1984**.

[3] A. L. Weber, *Journal of molecular evolution* **1981**, *18*, 24–29.

[4] A. L. Weber, *Biosystems* **1982**, *15*, 183–189.

[5] S. L. MILLER, M. PARRIS, *Nature* **1964**, *204*, 1248–1250.

[6] J. P. Ferris, *Science (New York, N.Y.)* **1968**, *161*, 53–54.

[7] A. D. Keefe, S. L. Miller, *Journal of molecular evolution* **1995**, *41*, 693–702.

[8] C. Huber, G. Wächtershäuser, *Science (New York, N.Y.)* **1997**, *276*, 245.

[9] C. de Duve, *Blueprint for a cell*. *The nature and origin of life*, N. Patterson, Burlington, N.C., **1991**.

[10] K. Zahnle, N. Arndt, C. Cockell, A. Halliday, E. Nisbet, F. Selsis, N. H. Sleep, *Space Sci Rev* **2007**, *129*, 35–78.

[11] N. T. Arndt, E. G. Nisbet, *Annu. Rev. Earth Planet. Sci.* **2012**, *40*, 521–549.

[12] a) S. J. Mojzsis, T. M. Harrison, R. T. Pidgeon, *Nature* **2001**, *409*, 178–181; b) M. M. Hirschmann, *Annu. Rev. Earth Planet. Sci.* **2006**, *34*, 629–653;

[13] a) J. D. Bernal, *Proceedings of the Physical Society. Section B* **1949**, *62*, 597–618; b) H. C. Urey, *Proceedings of the National Academy of Sciences* **1952**, *38*, 351;

[14] T. M. McCollom, *Annu. Rev. Earth Planet. Sci.* **2013**, *41*, 207–229.

[15] S. L. Miller, *Science (New York, N.Y.)* **1953**, *117*, 528–529.

[16] P. H. Abelson, *Proceedings of the National Academy of Sciences* **1966**, *55*, 1365.

[17] J. C. G. Walker, *Evolution of the atmosphere / James C. G. Walker*, Macmillan, New York, **1977**.

[18] J. F. Kasting, *Science (New York, N.Y.)* **1993**, *259*, 920.

[19] M. J. Russell, A. J. Hall, *Journal of the Geological Society* **1997**, *154*, 377–402.

[20] T. Tashiro, A. Ishida, M. Hori, M. Igisu, M. Koike, P. Méjean, N. Takahata, Y. Sano, T. Komiya, *Nature* **2017**, *549*, 516–518.

[21] M. Schidlowski, P. W. Appel, R. Eichmann, C. E. Junge, *Geochimica et Cosmochimica Acta* **1979**, *43*, 189–199.

[22] S. J. Mojzsis, G. Arrhenius, K. D. McKeegan, T. M. Harrison, A. P. Nutman, C. R. Friend, *Nature* **1996**, *384*, 55–59.

[23] E. J. Javaux, A. H. Knoll, M. R. Walter, *Nature* **2001**, *412*, 66–69.

[24] a) M. R. Walter, R. Buick, J. S. R. Dunlop, *Nature* **1980**, *284*, 443–445; b) D. R. Lowe, *Nature* **1980**, *284*, 441–443; c) J.-P. Duda, M. J. van Kranendonk, V. Thiel, D. Ionescu, H. Strauss, N. Schäfer, J. Reitner, *PloS one* **2016**, *11*, e0147629;

[25] J. L. Bada, *Earth and Planetary Science Letters* **2004**, *226*, 1–15.

[26] R. Amils in *Springer reference* (Ed.: M. Gargaud), Springer, Berlin, **2011**.

[27] G. Wächtershäuser, *Systematic and Applied Microbiology* **1988**, *10*, 207–210.

[28] a) G. Wächtershäuser, *Proceedings of the National Academy of Sciences* **1990**, *87*, 200–204; b) G. Wächtershäuser, *Microbiological reviews* **1988**, *52*, 452–484;

[29] G. Wächtershäuser, *Philosophical Transactions of the Royal Society B: Biological Sciences* **2006**, *361*, 1787-806; discussion 1806-8.

[30] G. Wächtershäuser in *Frontiers of Life*, **1992**.

[31] L. M. Barge, E. Branscomb, J. R. Brucato, S. S. S. Cardoso, J. H. E. Cartwright, S. O. Danielache, D. Galante, T. P. Kee, Y. Miguel, S. Mojzsis et al., *Origins Life Evol Biosphere* **2017**, *47*, 39–56.

[32] S. B. Hedges, *Nature reviews. Genetics* **2002**, *3*, 838–849.
[33] J. M. Edmond, C. Measures, R. E. McDuff, L. H. Chan, R. Collier, B. Grant, L. I. Gordon, J. B. Corliss, *Earth and Planetary Science Letters* **1979**, *46*, 1–18.
[34] V. Sojo, B. Herschy, A. Whicher, E. Camprubí, N. Lane, *Astrobiology* **2016**, *16*, 181–197.
[35] K. L. Rogers, M. D. Schulte, *Geobiology* **2012**, *10*, 320–332.
[36] W. Heinen, A. M. Lauwers, *Origins of life and evolution of the biosphere : the journal of the International Society for the Study of the Origin of Life* **1996**, *26*, 131–150.
[37] a) S. W. Fox, *The Origins of Prebiological Systems and of Their Molecular Matrices*. *Proceedings of a Conference Conducted at Wakulla Springs, Florida, on 27-30 October 1963 under the Auspices of the Institute for Space Biosciences, the Florida State University and the National Aeronautics and Space Administration*, Elsevier Science, Burlington, **2013**; b) T. M. McCollom, J. S. Seewald, *Chemical reviews* **2007**, *107*, 382–401; c) M. J. Russell, W. Martin, *Trends in biochemical sciences* **2004**, *29*, 358–363;
[38] Woods Hole Oceanographic Institution, "The Cauldron Beneath the Seafloor", to be found under https://www.whoi.edu/oceanus/feature/the-cauldron-beneath-the-seafloor/, **2021**.
[39] W. Bach, G. L. Fruh-Green, *Elements* **2010**, *6*, 173–178.
[40] a) J. L. Palandri, M. H. Reed, *Geochimica et Cosmochimica Acta* **2004**, *68*, 1115–1133; b) M. Schulte, D. Blake, T. Hoehler, T. McCollom, *Astrobiology* **2006**, *6*, 364–376;
[41] W. Martin, M. J. Russell, *Philosophical transactions of the Royal Society of London. Series B, Biological sciences* **2007**, *362*, 1887–1925.
[42] M. C. Weiss, M. Preiner, J. C. Xavier, V. Zimorski, W. F. Martin, *PLOS Genetics* **2018**, *14*, e1007518.
[43] G. E. Fox, E. Stackebrandt, R. B. Hespell, J. Gibson, J. Maniloff, T. A. Dyer, R. S. Wolfe, W. E. Balch, R. S. Tanner, L. J. Magrum et al., *Science (New York, N.Y.)* **1980**, *209*, 457–463.
[44] M. C. Weiss, F. L. Sousa, N. Mrnjavac, S. Neukirchen, M. Roettger, S. Nelson-Sathi, W. F. Martin, *Nat Microbiol* **2016**, *1*, 16116.
[45] C. Woese, *Proceedings of the National Academy of Sciences* **1998**, *95*, 6854–6859.
[46] O. Kandler, *J Biol Phys* **1995**, *20*, 165–169.
[47] G. Fuchs, *Annual review of microbiology* **2011**, *65*, 631–658.
[48] J. A. Baross, S. E. Hoffman, *Origins Life Evol Biosphere* **1985**, *15*, 327–345.
[49] S. W. Ragsdale, E. Pierce, *Biochimica et biophysica acta* **2008**, *1784*, 1873–1898.
[50] H. L. Drake, A. S. Gössner, S. L. Daniel, *Annals of the New York Academy of Sciences* **2008**, *1125*, 100–128.
[51] L. G. Ljungdahl, *Annual review of microbiology* **1986**, *40*, 415–450.
[52] H. G. Wood, *FASEB journal : official publication of the Federation of American Societies for Experimental Biology* **1991**, *5*, 156–163.
[53] a) J. R. Andreesen, L. G. Ljungdahl, *Journal of Bacteriology* **1973**, *116*, 867–873; b) I. Yamamoto, T. Saiki, S. M. Liu, L. G. Ljungdahl, *The Journal of biological chemistry* **1983**, *258*, 1826–1832;
[54] R. H. Himes, J. A. Harmony, *CRC critical reviews in biochemistry* **1973**, *1*, 501–535.
[55] a) M. R. Moore, W. E. O'Brien, L. G. Ljungdahl, *The Journal of biological chemistry* **1974**, *249*, 5250–5253; b) S. W. Ragsdale, L. G. Ljungdahl, *The Journal of biological chemistry* **1984**, *259*, 3499–3503;
[56] J. E. Clark, L. G. Ljungdahl, *The Journal of biological chemistry* **1984**, *259*, 10845–10849.
[57] P. A. Lindahl, *Angew. Chem.* **2008**, *120*, 4118–4121.
[58] a) C. L. Drennan, J. Heo, M. D. Sintchak, E. Schreiter, P. W. Ludden, *Proceedings of the National Academy of Sciences* **2001**, *98*, 11973–11978; b) H. Dobbek, V. Svetlitchnyi, L. Gremer, R. Huber, O. Meyer, *Science (New York, N.Y.)* **2001**, *293*, 1281–1285;

[59] S. W. Ragsdale, L. G. Ljungdahl, D. V. DerVartanian, *Biochemical and biophysical research communications* **1983**, *115*, 658–665.
[60] a) H. Dobbek, V. Svetlitchnyi, J. Liss, O. Meyer, *Journal of the American Chemical Society* **2004**, *126*, 5382–5387; b) J. Sun, C. Tessier, R. H. Holm, *Inorganic chemistry* **2007**, *46*, 2691–2699;
[61] S. W. Ragsdale, *Journal of inorganic biochemistry* **2007**, *101*, 1657–1666.
[62] T. I. Doukov, T. M. Iverson, J. Seravalli, S. W. Ragsdale, C. L. Drennan, *CRYSTAL STRUCTURE OF BIFUNCTIONAL CARBON MONOXIDE DEHYDROGENASE/ACETYL-COA SYNTHASE(CODH/ACS) FROM MOORELLA THERMOACETICA (F. CLOSTRIDIUM THERMOACETICUM)*, **2003**.
[63] V. Svetlitchnyi, H. Dobbek, W. Meyer-Klaucke, T. Meins, B. Thiele, P. Rmer, R. Huber, O. Meyer, *Crystal Structure of the monomeric acetyl-CoA synthase from Carboxydothermus hydrogenoformans*, **2003**.
[64] *Limnol. Oceanogr.* **1989**, *34*, 1150–1152.
[65] W. G. Dougherty, K. Rangan, M. J. O'Hagan, G. P. A. Yap, C. G. Riordan, *Journal of the American Chemical Society* **2008**, *130*, 13510–13511.
[66] D. EVANS, *Coordination Chemistry Reviews* **2005**, *249*, 1582–1595.
[67] J. M. Berg, J. L. Tymoczko, G. J. Gatto jr., L. Stryer, *Stryer Biochemie,* 8. Auflage ed., Springer Spektrum, Berlin, **2018**.
[68] D. Deamer, A. L. Weber, *Cold Spring Harbor perspectives in biology* **2010**, *2*, a004929.
[69] A. E. Senior, S. Nadanaciva, J. Weber, *Biochimica et Biophysica Acta (BBA) - Bioenergetics* **2002**, *1553*, 188–211.
[70] *Energy conversion leading to the origin and early evolution of life: did inorganic pyrophosphate precede adenosine triphosphate*, **1996**.
[71] W. Junge, H. Lill, S. Engelbrecht, *Trends in biochemical sciences* **1997**, *22*, 420–423.
[72] J. P. Abrahams, A. G. Leslie, R. Lutter, J. E. Walker, *Nature* **1994**, *370*, 621–628.
[73] G. D. Cody, N. Z. Boctor, T. R. Filley, R. M. Hazen, J. H. Scott, A. Sharma, H. S. Yoder, *Science (New York, N.Y.)* **2000**, *289*, 1337–1340.
[74] R. H. Crabtree, *The organometallic chemistry of the transition metals,* 6. ed. ed., Wiley, Hoboken, N.J., **2014**.
[75] C. de Duve, S. Vogel, *Aus Staub geboren*. *Leben als kosmische Zwangsläufigkeit*, Spektrum Akad. Verl., Heidelberg, **1995**.
[76] A. L. Weber, *Journal of molecular evolution* **1984**, *20*, 157–166.
[77] T. Wieland, E. Bokelmann, L. Bauer, H. U. Lang, H. Lau, *Justus Liebigs Ann. Chem.* **1953**, *583*, 129–149.
[78] M. C. Maurel, L. E. Orgel, *Origins of life and evolution of the biosphere : the journal of the International Society for the Study of the Origin of Life* **2000**, *30*, 423–430.
[79] a) M. A. Pasek, *Chemical reviews* **2020**, *120*, 4690–4706; b) N. N. Rao, M. R. Gómez-García, A. Kornberg, *Annual review of biochemistry* **2009**, *78*, 605–647;
[80] Y. Yamagata, H. Watanabe, M. Saitoh, T. Namba, *Nature* **1991**, *352*, 516–519.
[81] D. W. Deamer, *Microbiology and molecular biology reviews : MMBR* **1997**, *61*, 239–261.
[82] H. M. Leicester (Ed.) *Source Books in the History of the Sciences*, Harvard University Press, s.l., **1968**.
[83] W. J. Hagan, A. Parker, A. Steuerwald, M. Hathaway, *Origins of life and evolution of the biosphere : the journal of the International Society for the Study of the Origin of Life* **2007**, *37*, 113–122.
[84] D. Glindemann, R. M. de Graaf, A. W. Schwartz, *Origins of life and evolution of the biosphere : the journal of the International Society for the Study of the Origin of Life* **1999**, *29*, 555–561.
[85] R. M. de Graaf, A. W. Schwartz, *Origins of life and evolution of the biosphere : the journal of the International Society for the Study of the Origin of Life* **2000**, *30*, 405–410.

[86] A. W. D. Avison, *J. Chem. Soc.* **1955**, 732.
[87] R. Geuther, *Z Allg Mikrobiol* **1977**, *17*, 86–87.
[88] A. Whicher, E. Camprubi, S. Pinna, B. Herschy, N. Lane, *Origins of Life and Evolution of Biospheres* **2018**, *48*, 159–179.
[89] I. I. de Zwart, S. J. Meade, A. J. Pratt, *Geochimica et Cosmochimica Acta* **2004**, *68*, 4093–4098.
[90] D. Herschlag, W. P. Jencks, *Journal of the American Chemical Society* **1986**, *108*, 7938–7946.
[91] H. Baltscheffsky, A. Schultz, M. Baltscheffsky in *Matter, Energy, and Information in the Origin and Evolution of Life in the Universe*. *Proceedings of the Fifth Trieste Conference on Chemical Evolution* (Eds.: J. Chela-Flores, F. Raulin), Springer Netherlands, Dordrecht, **2012**.
[92] M. E. Jones, F. Lipmann, *Proceedings of the National Academy of Sciences* **1960**, *46*, 1194–1205.
[93] S. M. KRANE, M. J. GLIMCHER, *The Journal of biological chemistry* **1962**, *237*, 2991–2998.
[94] A. G. Cairns-Smith, *Genetic takeover and the mineral origins of life,* 1. paperback edition ed., Cambridge Univ. Press, Cambridge, **1987**.
[95] M. Hermes-Lima, A. Vieyra, *Origins Life Evol Biosphere* **1989**, *19*, 143–152.
[96] M. Hermes-Lima, A. Vieyra, *Journal of molecular evolution* **1992**, *35*, 277–285.
[97] L. M. Barge, I. J. Doloboff, M. J. Russell, D. VanderVelde, L. M. White, G. D. Stucky, M. M. Baum, J. Zeytounian, R. Kidd, I. Kanik, *Geochimica et Cosmochimica Acta* **2014**, *128*, 1–12.
[98] R. Krishnan, C. G. Riordan, *Journal of the American Chemical Society* **2004**, *126*, 4484–4485.
[99] G. Wächtershäuser, *Journal of molecular evolution* **2016**, *82*, 75–80.
[100] Daniel. Herschlag and William P. Jencks.
[101] D. H. Lee, S. Y. Kim, J.-I. Hong, *Angewandte Chemie (International ed. in English)* **2004**, *43*, 4777–4780.
[102] D. E. Koshland, *Journal of the American Chemical Society* **1952**, *74*, 2286–2292.
[103] J. Meyer-Fernandes, A. Vieyra, *Archives of biochemistry and biophysics* **1988**, *266*, 132–141.
[104] J. Eriksson, S. Karamohamed, P. Nyrén, *Analytical biochemistry* **2001**, *293*, 67–70.
[105] S. M. Steinberg, E. J. Poziomek, W. H. Engelmann, K. R. Rogers, *Chemosphere* **1995**, *30*, 2155–2197.
[106] in *UV Atlas of Organic Compounds / UV Atlas organischer Verbindungen*, Springer US, Boston, MA, **1967**.
[107] C. Huber, F. Kraus, M. Hanzlik, W. Eisenreich, G. Wächtershäuser, *Chemistry (Weinheim an der Bergstrasse, Germany)* **2012**, *18*, 2063–2080.
[108] J. Dewar, H. O. Jones, *Proceedings of the Royal Society of London* **1902**, *71*, 427–439.
[109] A. W. Budiman, J. S. Nam, J. H. Park, R. I. Mukti, T. S. Chang, J. W. Bae, M. J. Choi, *Catal Surv Asia* **2016**, *20*, 173–193.
[110] L. Mond, C. Langer, F. Quincke, *J. Chem. Soc., Trans.* **1890**, *57*, 749–753.
[111] W. Hieber, J. Ellermann, E. Zahn, *Zeitschrift für Naturforschung B* **1963**, *18*, 589–594.
[112] E. Weiss, H. Schmidbaur, H. Werner, W. A. Hermann, W. Beck, M. Herberhold, R. W. Hoffmann, G. Consiglio, O. Smrekar, *Angewandte Chemie International Edition in English* **1983**, *22*, 797–802.
[113] G. Bor, G. Sbrignadello, K. Noack, *HCA* **1975**, *58*, 815–833.
[114] M. D. Collins, P. A. Lawson, A. Willems, J. J. Cordoba, J. Fernandez-Garayzabal, P. Garcia, J. Cai, H. Hippe, J. A. Farrow, *International journal of systematic bacteriology* **1994**, *44*, 812–826.
[115] C. Kállay, I. Sóvágó, K. Várnagy, *Polyhedron* **2007**, *26*, 811–817.
[116] a) V. J. Starai, J. C. Escalante-Semerena, *Cellular and molecular life sciences : CMLS* **2004**, *61*, 2020–2030; b) M. Tobisu, T. Shimasaki, N. Chatani, *Chem. Lett.* **2009**, *38*, 710–711; c) R. C. Linck, C. W. Spahn, T. B. Rauchfuss, S. R. Wilson, *Journal of the American Chemical Society* **2003**, *125*, 8700–8701;

[117] O. Ganichkin, M. C. Wahl, *Crystal Structure of Moorella thermoacetica SelB(377-511)*, **2007**.
[118] F. García-Martín, M. Quintanar-Audelo, Y. García-Ramos, L. J. Cruz, C. Gravel, R. Furic, S. Côté, J. Tulla-Puche, F. Albericio, *Journal of combinatorial chemistry* **2006**, *8*, 213–220.
[119] P. E. Nielsen, M. Egholm, *Current issues in molecular biology* **1999**, *1*, 89–104.
[120] a) S. Kundu, S. Biswas, A. S. Mondal, P. Roy, T. K. Mondal, *Journal of Molecular Structure* **2015**, *1100*, 27–33; b) H. Unver, Z. Hayvali, *Spectrochimica acta. Part A, Molecular and biomolecular spectroscopy* **2010**, *75*, 782–788;
[121] J. F. KINCAID, J. S. STRONG, F. W. SUNDERMAN, *A.M.A. archives of industrial hygiene and occupational medicine* **1953**, *8*, 48–60.
[122] H. Behrens, E. Eisenmann, *Z. Anorg. Allg. Chem.* **1955**, *278*, 166–173.
[123] K. Hata, *New hydrogenating catalysts*. *Urushibara catalysts*, Halsted Press Division, Wiley, New York, **1972, 1971**.
[124] E. Riedel, *Anorganische Chemie,* 9. Auflage ed., De Gruyter, Berlin, Bosten, **2015**.